MONITORING OF CRUSTAL MOVEMENTS IN THE SAN ANDREAS FAULT ZONE BY A SATELLITE-BORNE RANGING SYSTEM

by
Muneendra Kumar

Prepared for

National Aeronautics and Space Administration
Washington, D. C.

Grant No. NGR 36-008-204
OSURF Project No. 3820-A1

The Ohio State University
Research Foundation
Columbus, Ohio   43212

August 1976

MONITORING OF CRUSTAL MOVEMENTS IN THE SAN ANDREAS FAULT ZONE BY A SATELLITE-BORNE RANGING SYSTEM

by

Muneendra Kumar

PREFACE

This project is under the supervision of Professor Ivan I. Mueller, Department of Geodetic Science, The Ohio State University and under the technical direction of Mr. James P. Murphy, Special Programs, Office of Applications, Code ES, NASA Headquarters, Washington, D.C. The Contract is administered by the Office of University Affairs, NASA, Washington, D.C., 20546.

This report was also submitted to the Graduate School of The Ohio State University as a partial fulfillment of the requirements for the Ph.D. degree.

ABSTRACT

The Close Grid Geodynamic Measurement System is conceived as an orbiting ranging device with a ground base grid of reflectors or transponders (spacing 1.0 to 30 km), which are projected to be of low cost (maintenance free and unattended), and which will permit the saturation of a local area to obtain data useful to monitor crustal movements in the San Andreas fault zone.

This investigation includes a station network of 75 stations covering an area between 36°N and 38°N latitudes, and 237°E and 239°E longitudes, with roughly half of the stations on either side of the faults. In addition, the simulation of crustal movements through the introduction of changes in the relative positions between grid stations, weather effect for intervisibility between satellite and station and loss of observations thereof, and comparative evaluation of various observational scheme/pattern have been critically studied.

The study considers laser radar as the main ranging system pending final selection from many possible candidates and the ranges used have been generated for standard deviations of 2 and 10 cm. The satellite orbit is inclined at 110° and slightly eccentric (e = 0.04) with orbital altitudes varying from 370 km to 930 km. Geometric and short arc modes are the two main methods for handling ranges and solution/adjustment of the system.

The constant rate of crustal motion has been assumed as 3 cm per year both in latitudinal and longitudinal directions. No vertical motion is consid-

ered. Using this rate, two time epochs, t_0 and t_1 ($= t_0 + 12$ months) are considered to investigate motion recovery.

The results have been analyzed in two stages: (1) Recovery analysis in terms of the differences between the actual and the recovered chords between any two stations to select the most optimum design of experiment, (2) Statistical analysis in terms of the conventional α and β errors for the recovery of motion rate for the selected design of experiment.

The geometric mode with minimum of five grid and three distant (fundamental) stations and mixed ranging to satellite and airplane seems to be most promising. The fundamental stations are distinguished from the grid station in their location and this location should be 'distant' enough from the area of crustal movement so that they can be considered stationary over the time span of the motion involved.

The recovery of motion rate for magnitude is quite straightforward, while for direction each case may require consideration on its own merit. The study also recognizes the sensitivity of the results/deductions obtained thereof to any design of experiment associated with them. For the specified setup, time interval between two sets of station recovery for different motion rate or ranging accuracies has also been suggested.

ACKNOWLEDGMENTS

TABLE OF CONTENTS

LIST OF TABLES

LIST OF FIGURES

1. INTRODUCTION

1.1 Historical Background

This study is the continuation of a recent simulation study "Error Analysis for the Proposed Close Grid Geodynamic Satellite Measurement System (CLOGEOS)," jointly undertaken by the author [Mueller et al., 1975]. It may be quite appropriate here to include a brief historical background of the problem which triggered the present experiment.

The scientific community has been for quite sometime actively engaged in the detailed study of the San Andreas fault system because of its great impact on the stability, growth and development of the surrounding areas in California and Mexico. The fault system lies along the boundary between the North American and the Pacific tectonic plates and comprises an extremely complex zone with relative slippages of varying rates of 1-6 cm per year, and spasmodic seismic activities [Drake et al., 1973].

The San Andreas "break" in the earth's crust is actually not one fault but a system of faults, most of which trend roughly northwest-southeast. The prominent exceptions are the east-west transverse ranges and faults that make up a band of some 150 km in width and extending inland between Los Angeles and Santa Barbara. However, in simple terms, the San Andreas fault system separates a northward-moving wedge of California, including Los Angeles, from the rest of North America.

In its complex entirety, it would be misleading to think of the San Andreas fault as an "isolated" mechanical system, or of the entire San Andreas fault zone as a "single" system. There is evidence that the part of the fault that lies in northern California, which was activated earlier, has moved farther than southern California, and may even be moving at a different rate -- a quite unlikely phenomenon since both these sections are considered to be

1

attached to the same Pacific plate. However, the compression in the trans-
verse ranges/faults may be attributed to this differential motion. Another
point of view is that all of the relative motion is not being taken up by the
San Andreas fault system alone but extends well inland.

The present understanding of the San Andreas fault system suggests
that at about 15 km depth the plates slip past one another fairly uniformly
along a steep contact [Savage and Buford, 1973], i.e., a condition of continu-
ous stable sliding may very well prevail at depth, as is evidenced by rather
uniform long-term displacement rates measured at the surface and by an
apparent absence of earthquake foci at depth greater than about 15 km. The
section north of Hollister (Figure 1-1) behaves as if the fault surfaces were
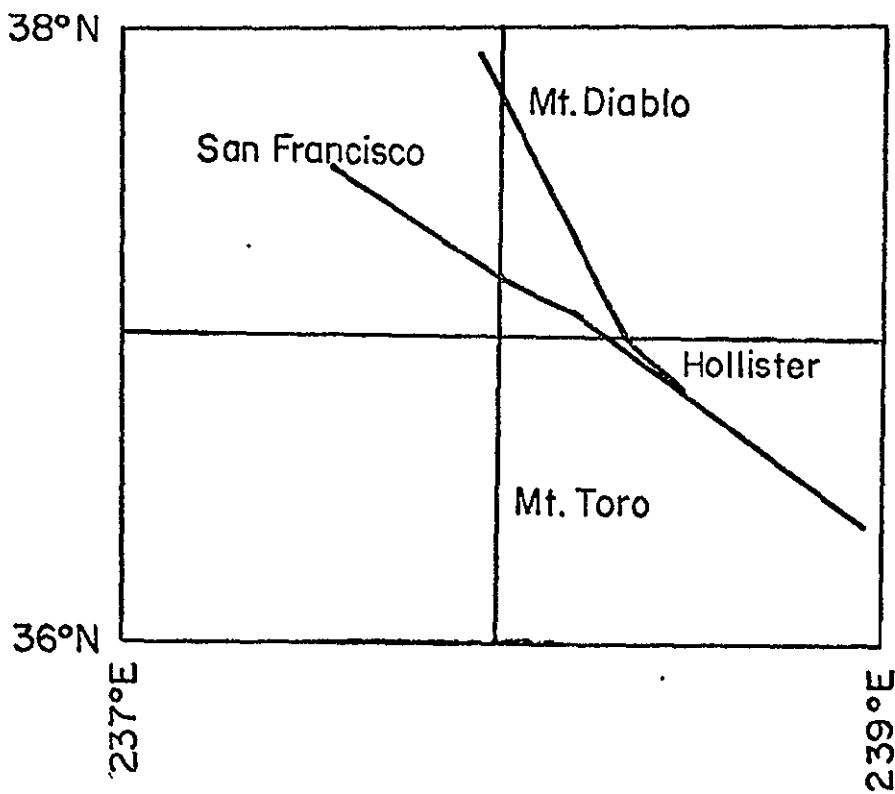
Figure 1-1. San Andreas Fault System in Central California

locked with strain accumulation in the vicinity of the fault system.

2

In the latter case where the fault surface behaves as "locked," Savage and Buford [1973] have obtained a rough estimate that, to include 90% of the relative motion, related measurements must extend across a belt of about 100 km on either side of the fault to span the zone of strain accumulation.

A review of some of the important current studies, both practical and theoretical, on the San Andreas fault system and other closely associated phenomena [Cox, 1968; Oliver et al., 1969; Scholz and Fitch, 1969; Savage and Bulford, 1970; Anderson, 1971; Bird and Isacks, 1972; NOAA, 1973 ; Savage and Bulford, 1973; Agreen and Smith, 1973; Scholz et al., 1973 ; Turcotte and Spence, 1974; Rodgers, 1975; Brown, 1975; Pope, 1966] indicates the following two main limitations which have all along been hampering a better insight into the problem:

(a) lack of "continuous" data to monitor, analyze and study the crustal/plate tectonics,

(b) lack of sufficient accuracy in the collected data vis-a-vis the order of magnitude of the motions involved.

In the case of traditional geodetic monitoring, the data available mostly consist of repeated surveys of triangulation, geodimeter or leveling networks and direct measurements of fault creep, where one or both of the above limitations are inherent. In addition, all such data have limited area coverage-- another obstacle that the measurements may not have extended sufficiently far enough from the fault to include the entire strain accumulation zone in the "locked" block-type section (s).

Thus, in cases where it may become necessary to extend the study of relative motion over extensive areas beyond the actual fault to span the zone of strain accumulation, the time span needed to provide such data coverage becomes an important factor. The brevity of time span for observations is also essential to assume that the observed stations do not move relatively during that period.

The system investigated in this study is free of all the above limitations. It provides accurate and continuously repeated measurements distributed over wide areas on both sides of the fault. Thus it is envisaged as a monitoring system which could register the time variant topography of the area covered on a continuous basis.

1.2 Review of Previous Works

The studies [Blaha, 1971b; Tsimis, 1973] elaborate the principle of multilateration and the report [Reilly et al., 1972] deals with the computer program for the determination of three-dimensional station coordinates and satellite ephemerides.

In another study [Escobal et al., 1973], making use of a system of six ground stations and one or two satellites with simultaneous slant ranges between them, numerical results presented indicate that relative station positions can be determined with an accuracy that is limited only by the hardware measurement system.

However, in the study mentioned earlier [Mueller et.al., 1975], the Close Grid Geodynamic Measurement System (CLOGEOS) was originally conceived as an active orbiting-ranging device with ground base reflectors or transponders in the San Andreas fault zone. It was envisaged that a grid of these reflectors/transponders which are projected to be of low cost (passive, maintenance free and unattended) will permit the saturation of a local area (spacing 0.5-50 km) to obtain data useful for geodynamic and geodetic purposes.

In the above investigation a first attempt was made with a grid of nine stations (Figure 1-2) with a spacing of five minutes of arc ($\Delta\phi=9.3$ km and $\Delta\lambda = 7.3$ km) to get an insight on how maximum accuracy of relative station position recovery can be achieved in a short time span, say three to five days.

From the numerous possible instrumental candidates, e.g., laser radar, RF radar or a combination of both operating in a continuous wave or pulse mode, providing ranges, range rates (Doppler) or range differences
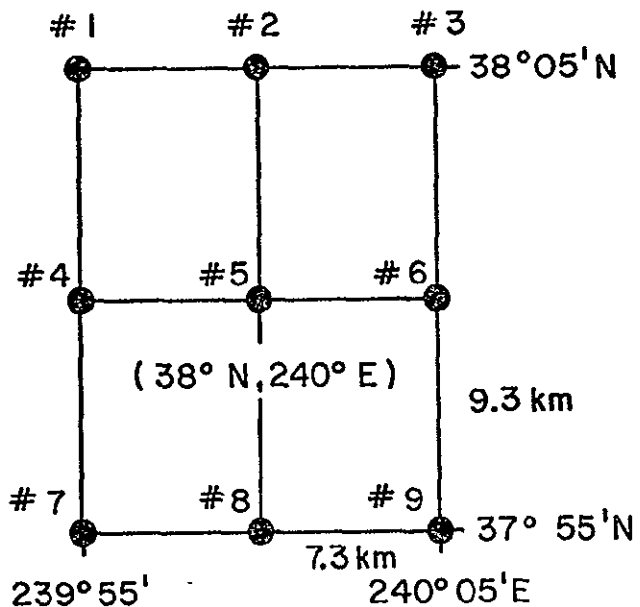
Figure 1-2. Nine-Station Configuration

(integrated Doppler), this study was carried out only with laser ranges of already feasible precision of 10 cm.

Two types of vehicles carrying the transmitter were considered: (1) three active satellites at altitudes of 392, 657, and 1007 km with nearly circular (e = 0.001) polar orbits --these altitudes were selected to avoid periods commensurate with the earth's rotation with the intention to suppress all possible resonances with the geopotential; (2) an airplane flying at an altitude of 9 km--these flights arranged from south to north.

With reference to Figure 1-2, if the ground stations and/or satellite points happen to be in critical configuration with each other, the solution for the system will be singular even when the number of observations is sufficient and the coordinate system is properly defined [Blaha, 1971b]. In practice, the case of near singularity or ill-conditioning also affects the solution and degenerates the recovery of the system when all the stations and/or the satellite points are near critical. In view of the above, the ellipsoidal height differences (Δh) between the nine stations were investigated as a parameter

5

for their effect on system's recovery. Three cases, viz., A, B, and C with Δh equal to 0, 100, and 1000 m were included in the study. (Figure 1-3).
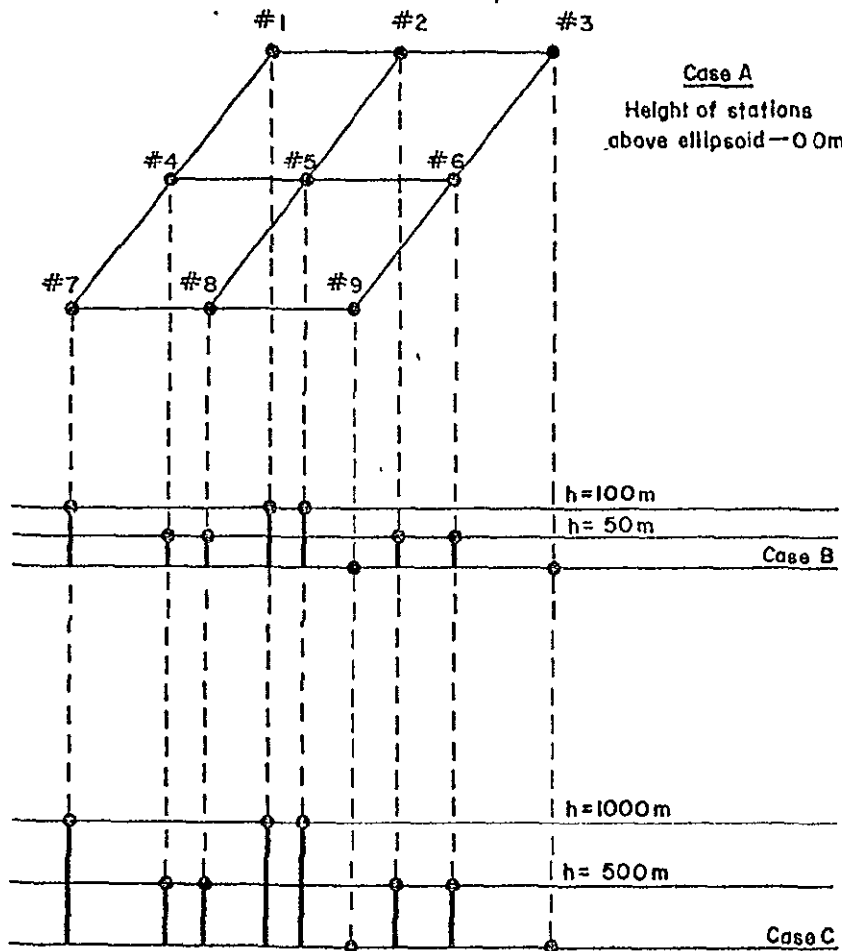
Figure 1-3. Diagrammatic Representation of Station Height Separation [from Mueller et.al., 1975].

To define the origin and orientation of the system in the short arc mode (see algorithm (2) of the following paragraph) and to distinguish them from the nine grid stations, three distant stations were selected outside the grid area and were referred to as "Fundamental" stations in the study. As a matter of convenience, these stations were located at future ground laser

station sites near San Diego and Quincy in California and near Bear Lake, Utah [Smith et al., 1974]. Figure 1-4 shows the location of grid and fundamental stations in the study. The broken line circles, which are marked U and L, represent the general coverage of the satellite orbits with 1007 km (upper) and 392 km (lower) altitudes respectively.

The ranges were simulated in two observational modes, simultaneous and nonsimultaneous (or sequential) and were then utilized in two different algorithms to compute relative positions of grid stations: (1) Geometric adjustment which takes advantage of the simultaneity of the observations leading to a very simple mathematical model but also involving degeneracies of near critical configurations in local networks as opposed to global networks. The definition of origin and orientation was obtained through "inner" constraints [Blaha, 1971a]. (2) Short arc adjustment which does not require simultaneous observations as of necessity and involve the bothersome critical configurations--however, in order to get stability in the solutions, the three distant fundamental stations had to be observed during each pass.

Since the range measurement system lacks coordinate definition, especially in the geometric mode, the recovery of the relative positions was expressed in terms of the estimable quantities, the lengths of the chords between the grid stations (Figure 1-4) and the angles between the chords. The recovery representation is in terms of absolute differences ($D_{R_{ij}}$) computed between the recovered and the true distances between the grid stations "i" and "j".

The geometric mode results indicated two possibilities to avoid the above-mentioned critical configurations (see Table 1-1, line 1) : (1) Separate stations in height either by introducing some height differences Δh (Figure 1-3)--a possibility only in the case of accommodating local topography (see Table 1-1, line 2), or by including into the observation-campaign the three fundamental stations (see Table 1-1, line 4)-- a stringent requirement of having favorable weather conditions at four different sites, viz., grid area and three

7

STATION SEPARATION
NORTH–SOUTH 5' ≈ 9.3 KM
EAST–WEST   5' ≈ 7.3 KM
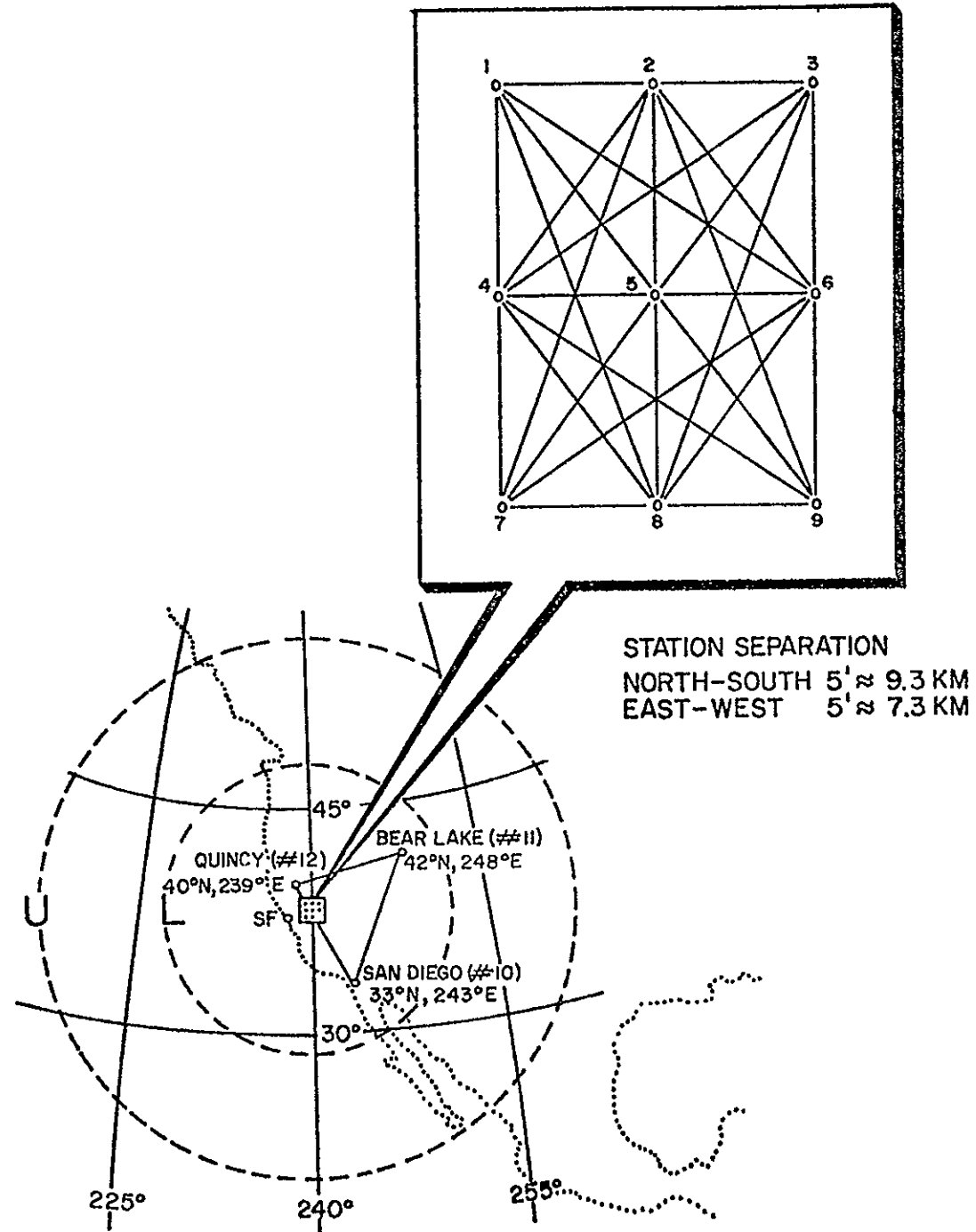
Figure 1-4.   Location of Grid and Fundamental Stations
[from Mueller et al., 1975]

Table 1-1

Recovery of Station-to-Station Distances[1]

36 Distances Between 9 Grid Stations, 500 Observations per Station
Accuracy of Range Measurements: σ_r = 10 cm

Mode	Δh (m)	No. of Grid Stations	No. of Fundamental Stations	Height (km) Satellite	Height (km) Airplane	Percentages of Absolute Differences $|D_R|$ 0-1 cm	1-2 cm	2-3 cm	3-4 cm	>4 cm	Maximum Difference	Maximum σ_R (cm)
Geometric	0	9	0	1007	---					100	669	569
Geometric	1000	9	0	1007	---	14	11	11	11	53	25	14
Geometric	0	9	1	1007	---	28	16	14	14	28	11	11
Geometric	0	9	3	1007	---	72	22	6			3	2
Geometric	0	9	0	392	9	69	28	3			3	4
Short Arc	0	9	3	1007	---	22	28	14	14	22	7	7

(Alternatives)

Note: For a graphical representation see Figure 1-5.

[1] From [Mueller et al., 1975]

fundamental stations. (2) Separate the ranging devices in height which in turn suggested the best (and most realistic) solution as the combination of an airplane and a satellite (see Table 1-1, line 5) thereby eliminating the need for fundamental stations. The only disadvantage of this mode is the instrumental problem related to the realization of simultaneous observations which for lasers may be overwhelming.

In the case of short arc mode results (see Table 1-1, line 6), it is important to note that a pass of four to ten minutes in length in time for satellite altitudes between 400 to 1000 km is extremely short in duration of time during which "expected" favorable weather conditions almost simultaneously at all four distant sites might be just as stringent a requirement as in the case of the geometric mode. Further, an improvement in ranging accuracy did not produce any significant difference in the system's recovery by the short arc mode.

Figure 1-5 shows a graphical representation of the results of the study, both in the geometric and in the short arc modes. In summary, the main conclusions of the study were the following:

(1) Ranging with $\sigma_r = 10$ cm and 500 observations per station can recover relative positions (or chords) between grid stations well ($\sigma_{R_{ij}} = 4$ cm and $|D_{R_{ij}}| = 3$ cm) for chord lengths varying from 7 km to 23 km in a limited grid of nine stations.

(2) Unit efficiency $\sigma_{R_{ij}} / \sigma_r$ can be achieved with fewer than 500 observations (about 50).

(3) Expected improvements in the ranging accuracy (to 1-2 cm) and in the corresponding precision makes the proposed system an excellent candidate for geodetic and geodynamic applications.

(4) As far as the mode of operation is concerned for a laser system, the trade-offs between the likelihood of having favorable weather conditions at the distant fundamental stations in the case of the short arc mode (possibly with a single satellite and nonsimultaneous ranging) and the
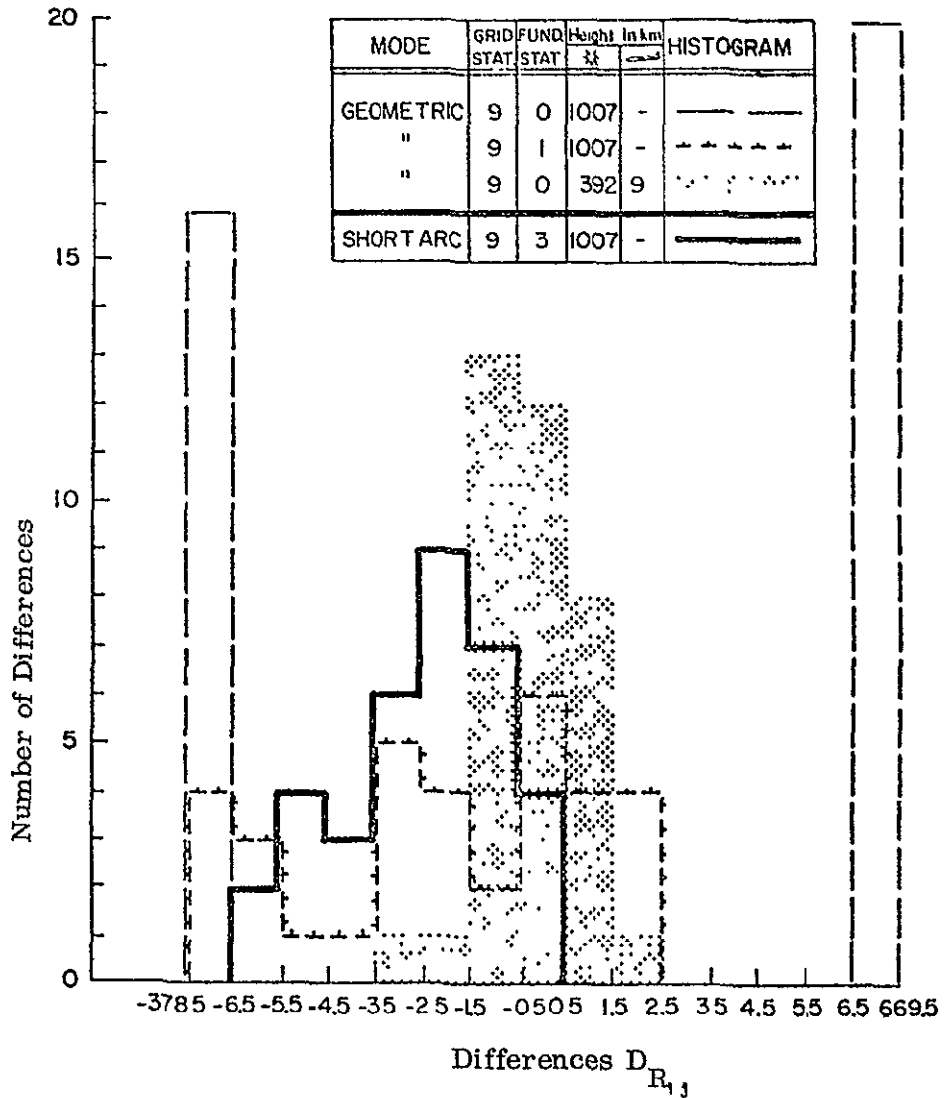
Figure 1-5. Recovery of Station-to-Station Distances
[from Mueller et al., 1975]

feasibility of overcoming problems in the geometric mode (satellite and airplane with simultaneous ranging) need to be considered.

The questions and recommendations which the study raised for future studies and investigations were as follows:

(1) At what stage do computational problems due to double precision arith-

metic start to dominate the ill-conditioning due to near critical config-
uration? Or, will quadruple precision arithmetic be able to cope with
problems in system's recovery arising from ill-conditioning due to near
critical configurations?

(2) The grid station network should be extended to a large grid, and an
observational scheme/procedure for the same is recommended.

(3) The case of very closely spaced (≈ 1 km) grid system should be in-
vestigated.

(4) In an extended network, actual changes in the relative positions of the
grid stations should be simulated and through successive recoveries
monitoring capabilities for these changes in relative positions studied
in the system.

(5) A short investigation should be made into the correctness of the step
and iterative adjustment including any pitfalls [Pope, 1972] and the
computational accuracy of geometric mode algorithms.

(6) Better algorithms for short arc adjustment should be devised to cater
for systematic effects at centimeter level, if necessary.

(7) An optimum estimation procedure for station recovery might be a geo-
metric mode which takes advantage of orbital constraints which connect
the different (unknown) satellite positions, or, the reverse--a short
arc mode which makes use of (near) simultaneities between observations.

The present study was initiated to accommodate some of the above recommenda-
tions.

1.3 Brief Description of the Present Study

The current study also envisages an active ranging satellite. The
laser radar has been retained as the main measurement system pending
final selection from many possible candidates. The inclusion of airplane
flights is treated as a special case of low flying satellite.

The selected satellite orbit is inclined at 110° and is slightly eccentric
($e = 0.04$). With this orbit, satellite passes were generated in a mesh pattern

over the grid area with perigee and apogee heights as 370 and 930 km respec-
tively. For low altitude ranges, the airplane flights are arranged south to
north at 10 km height.

The present simulation includes 75 stations covering an area 36°N and
38° N latitudes and 237° E and 239° E longitudes, with station-to-station
distance varying from 5-30 km with roughly half of them on either side of the
faults. In addition to the choice of three fundamental stations at distant ground
laser station sites outside the grid area, two other possible locations, viz.,
at the periphery and within the grid itself have been investigated. For densi-
fication of network and for the investigation of very closely spaced ($\approx$1 km)
grid, ten stations were replaced by a new set of ten stations at one-minute
spacing both in latitude and longitude.

The ranges generated were in two observational modes, simultaneous
and nonsimultaneous (or sequential). In case of simultaneous observations to
four or more stations, the geometric mode algorithm uses the satellite as the
common point for generating observations and ignores the fact that it moves
in the orbit. The other algorithm, the short arc mode, utilizes each observa-
tion individually thereby eliminating the need of simultaneity in observations.
The orbital constraints linking individual satellite positions become a part
of the algorithm and are made use of in obtaining a solution towards recovery
of station positions.

In addition, this study simulates various possible combinations of
observational patterns and station groupings both for geometric and short arc
modes, the effect of weather on visibility, the effect of crustal motion by the
introduction of changes in the relative positions of the grid stations, the effect
of varying accuracy of the observed ranges, and analyzes their role/effect on
the results.

It may be quite appropriate to mention here that the success of this
study depended to a very large extent on the successful setting up of the Goddard
Trajectory Determination System (GTDS) and Short Arc Geodetic Adjustment

13

(SAGA) computer programs, on the suitable modifications of these two programs and The Ohio State University Geometric and Orbital (Adjustment) Program (OSUGOP) as well. In addition, a new program for laser range generation (LRGP) was written. In view of this, four appendices have been added giving brief details about these programs and the modifications made for the present investigation.

The main contribution of this study lies in the attempt to answer the following questions:

A. How is the recovery of the relative positions (or chords) between grid stations at an epoch of time affected by

  a) the choice of fundamental stations

  b) the number of grid stations simultaneously observed in an event

  c) the number of grid stations observed in a pass

  d) the number of grid stations participating in any solution

  e) the densification of network

  f) the weather

  g) the number of observations to station

  h) the accuracy of ranging

  i) the observations from airplanes?

B. What are the statistical aspects of station position and chord length estimation?

C. For the recovery of the motion at a given grid station,

  a) what is the minimum time needed for a specified ranging accuracy (say $\sigma_r = 2\text{cm}$)

  b) how does this minimum necessary time depend on the ranging accuracy?

D. How are the specified motions of the plates recovered?

In brief, this study begins with detailed discussion in Chapter 2 of the mathematical models, procedure of recovery and statistical analysis, and details of data simulation. Chapter 3 includes the details of the experimental setup of stations, weather effect and crustal motion modeling, and of different

14

observational patterns. Following this, in Chapters 4 and 5 the information about the various solutions performed and the results are reported. A summary of main results and the conclusions thereof are included in Chapter 6.

2. MATHEMATICAL MODEL AND PROCEDURE OF RECOVERY

Out of the many possible candidates in measurement systems such as laser radar, RF radar, or a combination of both operating in continuous wave or pulse mode, this study again concentrates with the already feasible laser precision of 10 cm and expected precision of 2 cm [Byrns and Cooke, 1975]. This approach would allow the design of an optimum and operational drill now with laser ranges and still permit adaptation of the same drill with suitable modifications to any measurement system once the final choice is made at a later stage.

As regards the recovery of the relative positions of the grid stations and the velocity (or the differential position) vectors with the desired accuracy, two most promising methods are the geometric and short arc modes--the first involving the geometry of the system with its limiting critical degeneracies and the second following the orbital restraints with its complexities of the force model and equations of celestial mechanics. A brief and general description of mathematical models for geometric and short arc modes has been included here along with salient remarks/features pertaining to this study where appropriate.

2.1 Mathematical Model

(a) Geometric Mode

Following the treatment in [Krakiwsky and Pope, 1967] and [Mueller et al., 1973], the geometry of a topocentric range r_{ij} from any ground station P_i (u_i, v_i, w_i; $i = 1,2,3,4...$) to any satellite position Q_j (u_j, v_j, w_j; $j = 1,2,3,4...$) is given in Figure 2-1. Here, the coordinate system (earth fixed) is oriented towards the Greenwich Mean Astronomical Meridian (u-axis) and the Conventional International Origin (w-axis) -- both as defined by the Bureau
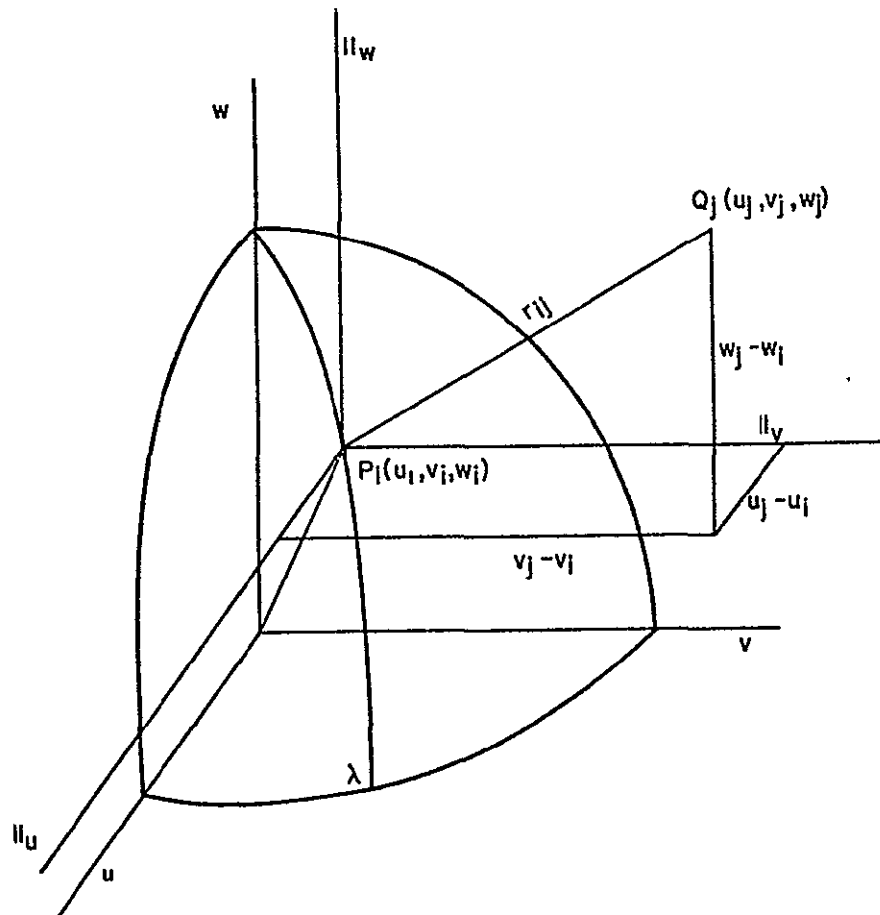
Figure 2-1. Geometry for a Topocentric Range

International de l'Heure (BIH)--while the v-axis forms a right handed system with u and w, and with u defines the average geodetic equator. Then, from Figure 2-1, the following relation can be written:

$$F_{ij} \equiv [(u_j - u_i)^2 + (v_j - v_i)^2 + (w_j - w_i)^2]^{\frac{1}{2}} - r_{ij} = 0 \qquad (2\text{-}1)$$

This basic mathematical model is solved through trigonometric computations based on simultaneous observations to or from a satellite (or airplane) from or to four or more ground stations (at least six in the case of a small network) [Blaha, 1971b; Escobal et al., 1973]. As the system extends with the increase of "i" or "j", the model becomes overdetermined and the unknown parameters are then recovered through an adjustment.

17

(b) Short Arc Mode

This mode of solution recognizes the fact that the satellite motion through space can also be represented by a set of three second-order differential equations. If these satellite orbit arcs defining its motion are restricted to 10 - 30 minutes in time, many approximations, namely in gravitational and nongravitational force models, are possible without jeopardizing the accuracy. As the solution in this mode does not involve geometry (in the same sense as geometric mode), this approach requires only nonsimultaneous (sequential) ranges.

The solution to the above-mentioned sets of differential equations at any assigned time (T) may be written in the following form

$$\bar{x}_{(T)} = \int_{t_0}^{T} (T-t)\, F_{(t)}\, dt \;+\; (T-t_0)\, \bar{\dot{x}}_{(t_0)} \;+\; \bar{x}_{(t_0)} \qquad (2\text{-}2)$$

whereby requiring six arbitrary constants of integration. In the present case the constants would be the position $\bar{x}_{(t_0)}$ and velocity $\bar{\dot{x}}_{(t_0)}$ vectors at epoch time "t_0", and the symbol $F_{(t)}$ describes the force function of the system at any arbitrary time "t" during the flight.

In this mode, the computer program used in the present study is Short Arc Geodetic Program (SAGA [Brown and Trotter, 1969], Appendix B) which employs a power series solution to the equations of motion [Hartwell, 1968] wherein each coefficient is formed in terms of its predecessors by means of recursive algorithms. Thus if x,y,z denote the geocentric inertial coordinates at any arbitrary time t relative to an adopted epoch t_0 , the power series solution is given as

$$
\begin{bmatrix} x & \dot{x} \\ y & \dot{y} \\ z & \dot{z} \end{bmatrix}_t
=
\begin{bmatrix} a_0 & a_1 & a_2 & \ldots & a_n \\ b_0 & b_1 & b_2 & \ldots & b_n \\ c_0 & c_1 & c_2 & .. & c_n \end{bmatrix}
\begin{bmatrix} 1 & 0 \\ t & 1 \\ t^2 & 2t \\ \vdots & \vdots \\ t^n & nt^{n-1} \end{bmatrix}
\qquad (2\text{-}3)
$$

18

The geocentric inertial coordinate system is here defined as oriented towards the mean vernal equinox (x-axis) and the mean north celestial pole (z-axis) at some selected fundamental epoch. The y-axis forms a right handed system with x and z-axes and with x-axis defines the mean celestial equator.

The coefficients in equation (2-3) are functions of initial state vector $(x_{t_0}, y_{t_0}, z_{t_0} ; \dot{x}_{t_0}, \dot{y}_{t_0}, \dot{z}_{t_0})$ and gravitational coefficients. In the program the series is truncated as the specified tolerance of 0.001 m is reached for the maximum value of t to be exercised for any given short arc. If t_0 is taken near the mid-arc, the radius of convergence for each expansion is sufficient to cater for arcs as long as one-third of a revolution for a nearly circular orbit. Keeping this in mind, the length of any arc in the current study was always kept less than one-fifth of a revolution.

If u_0, v_0, w_0 denote the earth-fixed coordinates of the center of mass, SAGA uses variational equations to relate errors in x_t, y_t, z_t to errors in adopted $\bar{U}_0$ and initial state vector at t_0. The matrix of partial derivative can then be represented as

$$M = \frac{\partial(x, y, z, t)}{\partial(u_0, v_0, w_0, x_{t_0}, y_{t_0}, z_{t_0}, \dot{x}_{t_0}, \dot{y}_{t_0}, \dot{z}_{t_0})}$$

$$= \begin{bmatrix} m_{11} & m_{12} & \dots & m_{19} \\ m_{21} & m_{22} & \dots & m_{29} \\ m_{31} & m_{32} & \dots & m_{39} \end{bmatrix} \qquad (2\text{-}4)$$

where each element is developed in the following polynomial form:

$$m_{kl} = (\alpha_0, \alpha_1, \alpha_2, \dots, \alpha_p)_{kl} \begin{bmatrix} 1 \\ t \\ t^2 \\ \vdots \\ t^p \end{bmatrix} \qquad (2\text{-}5)$$

19

If the state vector at time t in an earth-fixed system is denoted by $(\bar{U}, \bar{\dot{U}})$, then

$$
\begin{bmatrix} u_J \\ v_J \\ w_J \\ \dot{u}_J \\ \dot{v}_J \\ \dot{w}_J \end{bmatrix}_t
=
\begin{bmatrix} R & 0 \\ \dot{R} & R \end{bmatrix}
\begin{bmatrix} x \\ y \\ z \\ \dot{x} \\ \dot{y} \\ \dot{z} \end{bmatrix}_t
\tag{2-6}
$$

where the transformation matrix R and its derivative $\dot{R}$ are given as

$$
R = \begin{bmatrix} \cos \omega t & \sin \omega t & 0 \\ -\sin \omega t & \cos \omega t & 0 \\ 0 & 0 & 1 \end{bmatrix}
\tag{2-7}
$$

$$
\dot{R} = \omega \begin{bmatrix} -\sin \omega t & \cos \omega t & 0 \\ -\cos \omega t & -\sin \omega t & 0 \\ 0 & 0 & 0 \end{bmatrix}
\tag{2-8}
$$

where ω represents the earth's rotational angular velocity.

From equations (2-7) and (2-4), the partial derivative matrix can also be transformed to the earth-fixed system as

$$
M' = RM
\tag{2-9}
$$

20

Using now the values obtained in equations (2-3) and (2-6), the final mathematical model then becomes

$$r_{ij} = f(u_o, v_o, w_o, u_i, v_i, w_i, x_{t_0}, y_{t_0}, z_{t_0}, \dot{x}_{t_0}, \dot{y}_{t_0}, \dot{z}_{t_0}, t) \qquad (2-10)$$

where u_i, v_i, w_i are the earth-fixed coordinates of the ground station.

2.2 The Adjustment Scheme

2.2.1 Normal equations

(a) Geometric Mode

The mathematical model as given in equation (2-1) can be linearized by Taylor series expansion about the preliminary values of the ground stations, satellite positions and the observed ranges to obtain observational equation in the following matrix form [Uotila, 1967]:

$$BV + AX + W = 0 \qquad (2-11)$$

Here, corresponding to any observed range r_{ij}

$$B_{ij} = \frac{\partial F_{ij}}{\partial r_{ij}} = [0 \ \vdots \ -1 \ \vdots \ 0]$$

$$A_{ij} = \frac{\partial F_{ij}}{\partial u_j^0, \partial u_i^0} = [a_{ij} \ \vdots \ -a_{ij}]$$

$$a_{ij} = \left[\frac{u_j^0 - u_i^0}{r_{ij}} \quad \frac{v_j^0 - v_i^0}{r_{ij}} \quad \frac{w_j^0 - w_i^0}{r_{ij}} \right]$$

$$X_{ij} = [du_j \quad dv_j \quad dw_j \ \vdots \ du_i \quad dv_i \quad dw_i]^T$$

$$W_{ij} = r_{ij}^c \text{ (computed)} - r_{ij}^b \text{ (observed)}$$

The superscript " o " denotes the initial approximate values of the quantities involved. The approximate satellite positions (u_j^0, v_j^0, w_j^0) for any event are computed from a preliminary least squares adjustment for that event with observing ground station positions (u_i^0, v_i^0, w_i^0) held fixed. For this purpose in the computer, an approximate satellite height h is assumed and

the computations iterated to obtain satellite positions. It was noticed that with
the assumed satellite height (say, h =1000 km), the iteration failed to converge
for the airplane case while in the reverse assumption (h = 10 km), the iteration
did converge in less than 20 iterations to the satellite positions.

The satellite positions $(u_j^0$, v_j^0 , $w_j^0)$ so computed are then used to
compute the range r_{ij} from equation (2-1) to obtain the misclosure vector W_{ij} .
Also, in the present case the design matrix B becomes a negative unit matrix
[-I] and the residual matrix V_{ij} then corresponds directly to the observed
ranges r_{ij}^b .

If P is the weight matrix for the observed ranges, then the variation
function φ to be minimized is given as

$$\varphi = V^TPV + X^TP_xX - 2K^T(AX - V + W) \tag{2-12}$$

where

$P_x \equiv$ weight matrix for ground stations X_i and satellite positions X_j

$K \equiv$ vector of correlates or Lagrange multipliers

After enforcing the minimum condition for equation (2-12) and eliminat-
ing unknowns K and V, the expanded form of the equation for matrices A, P,
and P_x is as follows:

$$\begin{bmatrix} \sum_i a_{ij}^T p_{ij} a_{ij} + p_{x_j} & \vline & -a_{ij}^T p_{ij} a_{ij} \\ \hline -a_{ij}^T p_{ij} a_{ij} & \vline & \sum_j a_{ij}^T p_{ij} a_{ij} + p_{x_i} \end{bmatrix} \begin{bmatrix} X_j \\ \hline X_i \end{bmatrix}$$

$$+ \begin{bmatrix} \sum_i a_{ij}^T p_{ij} w_{ij} \\ \hline -\sum_j a_{ij}^T p_{ij} w_{ij} \end{bmatrix} = 0 \tag{2-13}$$

The matrix M in the above equations is defined as:

$$
M = \begin{bmatrix}
0 & \sin\varphi_0\,\alpha - \cos\varphi_0\,\eta & \begin{aligned} &-\cos\varphi_0\sin\lambda_0\,\alpha - \cos\lambda_0\,\xi \\ &-\sin\varphi_0\,\sin\lambda_0\,\eta \end{aligned} \\[2ex]
-\sin\varphi_0\,\alpha + \cos\varphi_0\,\eta & 0 & \begin{aligned} &\cos\varphi_0\cos\lambda_0\,\alpha - \sin\lambda_0\,\xi \\ &+\sin\varphi_0\cos\lambda_0\,\eta \end{aligned} \\[2ex]
\begin{aligned} &\cos\varphi_0\sin\lambda_0\,\alpha \\ &+\cos\lambda_0\,\xi \\ &+\sin\varphi_0\sin\lambda_0\,\eta \end{aligned} & \begin{aligned} &-\cos\varphi_0\cos\lambda_0\,\alpha \\ &+\sin\lambda_0\,\xi \\ &-\sin\varphi_0\cos\lambda_0\,\eta \end{aligned} & 0
\end{bmatrix}
$$

where $(\varphi_0,\ \lambda_0,\ h_0)$ are the geodetic coordinates of the initial point and $\eta,\ \xi,\ \alpha$ are the respective rotations about the above three axes.

Further, the three rotations $\eta,\ \xi,\ \alpha$ are related to the rotations $\epsilon,\ \psi$ and ω of Bursa's and Molodensky's models as

$$
\begin{bmatrix} \alpha \\ \xi \\ \eta \end{bmatrix} = \begin{bmatrix}
\sin\varphi_0 & \cos\varphi_0\sin\lambda_0 & \cos\lambda_0\cos\varphi_0 \\
0 & \cos\lambda_0 & -\sin\lambda_0 \\
-\cos\varphi_0 & \sin\varphi_0\sin\lambda_0 & \cos\lambda_0\sin\varphi_0
\end{bmatrix} \begin{bmatrix} \omega \\ \varphi \\ \epsilon \end{bmatrix} \tag{3}
$$

Also, if $\Sigma_{\alpha\xi\eta}$ and $\Sigma_{\omega\psi\epsilon}$ are the variance-covariance matrices in the two cases, then the principle of propagation of errors gives

$$
\Sigma_{\alpha\xi\eta} = G\Sigma_{\omega\psi\epsilon}G' \tag{4}
$$

where

$$
G = \begin{bmatrix}
\sin\varphi_0 & \cos\varphi_0\sin\lambda_0 & \cos\lambda_0\cos\varphi_0 \\
0 & \cos\lambda_0 & -\sin\lambda_0 \\
-\cos\varphi_0 & \sin\varphi_0\sin\lambda_0 & \cos\lambda_0\sin\varphi_0
\end{bmatrix}
$$

The above relations (3) and (4) would then supply independent rotational constraints in Veis's model.

rev. 9/8/76

As the satellite positions X_j are only necessary "enroute" to the final least squares adjustment for X_1 , these "nuisance" parameters are eliminated from equation (2-13) to obtain the final normal equations for geometric mode as

$$NX_1 + U = 0 \qquad (2\text{-}14)$$

Then, expanding the equation (2-14) for any k^{th} ground stations, the 3 x 3 blocks in N and 3 x 1 blocks in U are as given as

$N_{kk} \equiv$ 3 X 3 diagonal block for k^{th} station

$$(2\text{-}15)$$

$$= (\sum_j a_{kj}^T p_{kj} a_{kj}) - \sum_j \{(a_{kj}^T p_{kj} a_{kj})(\sum_i a_{1j}^T p_{1j} a_{1j})^{-1}(a_{kj}^T p_{kj} a_{kj})\} + p_{x_k}$$

$N_{k1} \equiv$ 3 X 3 off-diagonal block for k^{th} station corresponding to 1th station

$$= - \sum_j \{(a_{kj}^T p_{kj} a_{kj})(\sum_i a_{1j}^T p_{1j} a_{1j})^{-1} a_{1j}^T p_{1j} a_{1j}\} \qquad (2\text{-}16)$$

$U_k \equiv$ 3 X 1 block for k^{th} station

$$= -(\sum_j a_{kj}^T p_{kj} w_{kj}) + \sum_j \{(a_{kj}^T p_{kj} w_{kj})(\sum_i a_{1j}^T p_{1j} a_{1j})^{-1} \sum_i (a_{1j}^T p_{1j} w_{1j})\} \quad (2\text{-}17)$$

In the above equations (2-13) to (2-17), the $\sum_i$ denotes the summation over all ground stations involved in any event and $\sum_j$ over all events observed observed by ground stations k and/or 1. Further, in equation (2-13), the weight matrix P_{X_j} for satellite positions X_j is set equal to zero as there is no independent external source to give a priori estimates for these positions.

(b) Short Arc Mode

Equation (2-10) is linearized by Taylor series as follows:

$$r_{1j} = r_{1j}^0 + \frac{\partial r_{1j}}{\partial (u_0, v_0, w_0, u_1, v_1, w_1, x_{t_0}, y_{t_0}, z_{t_0}, \dot{x}_{t_0}, \dot{y}_{t_0}, \dot{z}_{t_0})}$$

$$X (\Delta u_0, \Delta v_0, \Delta w_0, \Delta u_1, \Delta v_1, \Delta w_1, \ldots \Delta \dot{z}_{t_0})^T \qquad (2\text{-}18)$$

In the above equation, r_{ij}^0 is the computed value of the range based on the initially assumed values of coordinates for center of mass for earth, ground stations and given value of the state vector and can be given as

$$r_{ij}^0 = f\{(u_0)^{0'}, (v_0)^0, \ldots (\dot{y}_{t_0})^0, (\dot{z}_{t_0})^0, t\} \qquad (2\text{-}19)$$

where superscript " 0 " denotes assumed or approximate value of the unknown to be obtained through adjustment. If (u_j^0) , (v_j^0) , (w_j^0) , $(\dot{u}_j^0)$, $(\dot{v}_j^0)$, $(\dot{w}_j^0)$ denotes the earth-fixed state vector of the satellite as determined from the integrator (equations (2-3) and (2-6)) based on the approximate state vector, then the partial derivatives of r_{ij} can be expressed as follows:

$$\frac{\partial r_{ij}}{\partial (u_i, v_i, w_i)} = - \left[\{(u_j)^0 - (u_i)^0 \}/r_{ij}^0, \ \{(v_j)^0 - (v_i)^0 \}/r_{ij}^0, \right.$$
$$\left. \{(w_j)^0 - (w_i)^0 \}/r_{ij}^0 \right] \quad (2\text{-}20)$$

$$\frac{\partial r_{ij}}{\partial (u_0, v_0, w_0, x_{t_0}, \ldots, \dot{z}_{t_0})} = - \frac{\partial r_{ij}}{\partial (u_i, v_i, w_i)} \cdot M' \qquad (2\text{-}21)$$

where M' is given by equation (2-9). Also, the approximate value of $\dot{r}_{ij}$ is obtained as

$$\dot{r}_{ij}^0 = - \frac{\partial r_{ij}}{\partial (u_i, v_i, w_i)} \begin{bmatrix} (\dot{u}_j)^0 \\ (\dot{v}_j)^0 \\ (\dot{w}_j)^0 \end{bmatrix} \qquad (2\text{-}22)$$

The ranges r_{ij} so computed (corresponding to the observations) are then used to form the discrepancy vector ϵ as

$$\epsilon = r_{ij}^0 \text{ (computed)} - r_{ij}^b \text{ (observed)} \qquad (2\text{-}23)$$

24

and a least squares adjustment from the discrepancy vector ϵ gives a correct-ed earth-fixed initial state vector at time t_0. This state vector transformed to an inertial coordinate system * can then be used again in equation (2-3) to iterate.

In general, the short arc programs are written to cater both for raw data and preprocessed data. In cases where the observations have not been preprocessed, a number of corrections, e.g., propagation delay, interstation timing offset (or bias), tropospheric and ionospheric refraction, clock correct-ion, frequency offset, etc., are taken into account depending upon the ranging system used. In the present study, corrections not relevant for laser ranging system were suppressed by assuming extremely small variances (as input in SAGA) instead of zero values. This procedure is possible as corrections involved are also treated as parameters in SAGA.

2.2.2 Weight matrix

(a) Geometric Mode

Each of the topocentric range r_{ij} from ground station i to satellite position j was considered independent; and if $\sigma^2_{r_{ij}}$ is the variance of the ob-served range in meters squared, then the weight $p_{r_{ij}}$ is given as

$$p_{r_{ij}} = \sigma^2_0 / \sigma^2_{r_{ij}} \tag{2-24}$$

where σ^2_0 is the a priori variance of unit weight. Thus, this makes the weight matrix P (equation (2-12)) as diagonal containing all the independent weights $p_{r_{ij}}$ as in equation (2-24) above. Two values for $\sigma_{r_{ij}}$, viz., 2 cm and 10 cm, were used in this mode.

In order not to prefer any station or stations over any other station for a "free" adjustment with inner constraint, no weights were assigned to ground stations.

---

* The program SAGA also accepts initial state vector in earth-fixed system, but then the iteration converges slower.

25

(b) Short Arc Mode

Table 2-1 shows the various standard deviations adopted for different parameters for the short arc adjustment in the present study.

Table 2-1

Assumed Standard Deviation for Short Arc Adjustment

Parameter	Assumed Standard Deviation	Unit	Remarks
State Vector (i) coordinate (ii) velocity	100.0 0.1	m m/sec	for each component for each component
Observed Range	10.0	cm	

The weight matrix P for observations in this case also contained only diagonal terms. Other parameters like frequency bias, drift and offset, refraction bias, clock synchronization, etc. were not considered.

2.2.3 Constraints

(a) Geometric Mode

As the range measurements inherently define only the scale in a system, the normal matrix (equation (2-14)) would still need origin and orientation to be defined. In the present study, the definitions for origin and orientation were obtained through inner constraints [Rinner et al., 1969 ; Blaha, 1971a] which can be represented in matrix form as

$$CX_i = 0 \tag{2-25}$$

where

26

$$C \equiv \left[\begin{array}{c} C_{origin} \\ \hline C_{orientation} \end{array}\right]$$

$$= \left[\begin{array}{ccc|ccc|c|c|c} \multicolumn{3}{c|}{\begin{array}{c} I \\ 3 \times 3 \end{array}} & \multicolumn{3}{c|}{\begin{array}{c} I \\ 3 \times 3 \end{array}} & & & \\ \hline 0 & w_1^o & -v_1^o & 0 & w_2^o & -v_2^o & & & \\ -w_1^o & 0 & u_1^o & -w_2^o & 0 & u_2^o & & & \\ v_1^o & -u_1^o & 0 & v_2^o & -u_2^o & 0 & & & \end{array}\right] \tag{2-26}$$

The number of 3 x 3 blocks in the equation (2-26) is the same as the total number of unknown ground stations, and geometrically interpreting, the inner constraints (for origin and orientation) adjust the system preserving the mean position and mean orientation of the ground stations involved.

The resulting solution--where the trace of the variance-covariance matrix (equation (2-28)) for the unknowns would be minimum compared to any other solution--is termed "free." Also, from equations (2-14) and (2-26), the final normal equation takes the following form:

$$\left[\begin{array}{cc} N & C^T \\ C & 0 \end{array}\right] \left[\begin{array}{c} X_1 \\ -K \end{array}\right] + \left[\begin{array}{c} U \\ 0 \end{array}\right] - 0 \qquad\qquad \tag{2-27}$$

whence the a posteriori "weight coefficient" matrix Q   for the unknown X is given as [Blaha, 1971a]

$$Q_x = \{N + C^T [CC^T]^{-1} C\}^{-1} \{I - C^T [CC^T]^{-1} C\} = N^+ \tag{2-28}$$

where N^+ denotes the pseudo-inverse of the normal matrix N [Bjerhammar, 1973].

However, in order to investigate the recovery of motion at grid stations (Question C, Section 1.3), the three distant ground laser stations were assumed stationary. In such cases, the geometric mode solution was obtained by constraining the coordinates of these distant stations and holding them as fixed.

(b) Short Arc Mode

In this mode, despite the dynamical constraints inherent in the short arc model, the system still needs origin and orientation definitions for stability purposes. One of the ways to achieve such a definition is to constrain any six coordinates between three "distant" fundamental stations in the system.

In the preliminary investigation [Table 5.3-2, Mueller et al., 1975], it was found that these three fundamental.stations must be observed in all the satellite passes which are included for solution—failing which the system's recovery of relative positions between ground stations shows rapid decrease in accuracy.

In the present investigation as an experiment, three fundamental stations were moved "closer" to the station grid itself to abate the influence of unfavorable weather conditions. To achieve this, the solutions in short arc mode were also run with the three fundamental stations as part of the grid where the average distance between fundamental stations is only 80 to 250 km as compared with 1000 km in an earlier study [Mueller et al., 1975].

2.2.4 Critical configuration and estimable quantities

In the present experiment the effects of limiting critical degeneracies of the geometric mode [Blaha, 1971b] have been reduced or eliminated by

(i)   the extension of the station grid to 75 stations spread over a larger area with differential heights of up to 1555 meters as topographically permitted in central California,

(ii)   the suitable observational patterns or station grouping observed in any event,

(iii)   the selection of an elliptic satellite orbit varying in height from 370 – 930 km.

The above experimental design has shown significant improvement in the recovery of relative positions even in cases where no fundamental stations and/or airplane observations are included (Section 1.2, Table 1-1).

28

It has been discussed earlier (Section 2.2.3) that a ranging system when solved in a geometric mode yields a design matrix A which is less than full column rank due to lack of origin and orientation definition. However, a least squares solution using pseudo-inverse gives a unique solution (minimizing both $V^T PV$ and $X^T X$) of equation (2-14) as

$$X_i = -N^+ U \tag{2-29}$$

In such cases, one method of computing pseudo-inverse [Bjerhammar, 1973] is to border the singular matrix N ($-A^T A$) by columns and/or rows which are orthogonal to all columns and/or rows of the matrix N, i.e., the method of applying inner constraints as shown in equation (2-27). Grafarend and Schaffrin [1974] have shown that in such solutions through pseudo-inverses, the solution vector X_i does not satisfy the relation

$$E(X_i) \neq X_T \tag{2-30}$$

where $E(X_i)$ denotes the expected value of X_i and X_T the true value. In other words, the vector X_i does not yield estimable quantities.

If any transformation matrix R satisfies the following necessary and sufficient condition [Rao, 1973]

$$R\{I - (A^T A)^+ (A^T A)\} = 0 \tag{2-31}$$

then the vector X_i' ($=RX_i$) is a vector of estimable quantities. Further, applying the principle of propagation of errors [Uotila, 1967], the variance-covariance matrix of X_i' is given as follows:

$$\Sigma_{X_i'} = R \Sigma_{X_i} R^T = R(N^+) R^T \tag{2-32}$$

if the a posteriori variance of unit weight $(\hat{\sigma}_o^2)$ is equal to 1.

Thus, in the geometric "free" solutions for ranging system through inner constraints (as investigated in the present study), two such estimable

29

quantities, obtainable from nonestimable quantities X_i , i.e., ground station coordinates, are the station-to-station distances R_{ij} and the angles θ_{ijk} between stations, i, j (and k).

The chords R_{ij} , angle θ_{ijk} , $\sigma_{R_{ij}}$ and $\sigma_{\theta_{ijk}}$ are then obtainable from the following relations:

$$R_{ij} = \{\Delta_{x_{ij}}^2 + \Delta_{y_{ij}}^2 + \Delta_{z_{ij}}^2\}^{\frac{1}{2}} \tag{2-33}$$

$$\theta_{ijk} = \cos^{-1}[\{\Delta_{x_{ij}}\Delta_{x_{jk}} + \Delta_{y_{ij}}\Delta_{y_{jk}} + \Delta_{z_{ij}}\Delta_{z_{jk}}\}/R_{ij}R_{jk} \tag{2-34}$$

$$\sigma_{R_{ij}}^2 = G \, \Sigma_{X_{ij}} G' \tag{2-35}$$

$$\sigma_{\theta_{ijk}}^2 = H \, \Sigma_{X_{ijk}} H' \tag{2-36}$$

where

$X_i \equiv x_i, y_i, z_i$ --rectangular coordinates of station "i"

$\Delta_{x_{ij}} = x_i - x_j$ ____

$\Delta_{y_{ij}} = y_i - y_j$

$\Delta_{z_{ij}} = z_i - z_k$

$$\Sigma_{X_{ij}} = {}_6\begin{bmatrix} \Sigma_{X_i} & \vdots & \Sigma_{X_i X_j} \\ \hline \Sigma_{X_j X_i} & \vdots & \Sigma_{X_j} \end{bmatrix}_6$$

$$\Sigma_{X_{ijk}} = {}_9\begin{bmatrix} \Sigma_{X_i} & \vdots & \Sigma_{X_i X_j} & \vdots & \Sigma_{X_i X_k} \\ \hline \Sigma_{X_j X_i} & \vdots & \Sigma_{X_j} & \vdots & \Sigma_{X_j X_k} \\ \hline \Sigma_{X_k X_i} & \vdots & \Sigma_{X_k X_j} & \vdots & \Sigma_{X_k} \end{bmatrix}_9$$

$$G = \left[\frac{\partial R_{ij}}{\partial x_i} \quad \frac{\partial R_{ij}}{\partial y_i} \quad \frac{\partial R_{ij}}{\partial z_i} \quad \frac{\partial R_{ij}}{\partial x_j} \quad \frac{\partial R_{ij}}{\partial y_j} \quad \frac{\partial R_{ij}}{\partial z_j} \right]$$

$$H = \left[\frac{\partial \theta_{ijk}}{\partial x_i} \quad \frac{\partial \theta_{ijk}}{\partial y_i} \quad \frac{\partial \theta_{ijk}}{\partial z_i} \quad \frac{\partial \theta_{ijk}}{\partial x_j} \quad \cdots \quad \frac{\partial \theta_{ijk}}{\partial z_k} \right]$$

Here, the typical partial derivatives in matrices G and H are given as

$$\frac{\partial R_{ij}}{\partial x_i} = \Delta_{x_{ij}}/R_{ij}$$

$$\frac{\partial R_{ij}}{\partial x_j} = -\frac{\partial R_{ij}}{\partial x_i}$$

$$\frac{\partial \theta_{ijk}}{\partial x_i} = \frac{\sin \theta_{ijk}}{R_{ij}^2 \, R_{jk}} \left\{ R_{ij} \Delta_{x_{kj}} - \cos \theta_{ijk} R_{jk} \Delta_{x_{ij}} \right\}$$

$$\frac{\partial \theta_{ijk}}{\partial x_j} = \frac{\sin \theta_{ijk}}{R_{ij}^2 \, R_{jk}^2} \left\{ R_{ij} R_{jk} (2x_j - x_i - x_k) + \cos \theta_{ijk} (R_{jk}^2 \Delta_{x_{ij}} + R_{ij}^2 \Delta_{x_{kj}}) \right\}$$

2.2.5 Recovery of velocity vector

In order to recover the velocity vector (Section 2.2.3 (a)) for any grid station X_i, Figure 2-2 shows a simple schematic diagram depicting the procedure followed in the present study.

Here, in Figure 2-2 the recovery scheme has been broken into two main steps. First, at step IA and/or IB the recovery of station positions at different time epochs; and second, at step II the geodetic monitoring of velocity $\overline{V}_k$ of crustal motion between two time epochs as explained in the following paragraphs.

Let X_{t_0} represent the position vector for any grid station at any arbitrarily chosen time epoch t_0. Then, modeling (or simulating) the crustal motion, subsequent grid station locations at the following time epochs separated

31
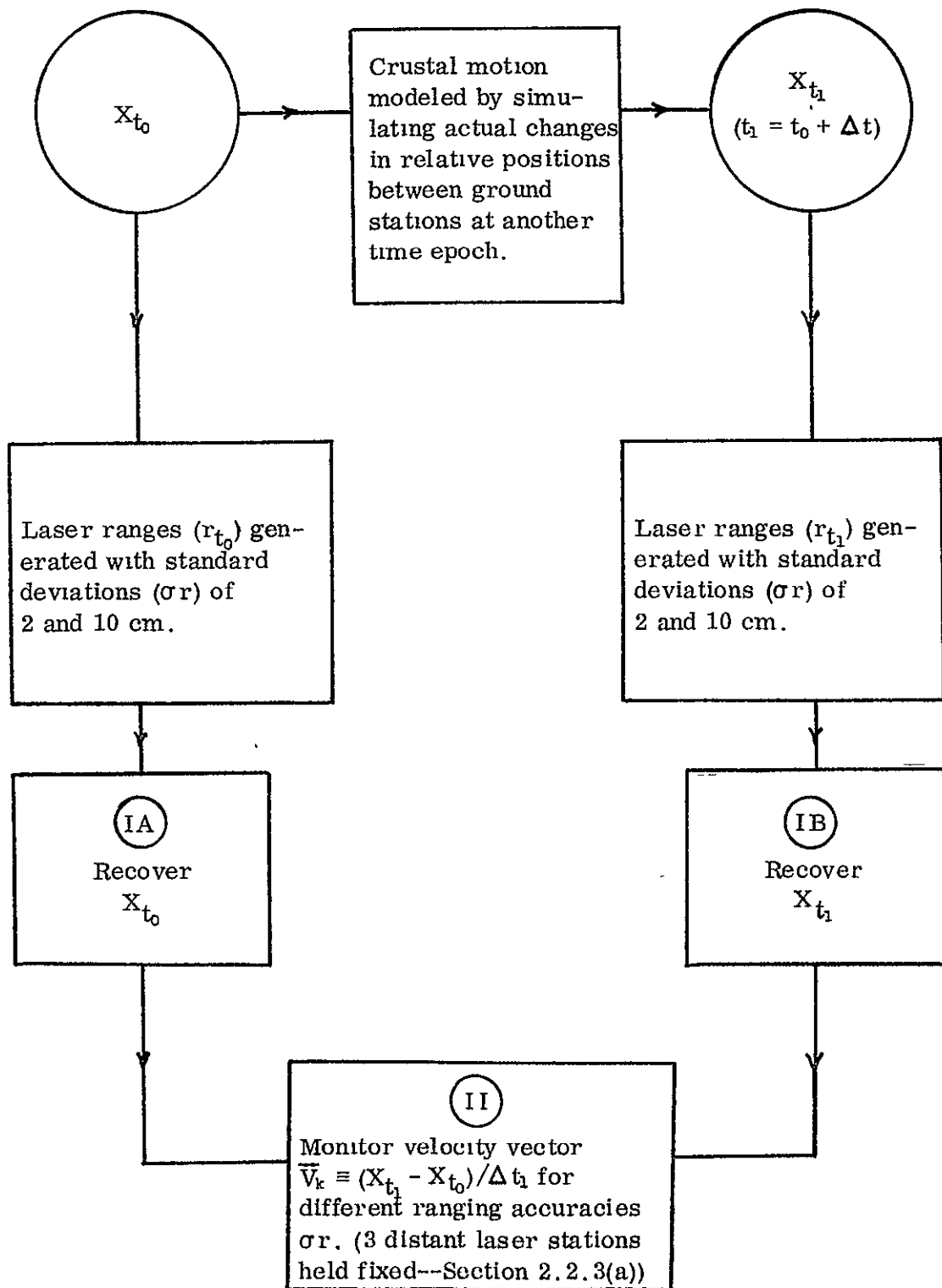
Figure 2-2   Schematic Diagram Showing Recovery of Station Positions
and Velocity Vectors

by any time interval Δt_k can be represented as X_{t_k} $(k = 1, 2, 3 \ldots)$ and the time interval is then defined as

$$\Delta t_k = t_k - t_{k-1} \qquad (2\text{-}37)$$

Now, if the position vectors for any grid stations can be recovered at any two successive time epochs, say t_{k-1} and t_k , then the velocity vector $\overline{V}_k$ of the crustal motion at that station can be modeled as

$$\overline{V}_k = \frac{X_{t_k} - X_{t_{k-1}}}{\Delta t_k} = \frac{\Delta X_k}{\Delta t_k} \qquad (2\text{-}38)$$

It is evident here that in practice it may not always be possible to set up the recovery procedure at "constant" time interval Δt. However, in the present simulation study this time interval Δt was set up as constant with a time interval of one year.

In the present investigation, step II was performed (with three distant laser stations held fixed--section 2.2.3 (a)) at two epochs t_0 and t_1 $(= t_0 + 12$ months) for 2 cm assumed standard deviation of laser ranging. The velocity vector $\overline{V}_1$ is then given as

$$\overline{V}_1 = (X_{t_1} - X_{t_0}) / \Delta_t \qquad (2\text{-}39)$$

The $\sigma_{\overline{V}_1}$ is then computed through error propagation [Uotila, 1967] from the following equation .

$$\sigma^2_{V_1} = G \, \Sigma_X \, G' \qquad (2\text{-}40)$$

where V_1 denotes the magnitude and

$$G = \left[\frac{\partial V_1}{\partial x_{t_1}} \quad \frac{\partial V_1}{\partial y_{t_1}} \quad \frac{\partial V_1}{\partial z_{t_1}} \quad \frac{\partial V_1}{\partial x_{t_0}} \quad \frac{\partial V_1}{\partial y_{t_0}} \quad \frac{\partial V_1}{\partial z_{t_0}} \right]$$

33

$$\Sigma_X = \begin{bmatrix} \Sigma X_{t_1} & 0 \\ 0 & \Sigma X_{t_0} \end{bmatrix}$$

A typical partial in G is given as

$$\frac{\partial V_1}{\partial x_{t_1}} = \frac{x_{t_1} - x_{t_0}}{V_1} \tag{2-41}$$

where

$$V_1 = \frac{\left\{ (x_{t_1} - x_{t_0})^2 + (y_{t_1} - y_{t_0})^2 + (z_{t_1} - z_{t_0})^2 \right\}^{\frac{1}{2}}}{\Delta t_1}$$

The three direction cosines A, B, and C are:

$$A = (x_{t_1} - x_{t_0}) / V_1 \tag{2-42}$$

$$B = (y_{t_1} - y_{t_0}) / V_1 \tag{2-43}$$

$$C = (z_{t_1} - z_{t_0}) / V_1 \tag{2-44}$$

Now

$$\sigma^2_{ABC} = H \Sigma_X H' \tag{2-45}$$

where

$$H = \begin{bmatrix} \dfrac{\partial A}{\partial x_{t_1}} & \dfrac{\partial A}{\partial y_{t_1}} & \dfrac{\partial A}{\partial z_{t_1}} & \dfrac{\partial A}{\partial x_{t_0}} & \dfrac{\partial A}{\partial y_{t_0}} & \dfrac{\partial A}{\partial z_{t_0}} \\[3mm] \dfrac{\partial B}{\partial x_{t_1}} & \dfrac{\partial B}{\partial y_{t_1}} & \dfrac{\partial B}{\partial z_{t_1}} & \dfrac{\partial B}{\partial x_{t_0}} & \dfrac{\partial B}{\partial y_{t_0}} & \dfrac{\partial B}{\partial z_{t_0}} \\[3mm] \dfrac{\partial C}{\partial x_{t_1}} & \dfrac{\partial C}{\partial y_{t_1}} & \dfrac{\partial C}{\partial z_{t_1}} & \dfrac{\partial C}{\partial x_{t_0}} & \dfrac{\partial C}{\partial y_{t_0}} & \dfrac{\partial C}{\partial z_{t_0}} \end{bmatrix}$$

34

Four typical partials in matrix H above are given as

$$\frac{\partial A}{\partial x_{t_1}} = \frac{\{(x_{t_1} - x_{t_0})^2 - V_1^2\}}{V_1^3} \tag{2-46}$$

$$\frac{\partial A}{\partial x_{t_0}} = -\frac{\partial A}{\partial x_{t_1}} \tag{2-47}$$

$$\frac{\partial A}{\partial y_{t_1}} = \frac{\{(x_{t_1} - x_{t_0})(y_{t_1} - y_{t_0})\}}{V_1^3} \tag{2-48}$$

$$\frac{\partial A}{\partial z_{t_1}} = \frac{\{(x_{t_1} - x_{t_0})(z_{t_1} - z_{t_0})\}}{V_1^3} \tag{2-49}$$

2.2.6 Recovery and statistical analysis

If $D_{R_{ij}}$ denotes the difference between the estimable quantity chord $\hat{R}_{ij}$ (obtainable from unbiased least squares estimator) and the actual R_{ij} between two grid stations "i" and "j", then

$$D_{R_{ij}} = \hat{R}_{ij} - R_{ij} \tag{2-50}$$

$$E(D_{R_{ij}}) = E(\hat{R}_{ij} - R_{ij})$$

$$= E(\hat{R}_{ij}) - E(R_{ij})$$

and using equation (2-30),

$$= R_{ij} - R_{ij}$$

$$= 0$$

Thus, in a design of experiment the deviation of $D_{R_{ij}}$ from its expected value can be interpreted to indicate the inherent limitations of that experi-

ment. These limitations themselves may be attributed to a particular source (or combination thereof) like lack of randomness in observational error, model deficiency, computational accuracy (obtainable through number of significant digits retained), truncation errors etc.

The importance of any simulation study also depends on the statistical analysis performed to determine and evaluate the chances for success (or failure) of the experiment, as specified in the investigation. Any statistical hypothesis leads itself to two alternatives and thus to two types of error:

(a) When the hypothesis is true, it would be an error to reject it. This type of error is called an α error, where α signifies some preassigned chance of rejecting the hypothesis.

(b) When the hypothesis is not true, a mistake in accepting it is called a β error.

Even though these two errors in any problem would not occur simultaneously, there is no way to determine which error, if either, is likely to be made. Controlling the chance of making the α error in any test, it would be most advantageous to have the chance of rejecting it (if the hypothesis is not true) to be as large as possible. This probability of rejecting a hypothesis is called the power of the test [Dixon and Massey, 1957] and is denoted in terms of $1-\beta$.

It may be pointed out here that declaring a hypothesis as not true implies the existence of some knowledge of alternative situations. In the current study, two such alternatives are whether any grid station in the fault zone shows some evidence of crustal movement or not. The risk of rejecting such evidence of any motion (when there has been an actual motion at any grid station) would be an α error at preassigned significance level (say 0.05). On the contrary, the chance of accepting such evidence of motion (when there has been no motion at all at the station) would involve a β error with an assigned power $1-\beta$ (say 0.80) or vice versa.

Using the above specification for α in the case of evidence of motion at a grid station, a two-sided test of the hypothesis $\mu = \overline{V}_1$, the critical region for any recovered velocity $\overline{V}_k$ with its standard deviation $\sigma_{\overline{V}_k}$ would be given as

$$\frac{\overline{V}_k - \overline{V}_1}{\sigma_{\overline{V}_k}} < -1.96 \quad \text{and} \quad \frac{\overline{V}_k - \overline{V}_1}{\sigma_{\overline{V}_k}} > 1.96 \qquad (2\text{-}51)$$

where $\overline{V}_1$ is true mean or theoretical velocity tested for the validity of the hypothesis at significance level $\alpha = 0.05$.

In the situation that the station has moved with a different velocity, i.e., $\mu = \overline{V}_1 + \Delta \overline{V}$, the computed quantity

$$d = \frac{(\overline{V}_1 + \Delta \overline{V}) - \overline{V}_1}{\sigma_{\overline{V}_k}} \qquad (2\text{-}52)$$

can be used to determine the power $1-\beta$ of rejecting the above hypothesis $\mu = \overline{V}_1$. Alternatively, the power $1-\beta$ can be preassigned at a large value (say 0.80). In such a case, from Table A-12b [Dixon and Massey, 1957] the value of d for power $1-\beta$ equal to 0.80 is 2.802 (for degree of freedom $>$ 36), and this value can then be used to evaluate $\Delta \overline{V}$ -- the limiting value at which the hypothesis (equation 2-52) can be rejected at the preassigned power. Similar test would apply for the case when any grid station shows evidence of no motion in the fault zone.

In the above statistical analysis, the equality of variance-covariance matrices at epoch t_0 and t_1 is inherently assumed. The hypothesis

$$H_0 \; : \; \Sigma_{X_{t_1}} = \Sigma_{X_{t_0}}$$

of the p-dimensional normal populations $N(\mu_i , \sigma_i)$ can be tested against the alternative

$$H_1 \; : \; \Sigma_{X_{t_1}} \neq \Sigma_{X_{t_0}}$$

through a test as suggested by G.E.P. Box in 1950 [Winer, 1962].

2.3 Data Generation

In the earlier study (Section 1.2), the investigations were carried out with three satellites in near circular ($e = 0.001$) polar orbits with altitudes between 392 km and 1007 km. However, in the current study the separation in vehicle heights was obtained by suitably selecting an eccentric ($e = 0.04$) orbit which more or less combined the altitude separation of the three orbits of the earlier study into one orbit (Table 2-2).

Also in one of the observations it was found that the recovery of east-west relative positions between grid stations (i.e., where the distance under consideration lay more or less perpendicular to the polar orbit) showed an abrupt deterioration compared to other chord distances. To avoid such a situation to happen again, the satellite orbit in the present case was also modified to 110° inclination (Table 2-2) to produce a mesh-like coverage over

Table 2-2

General Information for Satellite Orbit

Perigee Height	370 km
Apogee Height	930 km
Period	97 72 min
Inclination	110°
Eccentricity	0.04
Length of Long Arc	168 hrs
Available Short Arcs Over the Designated Area	21
Observational Time Span	Nov. 1, 1972 ($0^h 0$) to Nov. 8, 1972 ($0^h 0$)
Geopotential Model	GEM 6 (Degree and Order 15)
Atmospheric Density Model	Modified Harris-Priester

the study area (Figure 2-3).

Details of generated orbit, both long arc and short arcs, airplane flights, simulation of ranges and associated precision and accuracy of generated ranges are presented in the following sub-paragraphs:
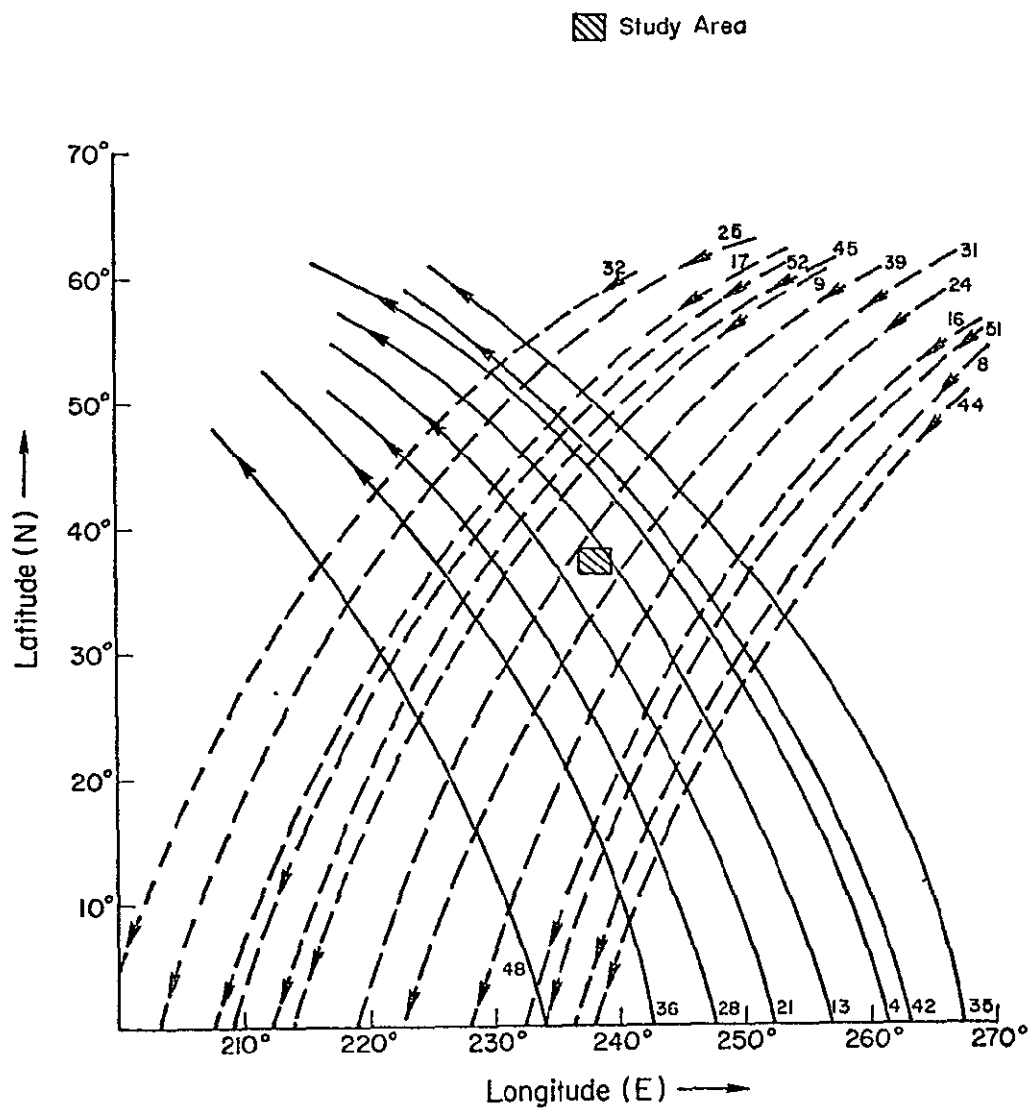
Figure 2-3.   Satellite Passes and General Coverage

2.3.1 Orbit setup

(1) Satellite Case

Table 2-2 and Figure 2-3 give the general information and the coverage about the satellite orbit selected. The solid and broken lines show passes from southeast to northwest and from northeast to southwest respectively.

To generate suitable short arcs over the selected study area with a dense distribution of satellite points from where the grid stations can be observed, the orbit generation was carried out in the following two steps.

A. Long arc. In view of the nonvisibility of the specified small study area from most of the satellite orbit, long arc over 168 hours was used only to select satellite positions in the complete arc where the satellite would be able to observe for the first time the designated grid stations. This requirement allowed the generation of the long arc with relaxed specifications, viz., with a potential field of degree and order 8; integration step size of 300 seconds; no polar motion, drag and solar radiation; and sparse density of satellite points every two minutes apart (in time).

The long arc was generated in True of Date (TOD) system using the Goddard Trajectory Determination System (GTDS) program (Appendix A).

B. Short arcs. From the above long arc, the portions were sorted out when the satellite in each such portion was over the study area under consideration. The "starting" satellite position coordinates for each over-pass were then used as input into GTDS program to generate short arcs to the positions where the satellite would not be able to see the grid stations.

In generating these short arcs, all possible/permissible refinements as available in GTDS, e.g., inclusion of the geopotential model GEM 6 [Lerch et al., 1974] up to degree and order 15, solar radiation and air drag effects, polar motion, luni-solar perturbations, etc., were utilized to simulate the orbit as near to reality as possible.

An extremely dense distribution of satellite points ($\Delta t = 1.0$ sec) over the selected area were generated (Figure 2-3). In the present simula-

40

tion only 21 passes were visible during a time frame of seven days, namely ,
4, 8, 9, 13, 16, 17, 21, 24, 25, 28, 31, 32, 35, 36, 39, 42, 44, 45, 48, 51,
and 52. These passes were then designated as (S) for reference purposes in
this report.

Further, the integration step size was also reduced to 1.0 sec in place
of default value of 24.0 sec used in GTDS so as to be compatible with the
desired density of satellite points and to increase the accuracy of the integrated
short arcs. All short arcs were generated in earth-fixed coordinate system.

In the present study it was noticed that the orbit generation program
GTDS (Appendix A) uses Atomic Time (UTC) in its orbit integration while the
input time for SAGA (Appendix B) is in Universal Time (UT1). Thus in order
to minimize the effect due to the difference between the above two inherited
time systems in the two main programs used in the present investigation, the
observational time span for orbit generation (Table 2-2) was selected in
November, 1972, when the time difference (UT1 - UTC) was minimum, i.e.,
less than 12 msec [Bureau International de L'Heure (BIH), 1973].

(2) Airplane Case

For the airplane case (designated as A in this report), the coverage
was retained from south to north as in the earlier study and the approximate
longitudinal spacing between any two consecutive flights was $0.^{o}05$. In all, 40
airplane flights were simulated. To cater for various densities of satellite
positions which may be needed in different solutions, the data points along the
airplane flights (A) were generated at $0.^{s}05$ interval.

It may be pointed out here that the above satellite orbit and airplane
flights setup provided the short arcs (S) to lie either northeast-southwest or
southeast-northwest configuration and the flights (A) in south-north direction
and thus this arrangement avoided the situation when all the data was more or
less along north-south setup [Mueller et al., 1975]. Table 2-3 gives a few
important details about the satellite short arcs and airplane flights and density
of satellite/airplane positions along any arc or flight per second of time.

Table 2-3

Generation Details for Short Arcs/Flights and Satellite Positions

Type of Short Arcs/ Flights	Height of Vehicle (km)	No. of Short Arcs/ Flights	Average Length of Each Short Arc/ Flight (in time)	Density of Satellite Position per second (in time)
Airplane (A)	10	40	30 sec	20
Satellite (S)	650[1]	21	15 min	1

[1]Average height--Refer Table 2-2 also.

2.3.2 Precision and accuracy of generated ranges

The ranges which have been utilized in the present experiment were considered to be free of systematic errors and generated with a Gaussian noise only.

It is reported that the next generation of satellite laser ranging system [Byrns and Cooke, 1975] is expected to be capable of ranging to low orbit and synchronous orbit satellites with 2 cm accuracy and precision. The above accuracy, with system modifications, may also be possible in the time scale of three to five years when the proposed satellite-borne ranging system becomes operational. This significant (and possible) improvement in accuracy of the system was taken into consideration while selecting the Gaussian noise level for range generation. Two different noises at one sigma level, viz., 2 cm and 10 cm, have been utilized in this study.

2.4 Data Reduction and Computations

2.4.1 Adjustment of data

(a) Geometric Mode

The simulated ranges under this mode are processed event-wise by The Ohio State University Geometric and Orbital (Adjustment) Program (OSUGOP) for Satellite Observations (Appendix C).

42

The OSUGOP requires observations in grouping by events. Since in geometric mode the time of an observation does not enter the computations, the time associated with an observation is used by the program to distinguish two events. The computer program allows a deviation of 0.0002 sec between different observations in an event. Thus, as and when the time of a new observation differs more than 0.0002 sec from the time of the previous observation, the program treats the new observation as part of the next event. In the present version of the program, an event is deleted whenever the number of stations observed in the event is less than four.

As the contribution from each new event is computed, the requisite blocks (equations (2-15), (2-16), and (2-17)) are formed and algebraically added to the normal equation matrices N and U. At the end of observational data, the contribution from the inner constraints (Section 2.2.3) is taken into account to obtain the final reduced normal equation.

(b) Short Arc Mode

In this mode of adjustment the simulated ranges are subjected to adjustment in Short Arc Geodetic Adjustment (SAGA) Program (Appendix B).

SAGA requires nonsimultaneous (sequential) range observations sorted out for a subset of ground stations observed in any given pass. At the same time when data is being read, appropriate constraints on ground station coordinates, state vector and other error model terms, as applicable for the problem under consideration, are also exercised. With reinitialization of error model coefficients, each observed station from the subset can introduce as many as seventeen new parameters peculiar to any pass—a patterned system of normal equations which grows in dimension both with the number of passes processed and number of parameters exercised on each pass.

In view of the above, SAGA employs second-order partitioned regression [Brown and Trotter, 1969] which then allows processing of an arbitrarily large number of passes. In this method, the parameters are arranged in the form :

13

(a) parameters common to solution (N),

(b) parameters common to different passes ($\dot{N}_i$, i = 1, 2, ..., n), and

(c) parameters pertaining to any particular pass ($\ddot{N}_{ij}$, j = 1, 2, ...,

m) where n and m denote the number of passes and the number of parameters in any pass respectively.

Parameters Related to Passes

Parameters Common to Solution	1st Pass				2nd Pass			3rd Pass		
$\sum\limits_{i=1}^{n} N_i$	$\overline{N}_1$	$\overline{N}_{11}$	$\overline{N}_{12}$		$\overline{N}_2$	$\overline{N}_{21}$		$\overline{N}_3$	$\overline{N}_{31}$	pass no.1 (i = 1)
$\overline{N}_1^T$	$\dot{N}_1$	$\overline{N}_{11}$	$\overline{N}_{12}$							
$\overline{N}_{11}^T$	$\overline{N}_{11}^T$	$\ddot{N}_{11}$								
$\overline{N}_{12}^T$	$\overline{N}_{12}^T$		$\ddot{N}_{12}$							
										pass no.2 (i = 2)
$\overline{N}_2^T$					N_2	$\overline{N}_{21}$				
$\overline{N}_{21}^T$					$\overline{N}_{21}^T$	$\ddot{N}_{21}$				
										pass no.3 (i = 3)
$\overline{N}_3^T$								$\dot{N}_3$	$\overline{N}_{31}$	
$\overline{N}_{31}^T$								$\overline{N}_{31}^T$	$\ddot{N}_{31}$	

Figure 2-4. Second-Order Partitioned Regression Setup for
Normal Matrix N (Arranged Pass-wise)

This order of arrangement of parameters then gives rise to a normal matrix of the form shown in Figure 2-4. If the normal matrix N is rearranged for three groups of parameters, then the setup would look as given in Figure

44

2-5. Then, the arrangement in Figure 2-5 for a second-order system takes the form of double application of the reduction of a first-order system.

Parameters Common to Solution	Parameters Common to Various Passes					Parameters Related to Different Passes			
$\sum_{i=1}^{n} N_i$	$\bar{N}_1$	$\bar{N}_2$	$\bar{N}_3$		$\bar{N}_n$	N_{11}	N_{22}	N_{33}	
$\bar{N}_1^T$	$\dot{\bar{N}}_1$					$\bar{N}_{11}$			
$\bar{N}_2^T$		$\dot{\bar{N}}_2$					$\bar{N}_{22}$		
$\bar{N}_3^T$			$\dot{N}_3$					$\bar{N}_{33}$	
$\bar{N}_n^T$					$\dot{N}_n$				
$\bar{N}_{11}^T$	$\ddot{\bar{N}}_{11}$					$\ddot{N}_{11}$			
		$\bar{N}_{22}^T$					$\ddot{N}_{22}$		
			$\bar{N}_{33}^T$					$\ddot{N}_{33}$	

Figure 2-5   Second-Order Partitioned Regression Setup for Normal Matrix N (Arranged Parameter-wise)

3. EXPERIMENTAL SETUP

3.1 Selection of Stations

3.1.1 Grid stations

A grid of 75 stations was laid over the San Andreas and Calaveras Faults in central California running about 75 km northwest and southeast of the junction of these faults located east of Monterey, California (Figure 3-1).

The grid points were located at existing geological survey stations of the National Center for Earthquake Research (NCER) wherever possible, while attempting to maintain a station separation of 5 -30 km maximum with roughly half of them on either side of the faults. A somewhat more dense network of stations has been located around the fault intersection east of Monterey for obvious reasons. The fault lines are shown in gross locations since the intricate structure is not required for this experiment.

When it was necessary to add new stations, an attempt was made to locate them conveniently at points that were readily definable in terms of latitude, longitude, and elevation while ensuring that opposing stations are far enough removed so as to be decidedly on opposite sides of a particular fault but close enough to the fault to register the desired relative crustal motion.

In order to study the capability of an active satellite-borne measurement system in recovering the relative position in an extremely dense network, stations 1021 to 1030 were replaced by an "alternate" grid of one-minute interval in latitude and longitude (Figure 3-1, insert) while retaining all other 68 stations at their original locations.

Table 3-1 is a tabulation of the grid points with numerals refering to an arbitrary numbering system. Stations identified by a three-letter code or

46
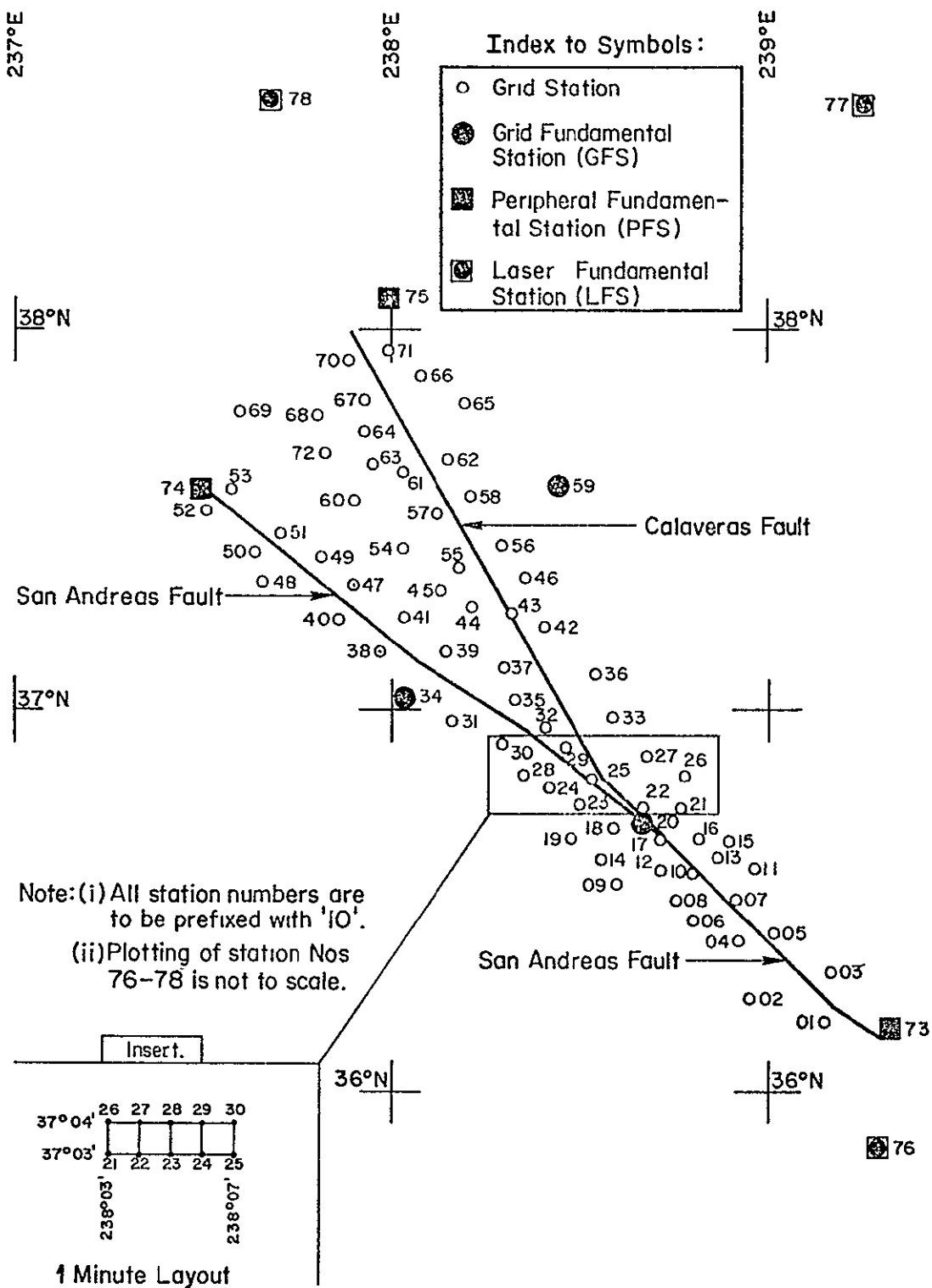
Figure 3-1   Grid and Fundamental Stations Layout

Table 3-1

Geodetic Coordinates of the 75-Station Grid and 3 Laser Stations[1]

at Epoch t_0

(Ellipsoidal Parameters[2]: a = 6378142 .0 m, 1/f = 298.25)

Station No.	Station Name	Geodetic Coordinates			Crustal Motion Zone[3]
		Latitude	Longitude	Height (m)	
1001	STN NO. 1001	36° 10′ 55.″200	239° 9′ 30.″200	10.0	III
1002	LDR	36 14 47.400	238 57 27.000	308.0	III
1003	GEOD	36 18 45.000	239 10 30.000	1367.0	I
1004	STN NO. 1004	36 23 45.000	238 55 30.000	305.0	III
1005	STN NO. 1005	36 25 0.0	239 1 12.000	832.0	I
1006	GEOD	36 26 54.000	738 49 18.000	1007.0	III
1007	BEN	36 30 36.000	238 55 28.200	448.0	I
1008	STN NO. 1008	36 30 30.000	738 45 54.000	757.0	III
1009	JHC	36 32 49.200	238 36 28.200	207.0	III
1010	BVL	36 34 30.600	238 48 39.600	510.0	III
1011	BGM	36 35 28.800	238 58 28.800	1217.0	I
1012	STN NO. 1012	36 35 6.000	238 43 15.000	914.0	III
1013	STN NO. 1013	36 36 54.000	238 52 30.000	607.0	I
1014	STN NO. 1014	36 36 45.000	238 34 6.000	607.0	III
1015	EMM	36 39 40.800	238 54 14.400	488.0	I
1016	EKH	36 39 52.800	238 49 33.000	342.0	I
1017	LWR	36 39 57.600	238 43 38.400	232.0	III
1018	STN NO. 1018	36 41 45.000	238 35 48.000	1003.0	III
1019	SRS	36 40 6.600	238 28 52.200	399.0	III
1020	CNR	36 42 33.000	238 39 24.000	305.0	III
1021	GEOD	36 44 42.000	238 46 45.000	697.0	I
1022	STN NO. 1022	36 44 48.000	238 40 30.000	257.0	I
1023	FRP	36 45 13.200	238 30 34.200	705.0	III
1024	SJG	36 47 52.800	238 25 34.200	171.0	III
1025	STN NO. 1025	36 48 15.000	238 33 0.0	305.0	II
1026	QSR	36 50 1.200	238 47 14.400	536.0	I
1027	LTR	36 53 4.200	238 41 30.600	183.0	I
1028	DIL	36 50 7.200	238 21 33.400	204.0	III
1029	STN NO. 1029	36 54 24.000	238 28 30.000	361.0	II
1030	STN NO. 1030	36 55 4.000	238 17 59.200	151.0	III
1031	PLV	36 58 37.200	238 10 4.200	158.0	III
1032	CHR	36 57 27.600	238 24 59.400	241.0	II
1033	FEL	36 59 0.0	238 35 54.600	323.0	I
1034	STN NO. 1034	37 2 36.000	238 2 15.000	973.0	III
1035	STN NO. 1035	37 1 58.800	238 20 6.600	11.0	II
1036	GHS	37 5 45.000	238 33 10.200	778.0	I

[1] Refer Section 1.2.

[2] [Mueller et al., 1973]

[3] Refer Figure 3-2.

48

Table 3-1 (cont'd)

Station No.	Station Name	Geodetic Coordinates			Crustal Motion Zone[3]
		Latitude	Longitude	Height (m)	
1037	CBO	37° 6' 42.600	238° 18' 40.200	192.0	II
1038	BCP	37 9 37.200	237 58 25.800	660.0	III
1039	ALM	37 9 30.000	238 9 10.800	244.0	II
1040	CRC	37 14 30.000	237 52 10.800	607.0	III
1041	STN NO. 1041	37 13 48.800	238 2 51.200	0.0	II
1042	STN NO. 1042	37 13 24.000	238 24 48.000	610.0	I
1043	COE	37 15 27.600	238 19 39.000	366.0	I
1044	SVC	37 17 6.600	238 13 39.000	128.0	II
1045	STN NO. 1045	37 19 5.500	238 8 21.300	456.0	I
1046	GEOD	37 20 48.000	238 22 0.0	1219.0	I
1047	STJ	37 20 1.800	237 54 31.200	122.0	II
1048	BGH	37 20 31.200	237 39 39.600	158.0	III
1049	SFT	37 24 19.800	237 49 27.000	143.0	II
1050	STN NO. 1050	37 25 18.000	237 38 42.000	641.0	III
1051	STN NO. 1051	37 27 48.000	237 43 6.000	61.0	I
1052	STN NO. 1052	37 31 42.000	237 31 6.000	132.0	III
1053	SAC	37 34 57.000	237 34 58.200	207.0	II
1054	STN NO. 1054	37 25 49.900	238 2 17.700	200.0	II
1055	STN NO. 1055	37 22 46.600	238 11 12.400	1555.0	II
1056	STN NO. 1056	37 26 18.000	238 18 0.0	1204.0	I
1057	MSJ	37 31 15.000	238 7 46.200	498.0	II
1058	STN NO. 1058	37 33 58.600	238 13 0.0	17.0	I
1059	MNR	37 35 40.800	238 21 46.800	500.0	I
1060	-CYH	37 33 32.400	237 54 22.800	38.0	II
1061	PAL	37 37 52.800	238 2 34.800	463.0	I
1062	STN NO. 1062	37 39 55.500	238 9 30.500	123.0	I
1063	CSH	37 38 52.800	237 57 25.800	170.0	II
1064	LCH	37 44 16.800	237 56 10.200	312.0	II
1065	MOR	37 48 40.800	238 11 45.000	792.0	I
1066	MDC	37 52 54.000	238 5 9.000	1173.0	I
1067	BOL	37 48 58.200	237 56 16.800	610.0	II
1068	MIL	37 46 52.800	237 49 27.000	90.0	II
1069	SFR	37 47 16.800	237 36 37.800	8.0	II
1070	BWR	37 55 27.000	237 53 36.000	221.0	II
1071	STN NO. 1071	37 57 0.0	237 59 24.000	313.0	I
1072	STN NO. 1072	37 41 0.0	237 50 0.0	6.0	II
1073	STN NO. 1073	36 10 0.0	239 20 0.0	0.0	I
1074	STN NO. 1074	37 35 0.0	237 30 0.0	0.0	III
1075	STN NO. 1075	38 5 0.0	238 0 0.0	0.0	I
1076	STN NO. 1076	33 0 0.0	243 0 0.0	0.0	
1077	STN NO. 1077	42 0 0.0	248 0 0.0	0.0	
1078	STN NO. 1078	40 0 0.0	239 0 0.0	0.0	

labelled "Geod" are existing National Center for Earthquake Research (NCER) seismograph and geodimeter stations respectively [Greensfelder, 1972; Bufe et al., 1975]. Those points with identification "Station No. ..." are nonexisting new stations which have been added to the grid. This table also contains the coordinates of the three distant ground laser station sites at San Diego, Bear Lake, and Quincy (Section 1.2), numbered from 1076 through 1078.

3.1.2 Fundamental stations

In the earlier study (Section 1.2) the importance and necessity of three distant "fundamental" stations outside the nine-station grid area was established for inclusion in the system.

However, as the present simulation extends over a large area (Figure 3-1), it was felt that it may be possible to select fundamental stations from the grid itself. Thus, three alternate methods of selecting fundamental stations were chosen:

(a) Laser Fundamental Stations (LFS)--In this choice the three distant ground laser stations (Nos. 1076, 1077, 1078) were retained at their original sites as used in the preliminary study (Figure 1-4). The locations of these fundamental stations are shown by the symbol ▓ in Figure 3-1 and to accommodate them in the figure their positional plotting is not to scale.

(b) Peripheral Fundamental Stations (PFS)--In this case three grid stations (Nos. 1073, 1074, and 1075) were selected at the periphery of the area covered by the station grid under consideration. These stations are shown by the symbol ▓ in Figure 3-1.

(c) Grid Fundamental Stations (GFS)--Here three grid stations (Nos. 1020, 1034, and 1059) were selected within the grid suitably located at the three vertices of a more or less equilateral triangle. These stations are shown by the symbol ● in Figure 3-1.

It may be noted here that the likelihood of having more or less favorable weather conditions at three PFS and the 72 grid station(s) might be just as

50

stringent (with the increase in the area covered by the grid) as in the former case of three "distant" LFS and nine grid station(s) (Section 1.2).

3.2 Crustal Motion Simulation

A number of papers on crustal motion in the San Andreas fault zone are available [Whitten, 1967a and b; Whitten, 1973; Holdahl, 1973; Greensfelder, 1972; Savage and Buford, 1970 and 1973; Meade, 1971 and 1973; Scholz et al., 1969; Turcotte and Spence, 1974; Rodgers, 1975; Brown, 1975] assigning either a linear or nonlinear model with respect to time or various drift rates in the area. However, for this study the crustal motion was modeled in the fault zone through a constant drift rate by creating changes in the relative positions of the grid stations.

Thus, for this purpose the area was subdivided into three sections (Figure 3-2) and the areas associated with individual grid stations are indicated in column 6 of Table 3-1. The stations in area I, east of Calaveras fault, were considered to be moving in a southeasterly direction with an annual rate of -1 marcsec in latitude and 1 marcsec in longitude. The stations in area II, between Calaveras and San Andreas faults, were assumed to be stationary, while stations in area III, west of San Andreas fault, were considered to be moving in a northwesterly direction with an annual rate of 1 marcsec in latitude and -1 marcsec in longitude. The above rate of motion represents about 3 cm per year drift in latitudinal and longitudinal directions or about 4 cm total horizontal motion per year. The station positions at epochs t_0 and t_1 (= t_0 + 12 mos.) were designated as CM00 and CM12 for reference purposes in this report.

3.3 Weather Effect Modeling

To simulate weather effects for landmarks or grid stations on a satellite pass over the area, the requirements placed upon any active satellite ranging system for a sighting of specific landmark(s) will result in one of two possible events:

(1) If the sighting is successful, then the ranging system continues with a prescribed sighting procedure, and

51
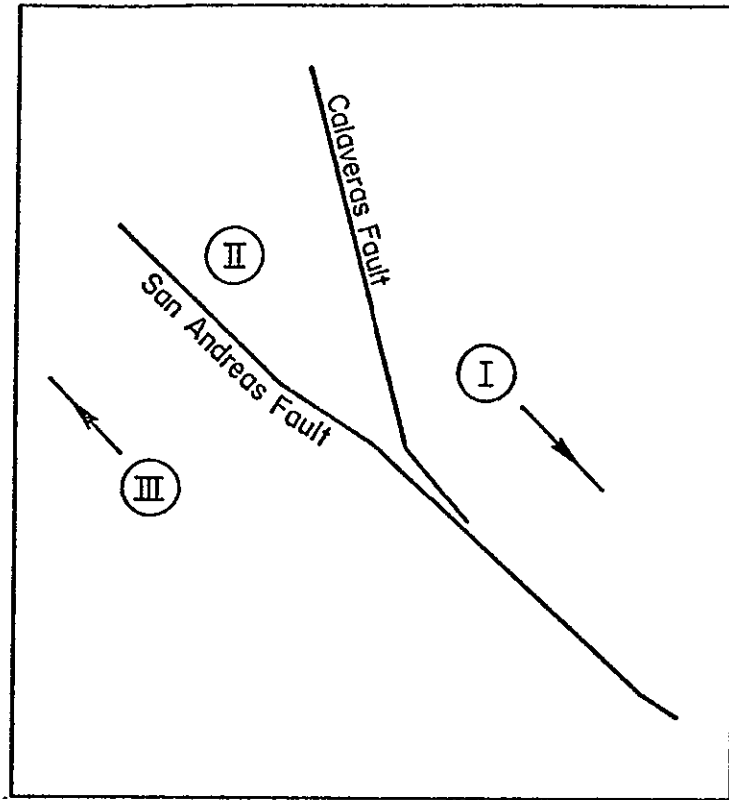
Figure 3-2.   Simplified Crustal Motion Pattern

(2) If the sighting is unsuccessful, because of weather obscuring the landmark, the system reorients the sighting mechanism for a try on the next landmark.

These events, consisting of a group of sightings for the geometric mode or individual sightings for the short arc mode, would require a different but predictable amount of time.   In the present state of operation of a laser system, each landmark scanning may take as small as 1 msec of "dwell" time allowing an acquisition out to 150 km [Wyman, 1970;personal communication, 1975]. During this time of acquisition and sighting, the spacecraft will have traveled over a certain distance along its orbit, and may have passed over a certain number of other landmarks, especially in a close and dense network, that cannot be used.

In studying the cloud cover distributions and adverse weather effects in the current investigation, two extensive simulation studies [Sheer et al., 1968; Daniels, 1973] were utilized. In the study [Sherr et al., 1968], the following questions were investigated:

(i) How many passes are required to give a probability of 95% (or some other level) of at least one clear pass over an area of about 500 km x 500 km?

(ii) If the number of passes required to reasonably assure one clear pass is excessive, what is the amount of pieced-together coverage expected in N passes?

(iii) How many passes are required to give a 90% (or some other level) probability that at least 90% (or some other fraction) of the area can be photographed?

To answer the above questions the study [Sherr et al., 1968] assumes that the cloud coverage is "randomly" scattered and probability distribution of piece-wise sighting (which includes total sighting) is a function of the number of passes of any satellite. In a simulation study covering an area of about 500 km x 500 km which assumes that favorable total sighting occurs every three days and in which the cloud distribution for the study area was generated from the spatial data, a number as an answer to question (i) above was that 28 passes must be programmed to provide 95% probability of encountering clear skies.

Further, Table 3-2 and Figure 3-3, reproduced from the above-quoted study, show the estimate of most probable coverage and probability of photographing a given percentage of the above-quoted target area respectively.

In the more recent study [Brown and Jayroe, 1973] carried out over a comparatively more cloudy section of the earth, the results obtained were more conservative. The results are made available in the following two forms. First, the satellite pass number and the probability of success were considered

Table 3-2

Most Probable Photographic Coverage
[Sherr et al., 1968]

No. of Passes:	1	2	3	4	5	6	7 or more
% Coverage:	55	75	88	94	97	99	100
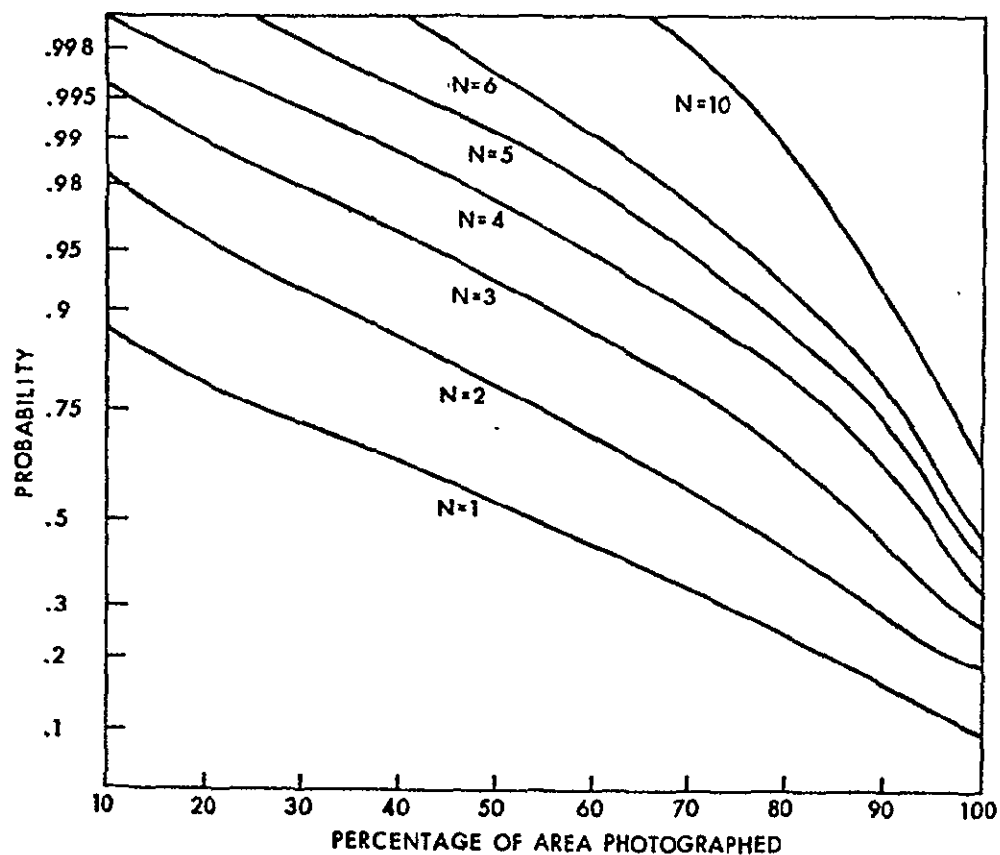
Figure 3-3. Probability of Photographing a Given
Percentage of a Target Area [Sherr
et al., 1968]

54

variable with the successful sighting of the required percentage coverage of the target area fixed. The plot in Figure 3-4 taken from this study gives the
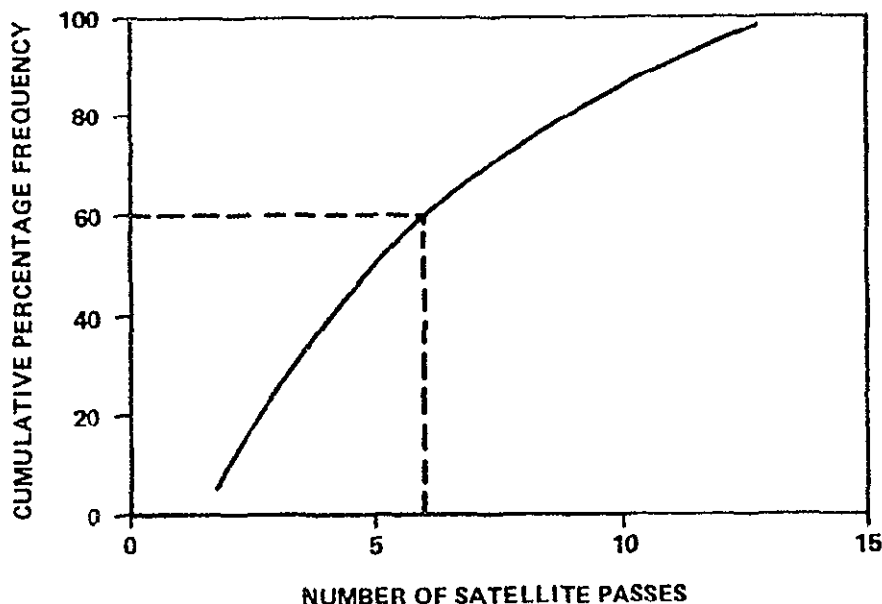
Figure 3-4. Probability of 95% Photographic Coverage of
Target Area [Brown and Jayroe, 1973]

probability of success versus the pass number, if 95% sighting coverage of the target area is needed, and shows that there is a 60% chance of sighting 95% target area in six satellite passes.

Second, the pass number is fixed while the percentage coverage of area sighted and the chance of success are treated variables. The plot in Figure 3-5 shows that after eight satellite passes there is a 60% chance of sighting 90% of the target area. Further, based on the statistics obtained from three study areas [Brown and Jayroe, 1973], 21 passes are required to be 95% confident of acquiring 95% of the target area (Figure 3-6). Figure 3-7 indicates that after ten passes there is 90% chance of covering 76% of the target area.

Compared to the area investigated by Brown and Jayroe [1973], the fault area in the present study is comparatively "cloud free" [Sherr et al.,
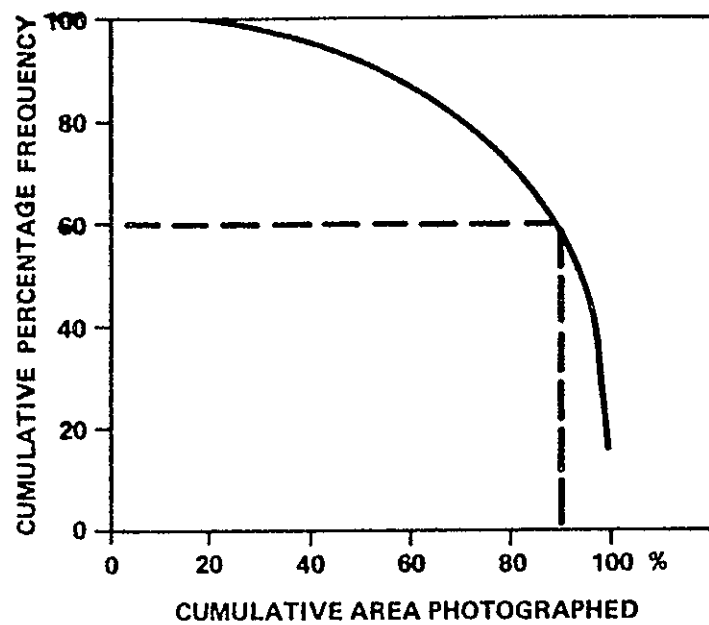
Figure 3-5   Photographic Coverage of Target Area After Eight
Satellite Passes [Brown and Jayroe, 1973]
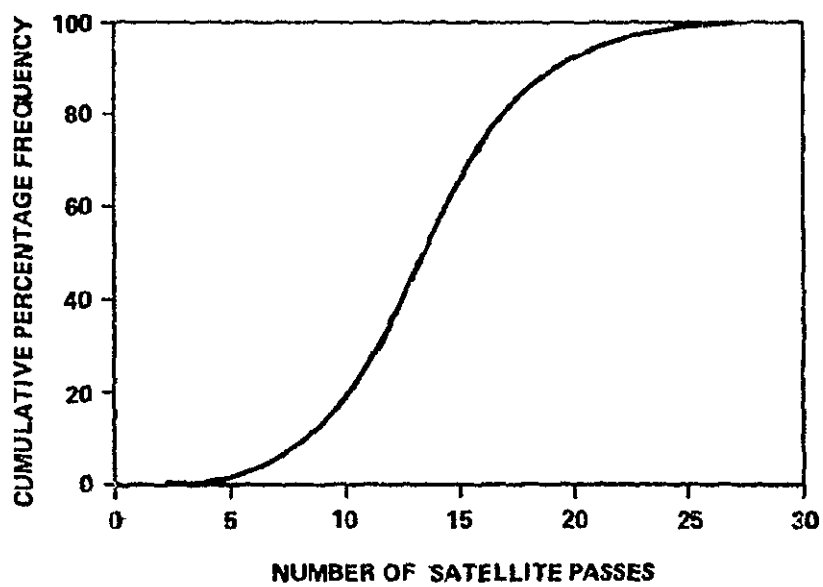
Figure 3-6   Analysis of at Least 95% Photographic Coverage
[Brown and Jayroe, 1973]
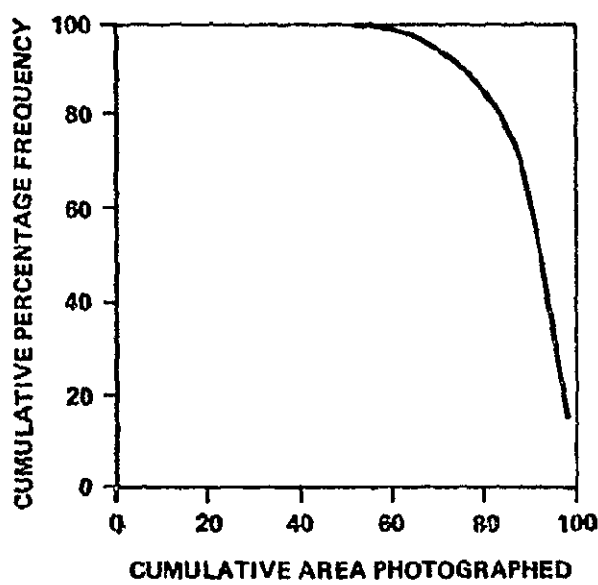
Figure 3-7   Analysis of Photographic Coverage After Ten Passes
[Brown and Jayroe, 1973]

57

1968]. This would imply that here the above statistical figures would be on the conservative side.

In addition, the study [Sherr et al., 1968] assigned a probability of sighting a landmark in a region depending upon the amount of cloudiness generally prevailing in that region. To achieve this, the clouds were classified in four groups, from clear in group 1 to mostly cloudy in group 4. For group 1 the probability of sighting a landmark was 95% which was decreased to 4% in group 4.

From the above perusal, it was assumed in the present investigation that 21 satellite passes would be sufficient for simulating the required data to cover the study area. To model the weather effect and study the resulting pattern with respect to visibility of a station from the satellite, the following procedure was adopted:

(a) The visibility from the satellite (or the participation of any station in any observation) is determined through a probability factor (PF).

(b) PF = 1 for any station signifies the participation of that station in any observation.

(c) PF < 1 for any station signifies that that station may or may not be able to participate in any observation.

In case (c), the computer generates a uniformly distributed random real number between 0.0 and 1.0 for each station sighting and if this random number is less than an assigned PF for the station, the observation is generated and the sighting is considered successful. Otherwise, the station is ignored and the cycle is continued with the next station.

The above procedure is no doubt more simplified than real nature. However it still can serve the purpose of randomly omitting station(s) in any given observational scheme/pattern for weather effect. The present method resulted in about 10% loss of observations.

58

3.4 Observation Pattern or Station Grouping

3.4.1 Geometric mode

A. Station Grouping with Fundamental Stations

(1) With peripheral fundamental stations (PFS). In this scheme the stations were grouped with a maximum of twelve observed (illuminated) by the satellite in any simultaneous event, but the group always included the PFS stations Nos. 1073, 1074, and 1075. Here, if the weather effect model is included, any event will involve the three PFS and a minimum of three other stations.

This group serves as a "standard" of comparison with other observational patterns.

(2) With grid fundamental stations (GFS). This grouping is the same as above except that the GFS Nos. 1020, 1034, and 1059 replace the three PFS. The total number of stations (including the three GFS's) "illuminated" by one event under this scheme was reduced, as a first alternative, to eight or nine and also made flexible as compared to Mode 1.

(3) With laser fundamental stations (LFS). This scheme is identical to (2) above except three LFS's Nos. 1076, 1077, and 1078 are now treated as fundamental stations. Stations Nos. 1021, 1031, and 1041 are excluded to keep the total number fixed at 75.

B. Station Grouping Without Fundamental Stations

(1) Stations in groups of eight or nine. In this scheme as the satellite reaches a prespecified elevation angle, the observational scheme involves eight or nine grid stations observed simultaneously (Figure 3-8). Two successive events are designed to have four or more common stations in an overlapping (leapfrogging) fashion.

(2) Stations in groups of six. This scheme differs from the previous one in that in any two successive events only four stations form the link. The total stations observed simultaneously in any event is also reduced to six (Figure 3-9).
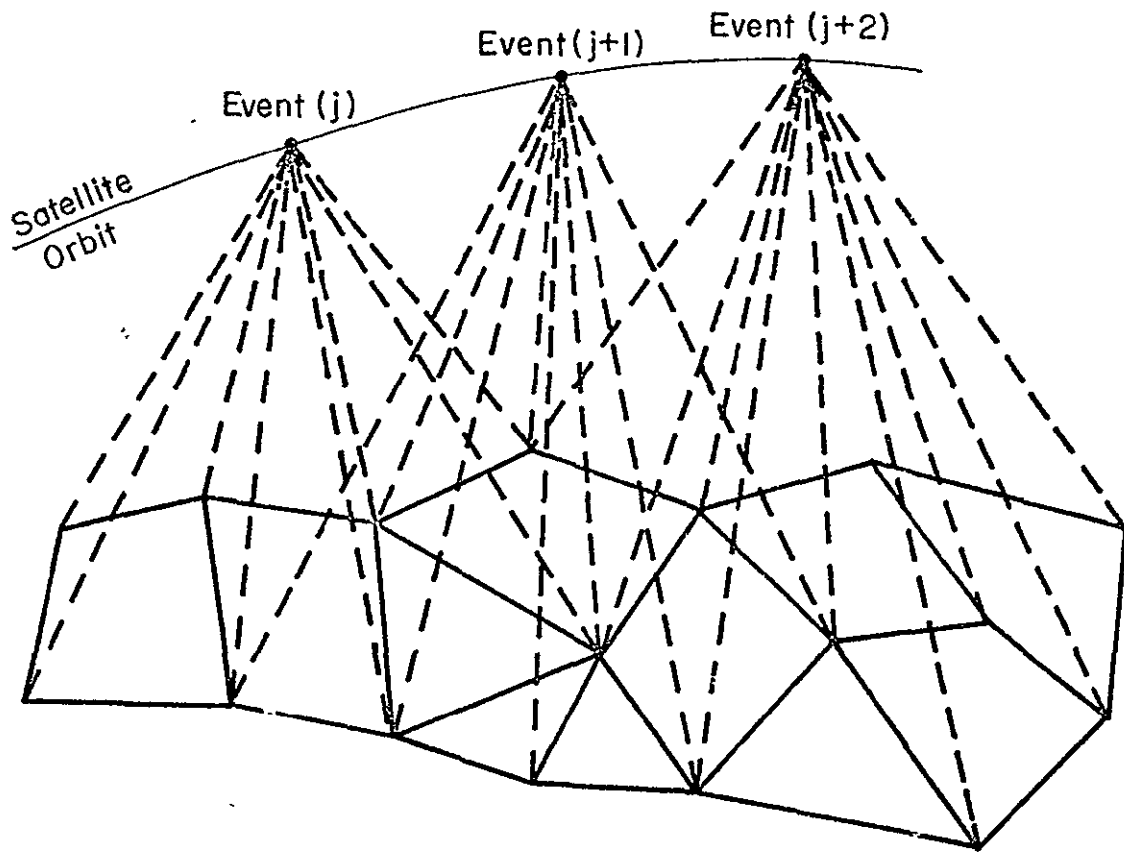
Figure 3-8. Stations in Groups of Eight or Nine

(3) Stations in groups of four. As a next alternative this scheme
envisages the start of an observational sequence with a group of only four
stations. Then from each group of four stations, two stations are dropped
and two new stations are included so that in any two successive events two
stations will always be common (Figure 3-10)

(4) Stations in fixed regional grouping (FRG). The design for this
scheme became necessary for the simulation of observations in an airplane
case (Section 2.3.1). Due to the close proximity of the airplane flights to
the ground (h = 10 km), the total number of 75 stations were grouped in
eleven regions (Figure 3-11) with each section having some common stations
with the adjoining section. Maximum number of stations in any section was
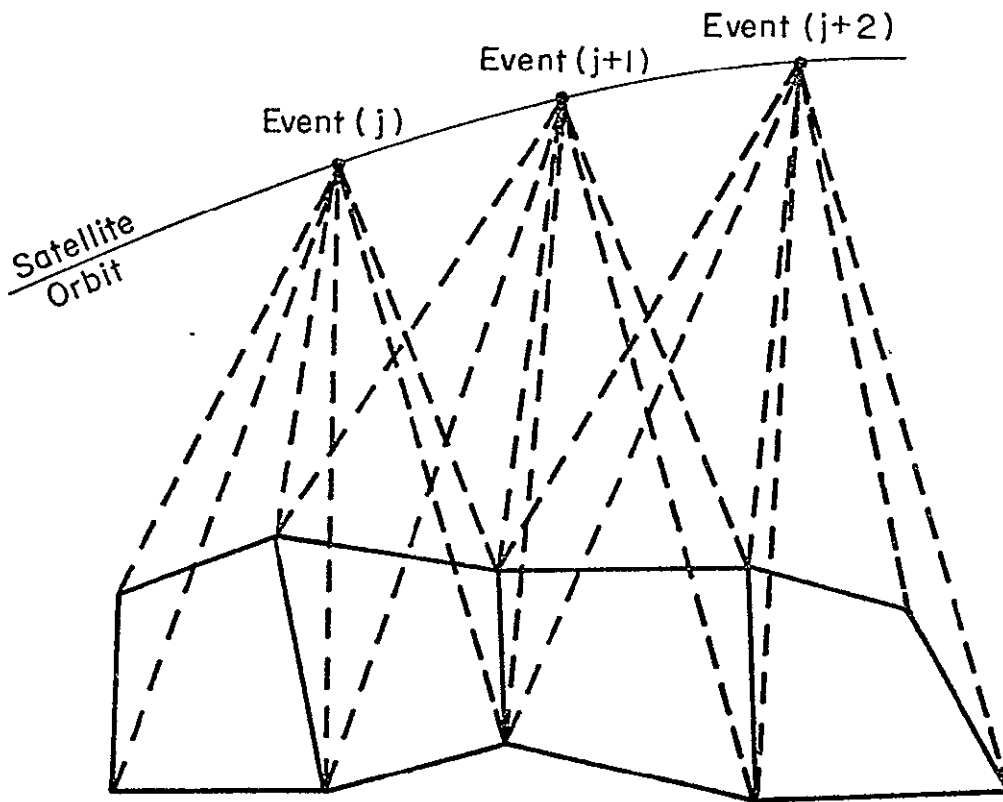
Figure 3-9. Stations in Groups of Six

restricted to nine. This regional grouping for airplane flights (A) has been termed as FRG for reference purposes in subsequent sections of this report.

3.4.2 Short arc mode

In this mode, the two main approaches were either to tackle the complete grid of 75 stations as one entity or to try to break up the full grid into two or more regional configurations.

The first approach was subdivided into two alternatives: (a) when all stations are observed by the satellite along all the passes, (b) when all the stations are observed by the satellite but not in all the passes.

For the second alternative, while conducting the earlier study [Mueller et al. , 1975], it was found that the participation of all the grid stations in each pass is not so critical as the participation of the three fundamental
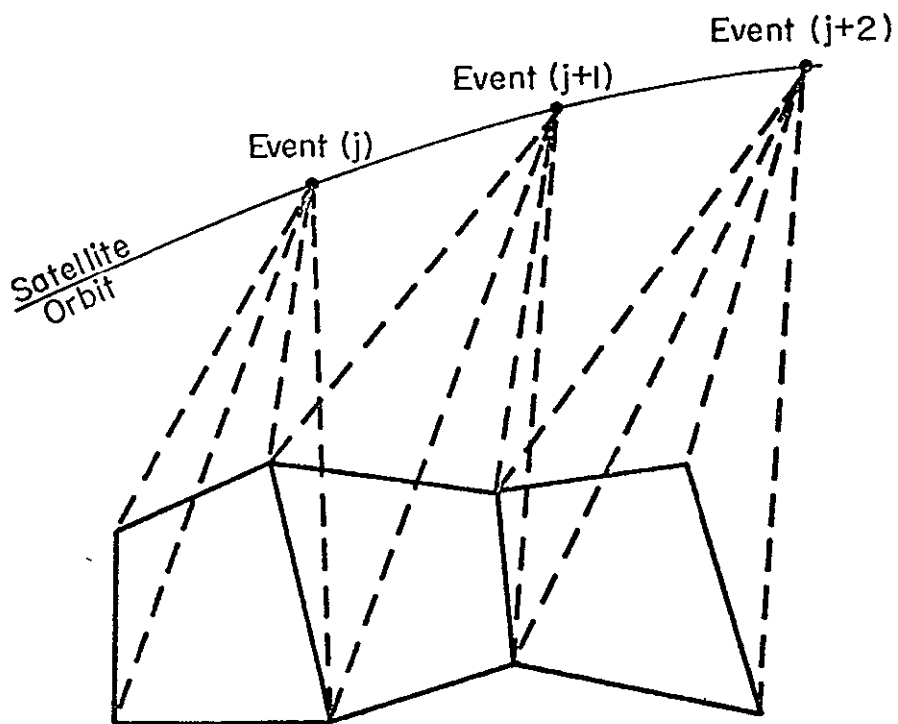
Figure 3-10. Stations in Groups of Four

stations and that the recovery starts deteriorating as the number of grid

stations observing any pass falls below two-thirds of the total number of

stations in any solution. To investigate this fact in case of an extended grid,

three solutions were set up with 25 stations (about 33%), 35 stations (about 50%),

and 50 stations (about 67%) to be observed in any single pass.

In the regional approach the grid was divided into three sections of about

25 stations each. The stations in each of these sections were observed to-

gether with the same GFS's (Figure 3-12).

3.5 Range Simulation

Using the short arcs (S),an airplane flights (A) and the Laser Range

Generation Program, LRGP (Appendix D), the ranges were generated with a

cut-off maximum zenith distance of 75° both for the geometric (event-wise) and

the short arc (station-wise) modes.
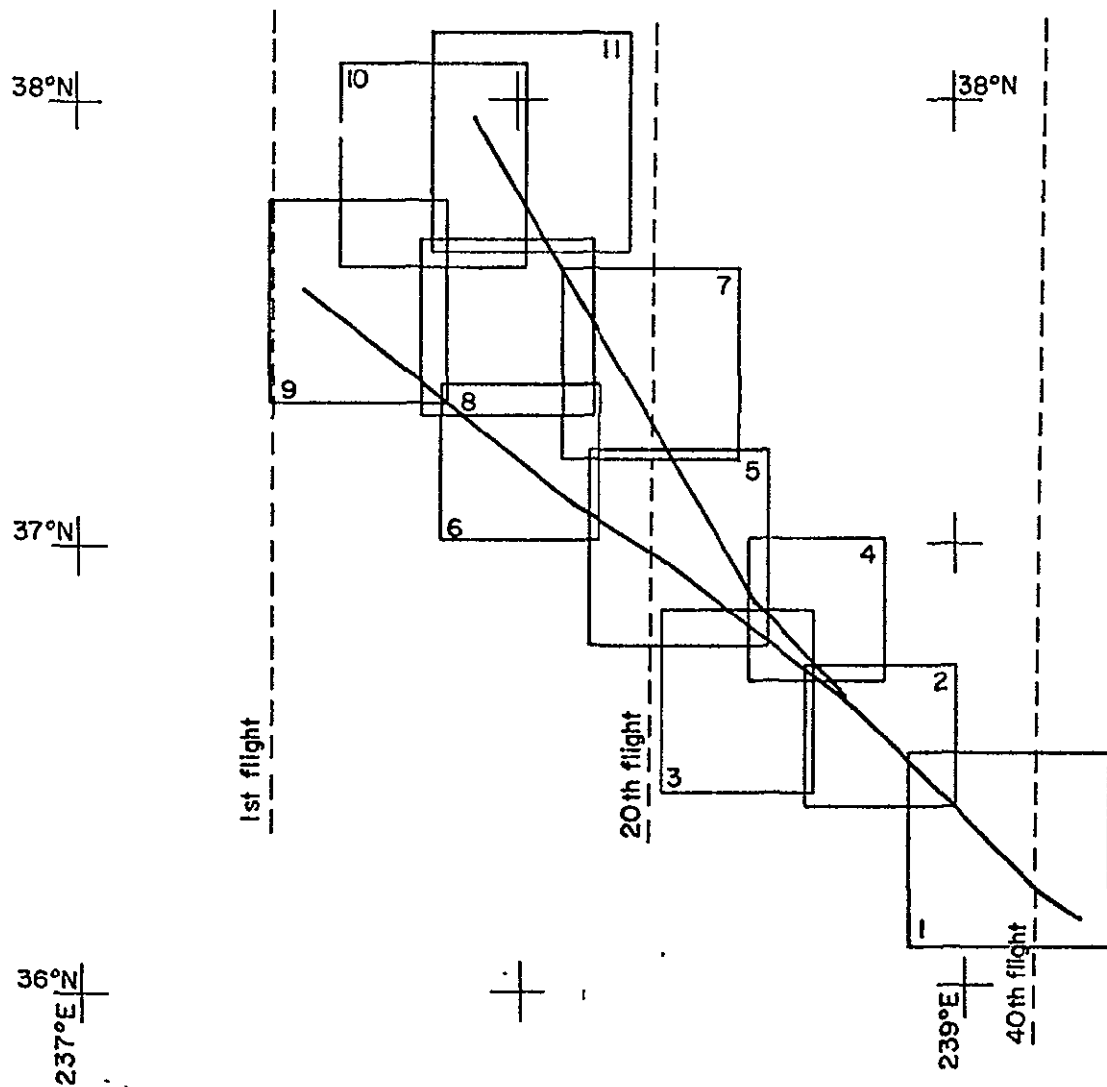
Figure 3-11   Station Grouping (Regional) for Airplane Flights
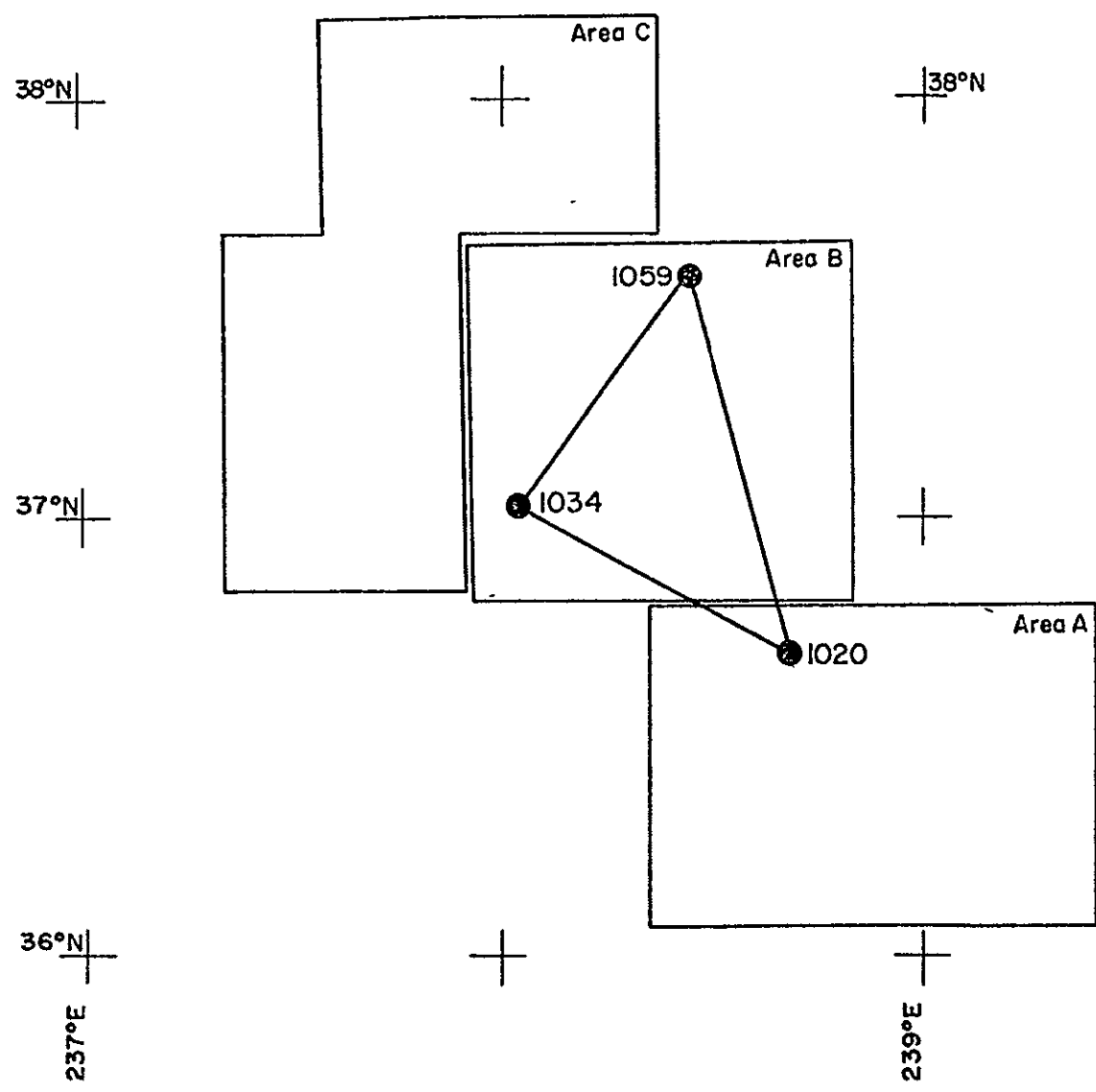
Figure 3-12   Regional Station Setup for Short Arc Mode

During the range generations the density of points was suitably altered in short arcs (S) and flights (A) to keep the number of ranges the same, as far as possible, for various observational pattern or station groupings.

4. SOLUTIONS PERFORMED

The feasibility of the geometric and short arc modes as possible means for determining the relative positions of the grid stations over a limited area with the required accuracy has already been established [Mueller et al., 1975]. In view of the questions to which answers are sought in the current analysis Table 4-1 gives the full listing of all solutions performed. To facilitate subsequent referencing, the various solutions have been designated by a number associated to the solution mode, geometric or short arc, under which they have been grouped. The associated numbers for geometric and short arc modes are 1 and 2 respectively. The numerical results are given and discussed in Section 5.

4.1 Geometric Mode Solutions

To perform the solutions in the geometric mode in order to obtain the adjusted station positions, The Ohio State University Geometric and Orbital (Adjustment) Program (OSUGOP) [Reilly et al., 1972] was suitably modified (Appendix C) to enlarge its scope and capability in handling an enlarged station network (up to 100 stations), large data sets and normal equations as input and/or output through magnetic tapes and disks, and mapping into estimable quantities and their variances.

All OSUGOP geometric solutions were performed using inner constraints [Blaha, 1971a], for the origin and orientation, except where otherwise stated (see Table 4-1) and are summarized under two main groups: (1) solutions with observations from satellite only, and (2) solutions with observations from both satellite and airplane-borne lasers.

Table 4-1

Summary of Solutions Performed

Solution No.	Station Type	Station Grouping or Stations/Pass	Observation Type	Type of Fundamental Stations Used	No. of Satellite Passes/Airplane Flights Used	Weather Effect Modeled	Ranging Accuracy (cm)	Remarks
GEOMETRIC MODE								
1-1	CM00	12	S	3 PFS	21	--	10	
1-2	CM00	8 or 9	S	3 GFS	21	--	2	
1-3	CM00	8 or 9	S	3 GFS	10	--	2	pass Nos. 4-28
1-4	CM00	8 or 9	S	3 LFS	10	--	2	pass Nos. 4-28. station Nos 1021, 1031, 1041 excluded 3 LFS held fixed
1-5	CM00	8 or 9	S	3 GFS	21	--	10	
1-6	CM00	8 or 9	S	3 GFS	10	--	10	pass Nos. 4-28
1-7	CM00	8 or 9	S	3 GFS	21	yes	10	
1-8	CM12	8 or 9	S	3 GFS	10	--	2	pass Nos 32-52
1-9	CM12	8 or 9	S	3 LFS	10	--	2	pass Nos. 32-52 station Nos. 1021, 1031, 1041 excluded 3 LFS held fixed
1-10	CM12	8 or 9	S	3 LFS	10	--	2	same as No. 1-9 but with inner constraints
1-11	CM12	8 or 9	S	3 GFS	10	--	10	pass Nos. 32-52
1-12	CM00	8 or 9	S	3 GFS	21	--	10	1-arc minute grid included for densification of network
1-12A	CM00	8 or 9	S	3 LFS	21	—	10	
1-13	CM00	4	S	--	21	--	10	
1-14	CM00	6	S	--	21	--	10	

67

Table 4-1 (Cont'd)

Solution No.	Station Type	Station Grouping or Stations/Pass	Observation Type	Type of Fundamental Stations Used	No. of Satellite Passes/Airplane Flights Used	Weather Effect Modeled	Ranging Accuracy (cm)	Remarks
1-15	CM00	6	S	--	10	--	10	pass Nos 4-28
1-16	CM00	8 or 9	S	--	21	--	10	
1-17	CM00	8 or 9 + FRG	S and A	3 GFS	21 and 40	--	10	
1-18	CM00	8 or 9 + FRG	S and A	3 GFS	21 and 40	yes	10	
1-19	CM00	6 + FRG	S and A	--	21 and 40	--	10	
1-20	CM00	8 or 9 + FRG	S and A	--	21 and 40	--	10	
SHORT ARC MODE								
2-1	CM00	75/pass	S	3 GFS	7	--	10	
2-2	CM00	50/pass	S	3 GFS	7	--	10	
2-3	CM00	35/pass	S	3 GFS	7	--	10	
2-4	CM00	25/pass	S	3 GFS	7	--	10	
2-5	CM00	35/pass	S	3 PFS	7	--	10	
2-6	CM00	35/pass	S	3 LFS	7	--	10	station Nos. 1021, 1031, 1041 excluded
2-7	CM00	17/pass	S	3 GFS	7	--	10	27 stations in solution
2-8	CM00	16/pass	S	3 GFS	7	--	10	25 stations in solution

4.1.1 Solutions with observations from satellite only

(1) Solution with peripheral fundamental stations $(\sigma_r = 10$ cm). The solution (No. 1-1) under this scheme was performed with station grouping as described in Section 3.4.1 (1). All the 21 satellite passes observe all the 75 grid stations and the average number of observations to each station (other than 3 PFS) per pass is 25. Twelve stations (nine grid stations and three PFS) were involved in any simultaneous event under ideal weather conditions.

The observational pattern, station grouping, and observation density in solution No. 1-1 and the results so obtained are viewed as "standard" for subsequent comparison with other geometric mode solutions under other observational schemes, density of observation, etc.

(2) Solution with grid fundamental stations. The solutions (Nos. 1-2, 1-3, 1-5, 1-6, 1-7, 1-8, 1-11, and 1-12) under this scheme have stations in groups of eight or nine (including 3 GFS -- Nos. 1020, 1034, and 1059 -- as fundamental stations). All 21 passes are involved except when otherwise stated. These solutions are subdivided for weather, crustal motion, special 1-arc minute grid for densification of network, different ranging accuracy σ_r, etc. as follows:

Solutions No. 1-2 $(\sigma_r = 2$ cm) and no. 1-5 ($\sigma_r = 10$ cm) involve station positions CM00 and the average number of observations to any grid station (other than 3 GFS) per pass is 25 without weather effect.

Solutions No. 1-3 ($\sigma_r = 2$ cm) and No. 1-6 ($\sigma_r = 10$ cm) differ from Nos. 1-2 and 1-5 as they use only the first ten passes, i.e., passes Nos. 4 - 28 (Section 2.3.1) which reduces the total number of observations to about one half.

Solution No. 1-7 ($\sigma_r = 10$ cm) corresponds to No. 1-5 but includes the weather effect as shown in Figure 4-1. As the GFS Nos. 1020, 1034, and 1059 are observed in each event (being fundamental stations), the PF value assigned to each of them is 1, i.e., only those events are considered when the weather at all the three GFS is clear.
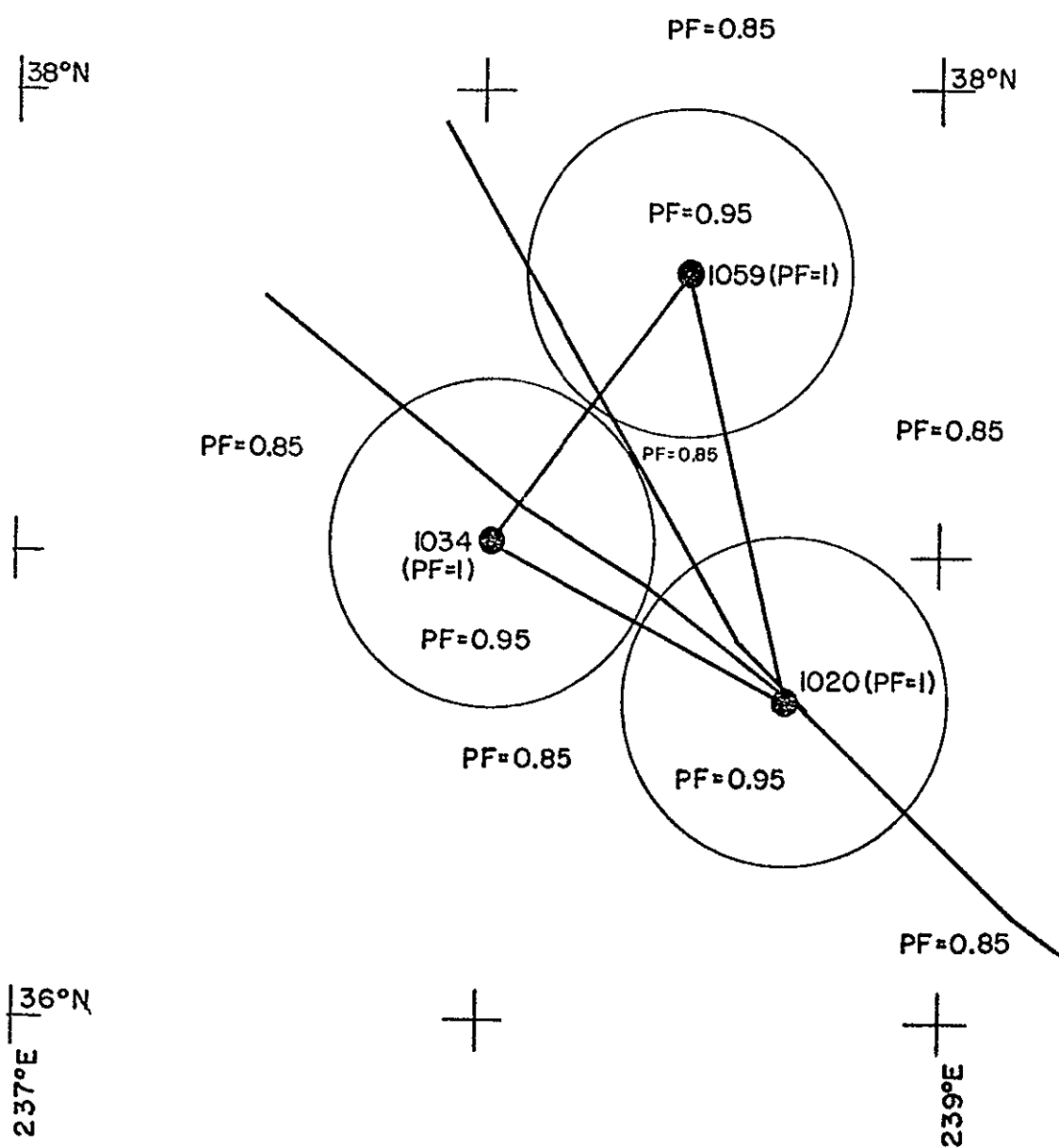
Figure 4-1   Schematic Weather Effect Modeling

With the above assigned condition at the three GFS, it is assumed that the weather at any other grid station is a function of its distance away from either of the GFS's. With this assumption, for stations within a radius of 25 km of the three GFS, the assigned PF value is 0.95 (Section 3.3) and in all other cases as 0.85--decreasing the probability of sighting with the distance from the three GFS's. This stipulation results in a loss of about 10% observations (compared to solution No. 1-5) to any grid station--the average per pass being 22.

Solution No. 1-8 ($\sigma_r = 2$ cm) and No. 1-11 ($\sigma_r = 10$ cm) differ from Nos. 1-3 and 1-6 as each takes into account the crustal motion model (Section 3.2) at epoch t_1 ($= t_0 + 12$ months) with station positions CM12. Other conditions remain the same.

Solution No. 1-12 ($\sigma_r = 10$ cm) differs from No. 1-5 in the setup that this experiment replaces ten stations, Nos. 1021 to 1030, by the alternate 1-arc minute grid (Insert, Figure 3-1) while the balance of 62 grid stations, three GFS and other observational features are kept the same.

This solution was designed to study the recovery of relative positions when a denser station network forms part of a larger grid.

(3) Solutions with laser fundamental stations. In the solutions (Nos. 1-4, 1-9, 1-10, and 1-12A), the observations for any event are to stations in groups of eight or nine (including 3 LFS Nos. 1076, 1077, and 1078 as fundamental stations). First two solutions are run towards recovery of velocity vector (Sections 2.2.5 and 3.2).

Solution No. 1-4 ($\sigma_r = 2$ cm) involves station positions CM00 at epoch t_0 with average number of observations to any station (other than three LFS) per pass as 25. First, ten passes, viz., 4 to 28 (Section 2.3.1) are used under ideal weather conditions. See Figure 2-3 for satellite pass configuration. Three LFS are held fixed (Section 2.2.3 (a)). Three grid stations, viz., 1021, 1031, and 1041 are excluded to keep the total number of stations in the solution fixed at 75.

71

Solution No. 1-9 (σ_r = 2 cm) involves station positions CM12 at epoch t_1 (= t_0 + 12 months) using last ten passes, viz., 32-52 (Figure 2-3). All other conditions remain the same as in solution No. 1-4.

Solution No. 1-10 (σ_r = 2 cm) uses inner constraints instead of 3 LFS held fixed (No. 1-9). All other conditions remain as in solution 1-9.

Solution No. 1-12A (σ_r = 10 cm) differs with No. 1-5 as this includes three LFS in place of three GFS. All other conditions remain the same.

(4) Solutions without fundamental stations. These solutions have no fundamental stations, i.e., all the 75 grid stations have equal chance of participating in any observation/event. However, the stations are observed by all the 21 satellite passes in the following station grouping in ideal weather.

Solution No. 1-13 (σ_r = 10 cm) contains the station grouping where the stations are coobserved in groups of four. The average number of observations to any station per pass is 25.

Solution No. 1-14 differs from No. 1-13 that in this experiment the stations are in groups of six. Other conditions remain the same. In addition, solution No. 1-15 has only 250 observations to each station while the rest of the conditions remain identical as in No. 1-14.

Solution No. 1-16 differs from No. 1-13 or 1-14 that here the stations are in groups of eight or nine. Other conditions remain the same.

4.1.2 Solutions with observations from both satellite and airplane

This section deals with the case when observations from the airplane are included in fixed regional grouping (Section 3.4.1 (6)) with observations from the satellite to improve the recovery of relative positions between grid stations (Section 1.2). Four typical cases of Section 4.1.1 were rerun as solutions Nos. 1-17 to 1-20 and their details are given below.

(1) Solutions with grid fundamental stations. Solution No. 1-17 (σ_r = 10 cm) was setup the same way as No. 1-5. The average number of observations (both from satellite and airplane) to any grid station per pass is 25. All other conditions remain the same.

72

Solution No. 1-18 ($\sigma_r = 10$ cm) differs from No. 1-17 by the fact that it includes the weather effect. The average number of observations to any grid station per pass is 22.

(2) Solutions without fundamental stations. Solution No. 1-19 ($\sigma_r = 10$ cm) corresponds to No. 1-14 and is to examine the effect of including observations from airplane when stations are coobserved in groups of six. All other conditions remain the same.

Solution No. 1-20 ($\sigma_r = 10$ cm) corresponds to No. 1-16 for station grouping of eight or nine. All other conditions are the same as in No. 1-19.

4.2 Short Arc Mode Solutions

The software used to generate solutions in the short arc mode to obtain adjusted station positions is a modified form of a Fortran program developed by Duane Brown Associates between 1968 and 1973 known as "The Short Arc Geodetic Adjustment" (SAGA) [Brown and Trotter, 1969 and 1973]. For a brief description of the same, see Appendix B.

All SAGA solutions were carried out using necessary origin and orientation definition by constraining six coordinates of three fundamental stations (Section 3.1.2). In the earlier study [Table 5.2.1, Mueller et al., 1975], it was noticed that a minimum of seven passes with 500 observations to any one grid station were needed to obtain an optimum recovery (Table 1-1). This specification has been retained.

·Brief descriptions of short arc mode solutions and their setup are as follows:

4.2.1 Complete solutions

A solution in which all the grid stations and the three fundamental stations are observed by all the selected satellite passes has been designated as "complete" and is viewed as "standard" for subsequent comparisons with other short arc mode solutions.

73

Solution No. 2-1 ($\sigma_r = 10$ cm) under this experiment has the average number of observations to any station as 500 and the three GFS Nos. 1020, 1034, and 1059 are held fixed for necessary constraints.

4.2.2 Partial solutions

In comparison to complete solution (Section 4.2.1), a solution in which the selected passes observe to some of the grid stations has been named as "partial."

Solutions Nos. 2-2, 2-3, and 2-4 include only about 67%, 50%, and 33% of the grid stations (i.e., about 50, 35, and 25 stations) respectively per pass (Section 3.4.2). However, three GFS are always observed in all the selected passes. All other specifications are the same as in No. 2-1.

Additional two solutions (Nos. 2-5 and 2-6) correspond in all respects to No. 2-3 except that these are with three PFS and LFS respectively. In solution No. 2-6, the three LFS are added after deleting three grid stations (Nos. 1021, 1031, and 1041) to keep the total number of stations at 75 (Table 4-1).

4.2.3 Regional solutions

In this setup, two solutions Nos. 2-7 and 2-8 are with 27 and 25 stations (including three GFS) respectively. The areas covered by the above solutions are the ones designated "A" and "B" respectively in Figure 3-12.

5. RESULTS

In the present investigation, as the station grid is enlarged, the importance of the following inherent characteristics of the geometric and short arc modes towards the success of geodetic monitoring stands out more and more:

(a) In the geometric mode, the failure of the satellite to pick up a station from any particular station grouping observed simultaneously may result in a possible loss of only one event. This situation occurs when the number of stations in the group falls below four.

(b) In the short arc mode the failure of the satellite to pick up three distant fundamental stations results in the complete loss of the entire pass (Section 1.2). As pointed out earlier (Section 3.4.2), the participation of "all" the grid stations in observations from an overpass is not as essential as participation of the three fundamental stations, but the recovery of the system does indicate adverse effects with the decrease in percentage of the total number of grid stations (from the entire network) observed in any single over pass. This may result in a possible loss of an entire pass. Further, the likelihood of having favorable weather conditions at some minimum number of grid stations to avoid the possible loss of the satellite pass would become more and more restrictive as the number of stations would grow in the network.

Tabulated results contain references to related solutions, details of which are available in Section 4.

5.1 Geometric Mode

In the earlier study (Section 1.2), in addition to the investigation of the recovery of chord distances (R_{ij}) between any two grid stations, a variance analysis for the angles, θ and ψ, between the chords was also performed (Figure 5-1). The general behavior of the "horizontal" angles θ
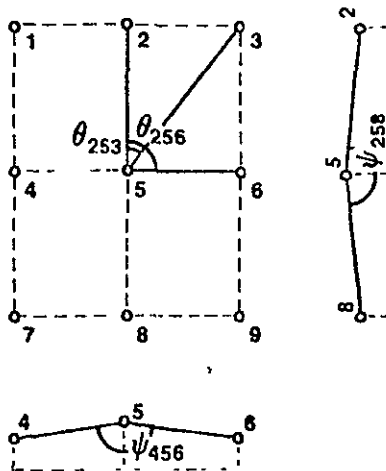
Figure 5-1. Diagram Showing Definition of Angles
θ, ψ in a Station Grid [Mueller et al., 1975]

is very similar to the behavior of chord distances while the "vertical" angles ψ can be related to the strength of the network in the vertical direction, i.e., in height (Section 2.2.4).

In view of the above, a representative chain of braced quadrilaterals and polygons running through the study area was selected to investigate the questions listed in Section 1.3 (Figure 5-2). This chain contains chord lengths (across faults) from 14.6 km ($r_{1001-1003}$) to 57.2 km ($r_{1003-1009}$) and angles θ and ψ of varying magnitude. In certain investigations some minor modifications became necessary to this chain and these changes are commented on at appropriate places. To study the recovery of velocity vector, the grid stations are analyzed for each of the three zones shown in Figure 3-2.

Results for distances greater than 60 km are also included in some cases for academic interest. Even though these longer chords do not relate to
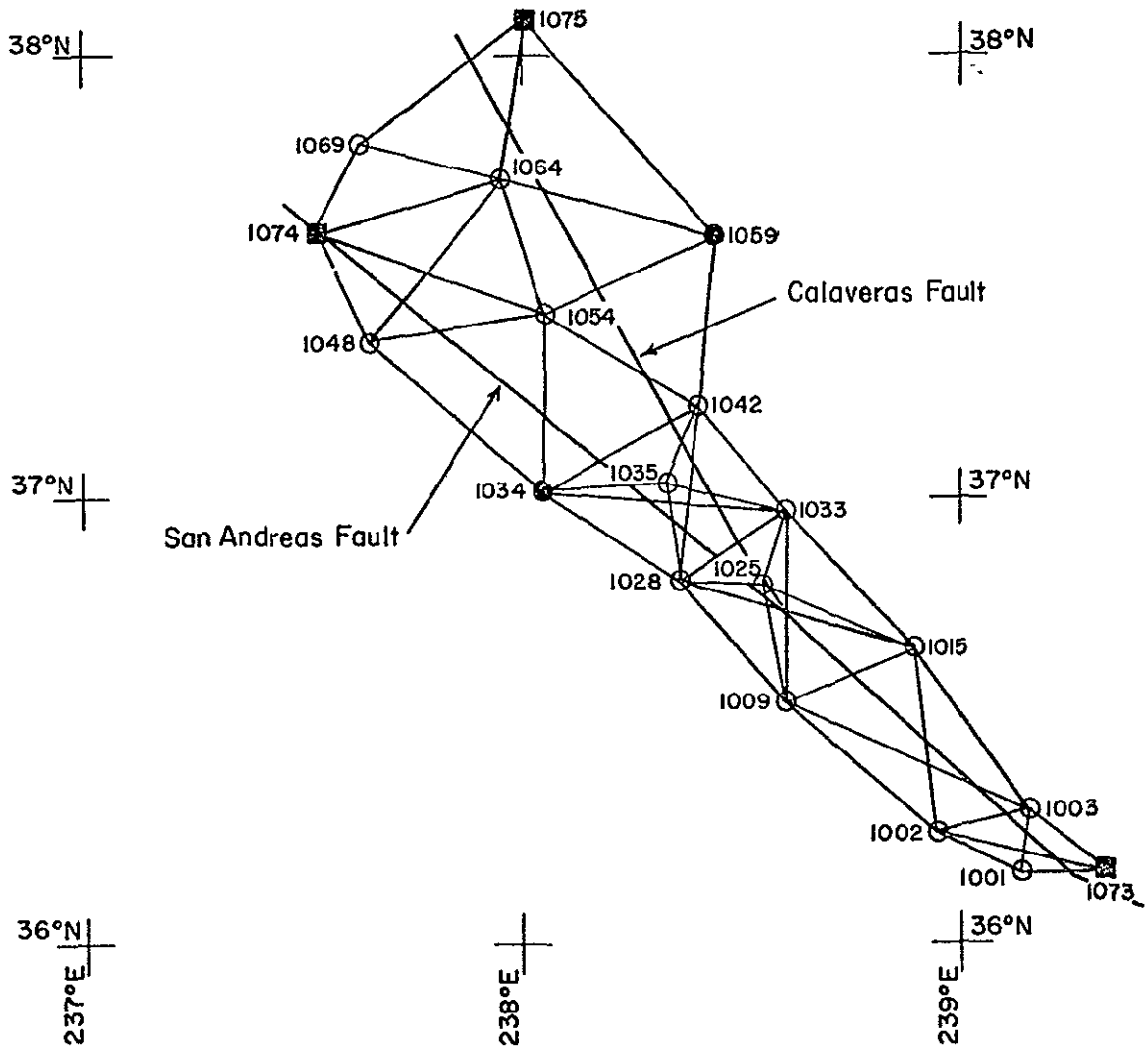
Figure 5-2. Representative Chain of Quadrilaterals
and Polygons for Stations

"adjacent or neighboring" stations in the present grid and thus are not relevant in the monitoring, their recovery behavior contains some interesting information.

It may be mentioned here that a posteriori variance of unit weight, σ_0^2, varied between 0.91 and 1.02 for all the solutions.

5.1.1 Grid and fundamental stations

In this subsection, the effect of different combinations of station grouping and fundamental stations is analyzed. The case of "densification of control" as part of a larger network is also included to study the recovery of relative positions in the 1 km range.

(1) Grid station grouping. Tables 5-1 and 5-2 and Figures 5-3 and 5-4 show the effect of station grouping and the number of stations participating in an event in terms of the standard deviations $\sigma_{R_{ij}}$ and relative standard deviations $\sigma_{R_{ij}}/R_{ij}$ for different chord lengths. The distances selected vary from 14.62 km to 243.46 km with an increment of about 20 km.

All the tabulated/plotted results indicate that

(i) the station grouping in fours (Section 3.4.1) does not give satisfactory solution. The behavior of $\sigma_{R_{ij}}$ and $\sigma_{R_{ij}}/R_{ij}$ is erratic, unpredictable, and shows no trend. The same behavior is reflected in case of angles θ_{ijk} and ψ_{ijk}.

(ii) The station grouping in sixes shows a significant improvement which is more marked in the case of angles θ_{ijk} and ψ_{ijk} as compared to chords.

(iii) The station grouping in eights or nines shows a further overall improvement.

Table 5-3 shows detailed results of recovery for the chord distances up to a length of 60 km between "adjacent" stations (Figure 5-2) in terms of difference $D_{R_{ij}}$ for various station groupings and different choices of·funda-

78

Table 5-1

Effect of Station Grouping and Fundamental Stations

on Precision of Chord Recovery, Geometric Mode

(500 observations to each station; $\sigma_r = 10$ cm)

Solution No.	R_{ij} (km) / Station Grouping per Event ij	14 62 / 1001 1003	21.60 / 1003 1073	45.78 / 1002 1009	57 15 / 1003 1009	77 60 / 1009 1073	102.07 / 1001 1033	121 84 / 1003 1042	138.54 / 1001 1034	159 63 / 1003 1059	185 59 / 1001 1048	204.11 / 1001 1064	222 51 / 1003 1075	243.46 / 1073 1075	Remarks
1-13	4	16/11	25/12	12866/281	3557/62	11000/142	6078/60.	9840/81.	12035/87	10891./68.	10766./92.	12178/60.	8490/38	8143/33.	no fundamental stations
1-14	6	3/2.	4/2.	9./2.	11/2	14/2	16/2.	19/2.	22/2	25./2	27/1.	28/1	30/1.	33/1	no fundamental stations
1-16	8 or 9	3/2	3/1	6./1	7/1	10/1	12/1	14/1	16/1	19/1.	22/1.	23/1	26/1	28/1	no fundamental stations
1-5	8 or 9	3/2.	3/1.	4./2.	6./1.	8/1	8/1	10/1	12./1	13/1	16/1.	16./1.	18/1	20/1	with GFS
1-1	12	1/0.7	1./0.5	1./0.2	2/0.3	2./0 3	2/0 1	3/0 2	3/0 2	4./0 3	4/0 2	5/0.2	5/0 2	6/0 2	with PFS

Refer Figure 5-2.
Tabulated values are $\sigma_{R_{ij}}$ (cm), upper number, and $\sigma_{R_{ij}}/R_{ij}$ (ppm), lower number.

Table 5-2

Effect of Station Grouping and Fundamental Stations

on Precision of Angle Recovery, Geometric Mode

(500 observations to each station; $\sigma_r = 10$ cm)

Solution No.	θ, ψ_{ijk} / Station Grouping per Event / ijk	θ		ψ			Remarks
		$\sim 45°$	$\sim 94°$	$\sim 160°$ E-W alignment	$\sim 150°$ N-S alignment	$\sim 170°$ NW-SE alignment	
		1001-1073-1003	1003-1015-1009	1034-1054-1064	1059-1064-1074	1015-1033-1042	
1-13	4	9.477	4331.8	6.576	7 112	5.382	no fundamental station
1-14	6	1 877	2.615	1.924	2.036	1.022	no fundamental station
1-16	8 or 9	1 584	2.270	1.327	1.464	0.957	no fundamental station
1-5	8 or 9	1.109	1.866	0.804	1.372	0.781	with GFS
1-1	12	0.529	0.668	0.344	0.498	0.333	with GFS

Refer Figure 5-1.
Tabulated values are $\sigma_{\theta, \psi_{ijk}}$ (rad. $\times 10^6$).

Figure 5-3 Effect of Station Grouping and Fundamental Stations[1] on Precision of Chord Recovery, Geometric Mode (500 observations to each station; $\sigma_r = 10$ cm)
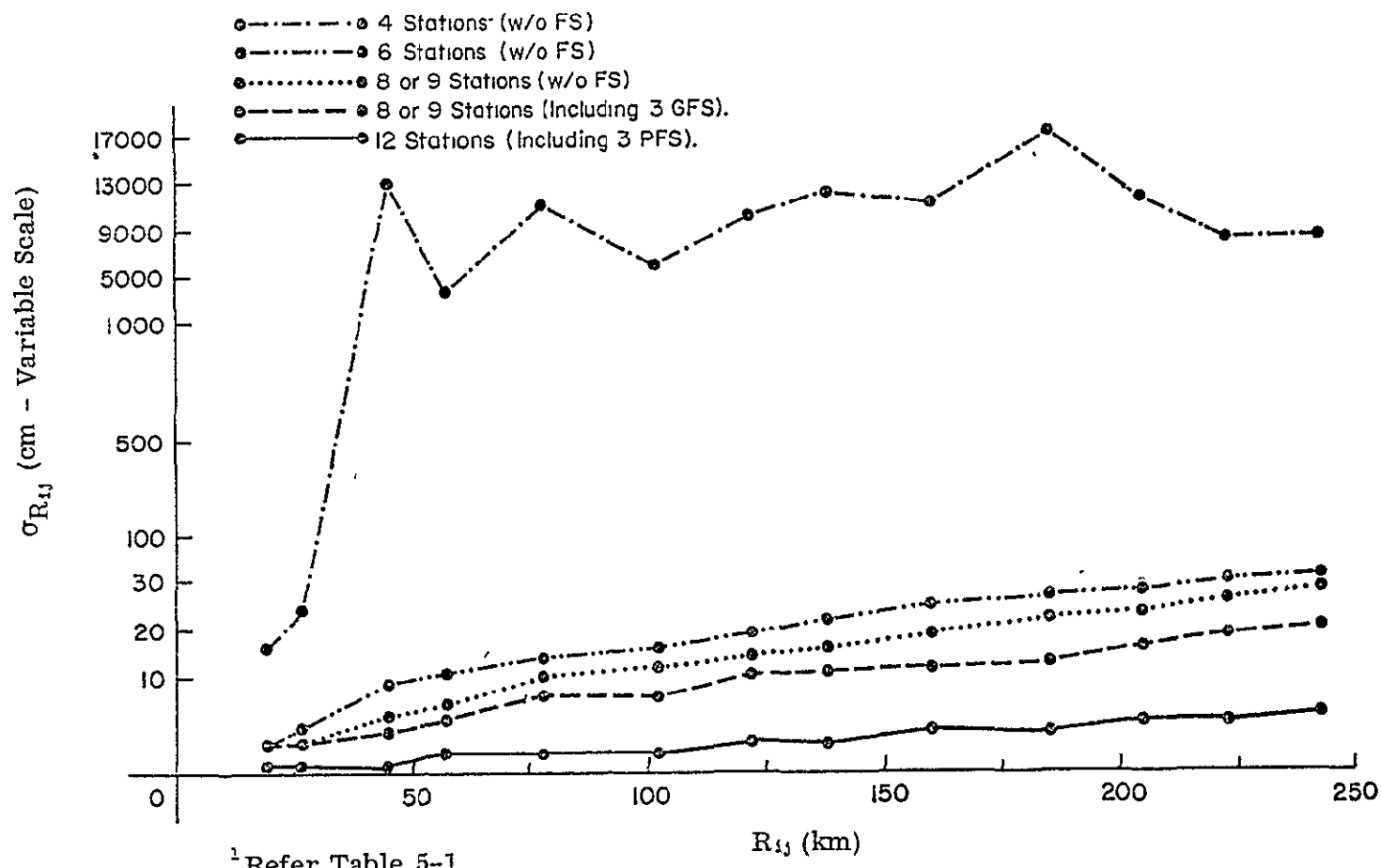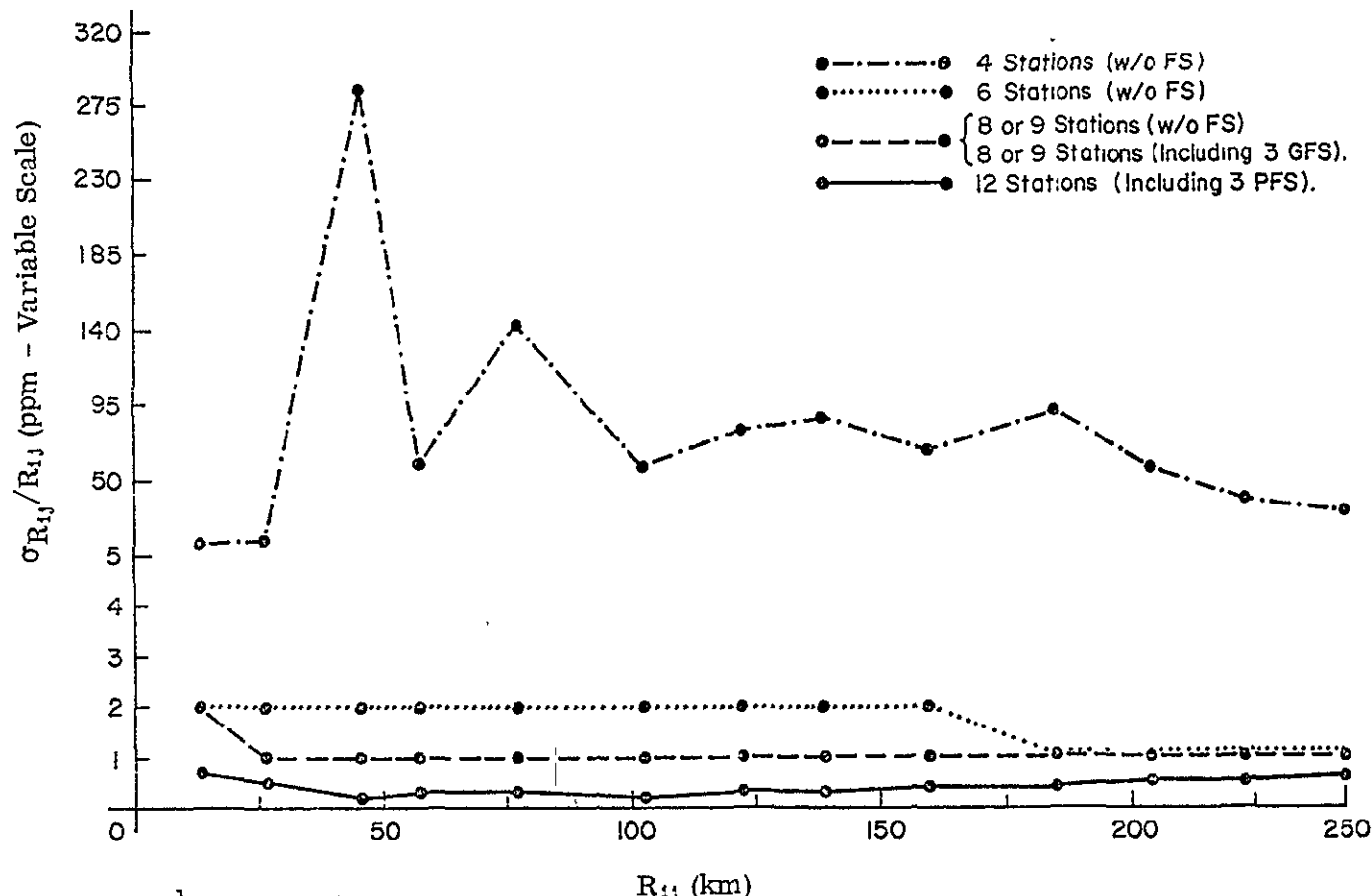
[1]Refer Table 5-1.

Figure 5-4   Effect of Station Grouping and Fundamental Stations[1] on Relative
Precision of Chord Recovery, Geometric Mode
(500 observations to each station; σ_r = 10 cm)

[1] Refer Table 5-1.

mental stations. The differences $D_{R_{ij}}$ are computed between the recovered
and the true distances between the grid stations "i" and "j".

It is seen again that only station groupings in eights or nines are
promising.

(2) Fundamental stations. The trend in improvement in the recovery
of chords with the increase in number of stations participating in any event
(Table 5-3) becomes more significant with the inclusion (or treatment) of
certain grid stations as fundamental stations. As the case of including three
fundamental stations within the station grouping of fours or sixes would be
too restrictive in the selection (or dropping) of stations in any event, these
options were not attempted under this scheme.

The recovery of chords for the station grouping in eights or nines with
three GFS's improves further (line 4, Table 5-3) over the case with no funda-
mental stations (line 3, Table 5-3).

When the station grouping is changed to 12 including three PFS's (line
5, Table 5-3), or to eight or nine with LFS (line 6, Table 5-3), the recovery
is still more promising in all respect.

(3) Densification of control. Table 5-4 shows the variance analysis
with respect to the recovery of one-minute grid stations for densification of
control. These results then indicate that the standard deviation $\sigma_{R_{ij}}/R_{ij}$
for one-minute grid stations are comparable to the values in Tables 5-1 and
5-2, while the same, as expected, is not true for the angles θ and ψ. Table
5-5 indicates the results for recovery of distances in case of one-minute grid
of 10 stations.

5.1.2 Weather effect

Table 5-6 contains the comparative results for the case where weather
effect has been modeled with about 10% loss in observations to each station.
It may be pointed out here that this loss in observations not only affects the
total number of observations to any station in any solution, but also the

83

Table 5-3

Effect of Station Grouping and Fundamental Stations

on Recovery of Chords ($R_{ij} \leq 60$ km), Geometric Mode

(500 observations to each station; $\sigma_r = 10$ cm)

Solution No.	Station Grouping per Event	Fundamental Stations Used	Percentage of Absolute Differences $|D_{R_{ij}}|$ [1]							Maximum $|D_{R_{ij}}|$		Relative Precision [2]
			0-1 cm	1-2 cm	2-3 cm	3-4 cm	4-5 cm	5-10 cm	>10 cm	cm	ppm	$\sigma_{R_{ij}}/R_{ij}$ ppm
1-13	4	--	3	2	5	8	5	22	55	66.7	14.0	281
1-14	6	--	18	15	5	8	7	22	25	28.2	7.0	11
1-16	8 or 9	--	22	10	10	30	10	13	5	13.3	3.0	7
1-5	8 or 9	3 GFS	57	20	17	4	2	--	--	5.0	2.5	6
1-1	12	3 PFS	77	20	3	--	--	--	--	3.0	0.5	2
1-12A	8 or 9	3 LFS	92	8	--	--	--	--	--	1.1	0.2	0.4

1 Total number of chords tested: 74
2 The number tabluated is for the worst case in the solution.

Table 5-4

Effect of Densification of Network

on Precision of Chord Recovery ($R_{ij} \leq 5$ km), Geometric Mode

(500 Observations to Each Station; $\sigma_r = 10$ cm)

Solution No.	Station Grouping per Event	$\sigma_{R_{ij}}$(cm), Upper Number $\sigma_{R_{ij}}/R_{ij}$(ppm), Lower Number				$\sigma_{\theta}, \psi_{ijk}$ (radians × 10^6)		
		Chords R_{ij} (km)				θ_{ijk}		ψ_{ijk}
		1.5	2.4	3.0	4.8	~45°	~90°	~180° (E-W)
1-12	8 or 9 with 3 GFS	$\dfrac{1.6}{1.1}$	$\dfrac{1\ 5}{0.6}$	$\dfrac{1.6}{0.5}$	$\dfrac{1.7}{0.4}$	9.5	12.9	16.6

Table 5-5

Effect of Densification of Network

on Recovery of Chords ($R_{ij} \leq 5$ km), Geometric Mode

(500 Observations to Each Station; $\sigma_r = 10$ cm)

Solution No.	Station Grouping per Event	Percentage of Difference $|D_{R_{ij}}|$			Maximum Difference $|D_{R_{ij}}|$	
		0-1 cm	1-2 cm	2-3 cm	cm	ppm
1-12	8 or 9 with 3 GFS	44	46	10	2.6	6.5

Table 5-6

Effect of Weather for Satellite and/or Airplane Observations
on Recovery of Chords and Angles, Geometric Mode

Solution No.	Station Grouping per Event	Type of Observation	No. of Observations to Each Station $\sigma_r = 10$ cm	Maximum Differences $|D_{R_{ij}}|$ (cm) for Different Chord Lengths (km)													Spread of $\sigma_{R_{ij}}$ (cm) and σ_θ, ψ_{ix} (radians X 10^6)			
				< 20	20 to 40	40 to 60	60 to 80	80 to 100	100 to 120	120 to 140	140 to 160	160 to 180	180 to 200	200 to 220	220 to 240	> 240	$\sigma_{R_{ij}}$ Min.	$\sigma_{R_{ij}}$ Max.	σ_θ, ψ_{ix} Min	σ_θ, ψ_{ix} Max
1-5 (no weather effect)	8 or 9 (including GFS)	S	500	1	3	5	6	4	6	4	5	4	5	6	6	3	2.9	20 1	0.11	3.01
1-7 (with weather effect)		S	450	5	6	7	9	11	12	7	11	11	8	7	10	3	3.1	22.1	0.11	3 30
1-17 (no weather effect)	8 or 9 (including GFS)	S + A	500	1	3	2	3	2	3	2	5	2	4	4	3	3	0.5	4.2	0.05	1.63
1-18 (with weather effect)		S + A	450	2	4	5	5	4	4	5	5	8	6	8	6	2	1.0	7.0	0.08	2.35

station grouping from event to event. However, those events where the number of stations becomes less than six are eliminated.

In case of chords up to 60 km, a general deterioration of 1-3 cm in the recovery of difference $D_{R_{ij}}$ is noticed--this adverse increase in differences reaches a maximum value of 7 cm for longer chords in case of satellite observations only. The analysis for angles shows insignificant changes.

5.1.3 Observations from airplanes

Table 5-7 contains the results when airplane observations are mixed with satellite observations and compared to similar satellite only cases.

The improvement is overall in all the cases but more marked in the case of station grouping of sixes without fundamental stations. Here this mode of observations almost becomes as good as "standard" Solution No. 1-1 (line 5, Table 5-1).

5.1.4 Precision of ranging

The overall effect on system's recovery due to change in precision of ranging (Section 2.3.3) has been analyzed in Table 5-8. The data used in the two solutions compared employs different (but adjacent) satellite positions selected from the same passes and was generated with two different random numbers for imposing the respective noises.

The table contains the effect on the recovery of chords in terms of differences $D_{R_{ij}}$ (cm) and on the precision $\sigma_{\theta_{ijk}}$ and $\sigma_{\psi_{ijk}}$ (radians x 10^6) for varying σ_r for laser ranges. The numbers (except for some minor differences) show proportional changes in recovery and precision vis-a-vis the change in ranging precision. The minor differences may be attributed to the different randomness in the data used.

5.1.5 Number of observations per station

In the preliminary study it was noticed that, for a small grid of nine stations in noncritical configuration, the optimum number of observations per station (in terms of obtaining the efficiency ratio $\sigma_{R_{ij}}/\sigma_r$ equal to 1) could

Table 5-7

Effect of Combining Satellite and Airplane Observations

on Precision of Chord Recovery, Geometric Mode

(500 Observations to Each Station; $\sigma_r = 10$ cm)

88

Solution No	Station Grouping per Event	Type of Observation R_{ij} (km) / i-j	14.62 1001/1003	21.60 1003/1073	45 78 1002/1009	57.15 1003/1009	77 60 1009/1073	102.07 1001/1033	121 84 1003/1042	138.54 1001/1034	159.63 1003/1059	185 59 1001/1048	204.11 1001/1064	222.51 1003/1075	243 46 1073/1075
1-14	6 w/o FS	S	3/2	4/2	9./2	11/2.	14/2	16/2.	19/2	22/2	25./2	27./1.	28/1	30/1	33/1
1-19		S + A	2/1.	2/1	2./0.5	2/0 4	3/0 4	3./0.3	4/0 3	4/0 3	4/0.3	5./0 3	5/0.3	5./0.3	5/0 3
1-3	8 or 9 with GFS	S	3/2	3./1	4/2	6/1.	8/1.	8/1.	10/1	12./1.	13/1	16/1	16/1	18./1.	20./1
1-17		S + A	2/1	2/1	2./0 4	2./0.4	2./0 3	2/0 2	3/0 2	3./0 2	3/0.3	4/0 2	4./0.2	4./0.2	4/0.2

Note· Tabulated values are $\sigma_{R_{ij}}$(cm), upper number; and $\sigma_{R_{ij}}/R_i$(ppm), lower number.

Table 5-8

Effect of Ranging Precision on Recovery of Chords,

Geometric Mode

(500 Observations to Each Station)

89

Solution No.	Station Grouping per Event	Ranging Precision σ_r (cm)	Maximum Difference $|D_{R_{ij}}|$ (cm) for Different Chord Lengths (km) [1]													Spread of $\sigma_{R_{ij}}$ (cm) and $\sigma_{\theta}, \psi_{ijk}$ (rad. $\times 10^6$)			
			< 20	20 to 40	40 to 60	60 to 80	80 to 100	100 to 120	120 to 140	140 to 160	160 to 180	180 to 200	200 to 220	220 to 240	> 240	$\sigma_{R_{ij}}$		$\sigma_{\theta}, \psi_{ijk}$	
																Minimum	Maximum	Minimum	Maximum
1-2	8 or 9 with 3 GFS	2	0 5	1.1	1.3	1.6	1 6	1.8	1.8	1.7	2.0	2.1	2.4	2.4	0.5	0.6	4.0	0.02	0.55
1-5		10	1.2	3.4	5.0	5.6	4.3	5.7	3.9	5.0	3.9	5 3	5.6	6.2	2.8	2.9	20 1	0.11	3 01

[1] Total number of chords: 120

be as low as 20-50. However, to recover chords between grid stations in the desired centimeter level ($|D_{R_{ij}}| < 3$ cm), this optimum number was found to be 500 (section 1.2).

In the current investigation, the effect of number of observations to each station for two main station groupings and different ranging precisions has been further studied. The case of 500 observations to a station uses all the 21 satellite passes while the other case involves the first ten passes, viz., 4 to 28 (Section 2.3.1). The random number used to incorporate noise was different in each case.

Table 5-9 compiles comparative results for the effect of number of observations per station in an extended station grid, both in terms of σ_R and $|D_R|$ for chords up to 60 km. The tabulated values of σ_R and $|D_R|$ do not refer to the same chord.

In the case of station grouping in eights or nines with 3 GFS, the decrease in observations per station from 500 to 250 results in a deterioration of about 50% both in σ_R and $|D_R|$. However, this deterioration is about 100% in the case of stations in groups of six and without any fundamental station.

5.1.6 Accuracy estimation

Figure 5-5 shows the error ellipses for φ and λ at the selected grid stations and chords between them (Figure 5-2) for solution No. 1-10, i.e., with inner constraints only (Table 4-1). The ellipses for different chords show better recovery precision in the center of the grid as compared to SE and NW corners and the maximum error (as shown by the error ellipses) is about 1.5 cm in length. The differences $D_{R_{ij}}$ for some of the chords have also been indicated in Figure 5-5, along side the ellipses, for comparison.
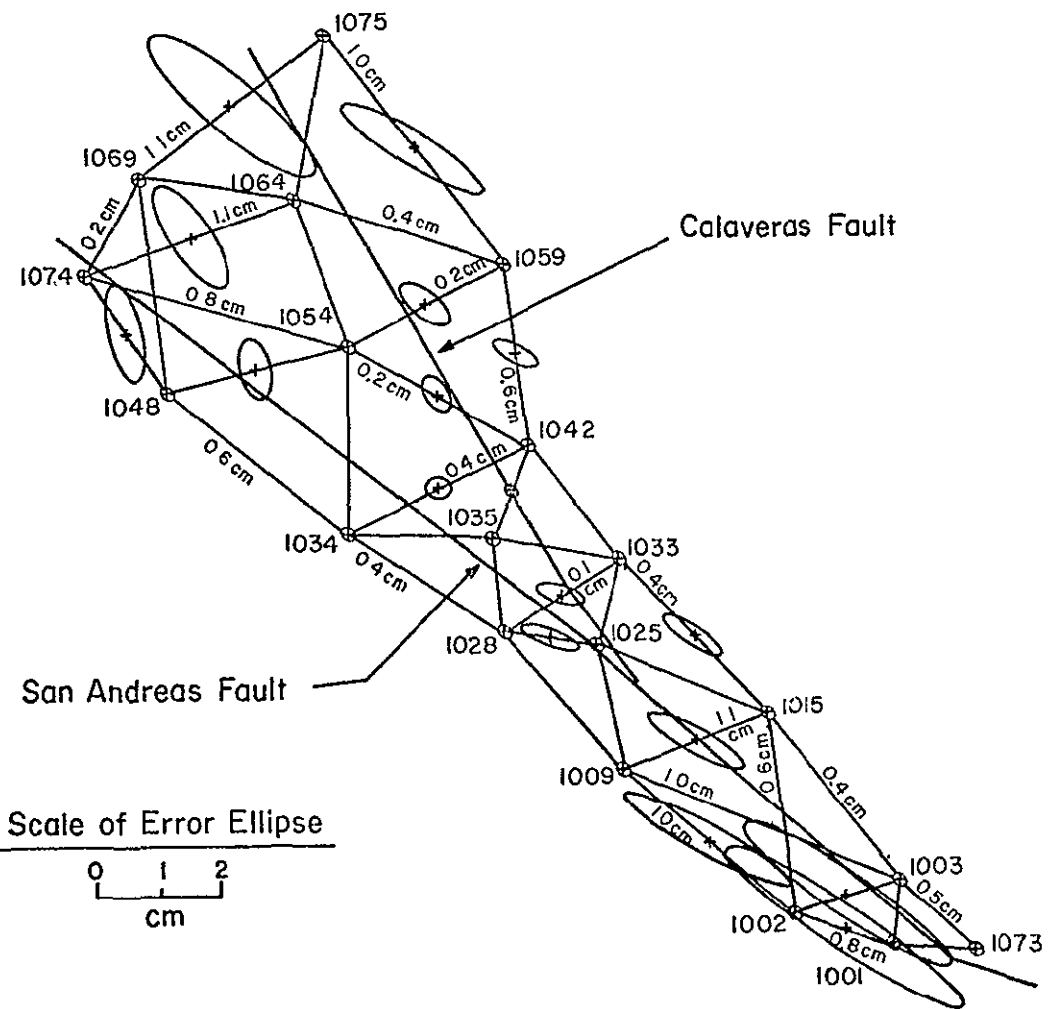
In comparison, when the same data (as in the above case) is solved with three LFS's held fixed (Solution No. 1-9), the error ellipses show a very uniform trend in size and shape over the entire grid (Figure 5-6). In

Table 5-9

Effect of Number of Observations to Each Station, Geometric Mode
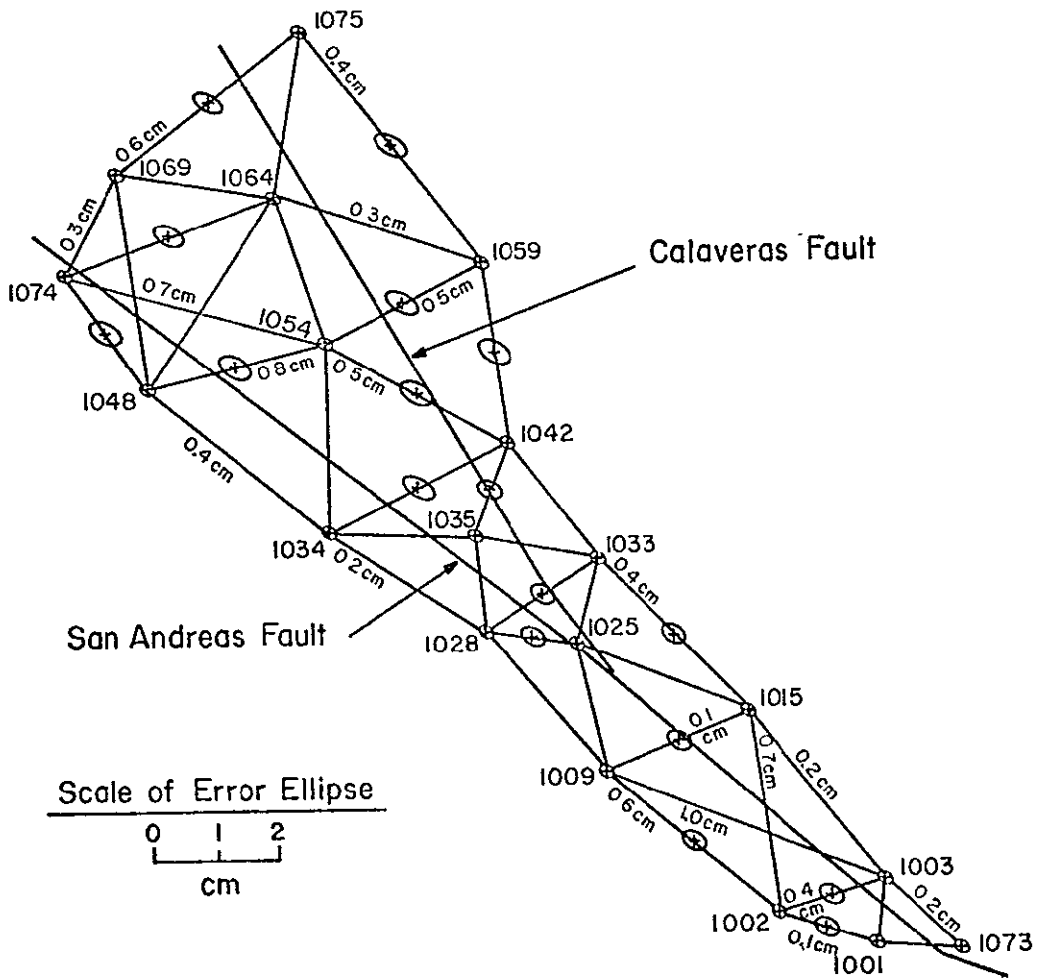
Solution No.	No. of Observations to Each Station	Station Grouping per Event	Maximum σ_R (cm) and Maximum Absolute Difference $	D_R	$ for Chords up to 60 km[1]				Remarks
			$R \leq 40$ km		$R \leq 60$ km		
			σ_R	$|D_R|$	σ_R	$|D_R|$	
1-5	500	8 or 9	5.0	3.4	6.5	5.0	$\sigma_r = 10$ cm
1-6	250	with 3 GFS	7.8	5.5	10.3	6.5	
1-14	500	6	10.6	21.7	12.8	28.2	"
1-15	250	no FS	21.7	44.8	27.5	47.7	
1-2	500	8 or 9	1.0	1.1	1.2	1.3	$\sigma_r = 2$ cm
1-3	250	with 3 GFS	1.5	1.4	2.0	1.9	

[1] Tabulated values do not refer to the same chord.

91

Figure 5-5. Error Ellipses for Solution No. 1-10 with
Inner Constraints, Geometric Mode

Note : The numbers entered along the
chords are $D_{R_{ij}}$

Note: The numbers entered along chords are $D_{R_{ij}}$

Figure 5-6: Error Ellipses for Solution No. 1-9 with Three Laser Fundamental Stations (LFS) Held Fixed, Geometric Mode

93

this case, the maximum error for any chord is about 0.5 cm. The differences $D_{R_{ij}}$ show no significant change from Solution No. 1-10.

5.1.7 Crustal motion

In order to recover the simulated crustal motion (Section 3.2), two solutions, Nos. 1-4 and 1-9, were carried out with $\sigma_r = 2$ cm at epoch t_0 and t_1 ($= t_0 + 12$ months) respectively. In these solutions three distant laser fundamental stations, viz., 1076, 1077, and 1078 were assumed stationary and their positions at epoch t_0 were held fixed in both solutions.

Using the results of the above-mentioned solutions, Figure 5-7 shows the recovered velocity vectors at some of the grid stations (Figure 5-2) for three areas of Figure 3-2. In the case of areas I and III, the directions of velocity vectors are consistent with the simulated directions; while for area II, there is no systematic pattern, as expected.

Noting that the velocity vectors in Figure 5-7 are recovered through error propagation from a very large number of observations, the normal distribution is assumed in computing the confidence interval for the true or theoretical mean $\mu = \overline{V}$ taking $\alpha = 0.05$, and rejection criteria $\overline{\Delta V}$ for power $1-\beta$ equal to 0.80 and 0.90 (section 2.2.6).

Table 5-10 shows the results regarding the recovery of velocity vector $\overline{V}_i$ at individual stations for three areas I, II, and III (Figure 3-2), confidence interval at significance level $\alpha = 0.05$ and rejection criteria $\overline{\Delta V}$ for power $1-\beta$ equal to 0.80 and 0.90. Time interval considered for computing the velocity vector in Table 5-10 between the two recoveries is 12 months. It will be seen that the magnitude of the velocity vector is recovered better in comparison to its direction as the direction recovery is more sensitive to small deviations in the system's performance. For area II, the recovery for direction cosines is too arbitrary.

Knowing the simulation setup, Table 5-11 groups the results of Table 5-10 area-wise with respect to block velocity vector(for weighted mean $\overline{V}$).

94

For Area II.
μ = 0.0 cm
$\bar{x}$ = 0.6 ± 0.1 cm

38°N

1075 (4 2 ± 0 4)

38°N

1069 (0.5 ± 04)

1064 (0.5 ± 0.3)

1074 (3 3 ± 0 4)

1059 (4.2 ± 0.4)

Calaveras Fault

I

1054 (0.7 ± 0.4)

1048 (4.0 ± 0.4)

For Area
μ = 4.0 cm
$\bar{x}$ = 4.1 ± 0.1 cm
For Area

For Area
I μ = 4.0 cm
   $\bar{x}$ = 3.9 ± 0.1 cm

1042 (3.8 ± 0.4)

37°N

III

1034 (4.3 ± 0.4)

1035 (0.5 ± 0.4)

1033 (3.7 ± 0 4)

37°N

1028 (4.3 ± 0.4)

1025 (1.1 + 0.5)

San Andreas Fault

1013 (4.0 ± 0.4)

1009 (3.7 ± 0.4)

1003 (3.7 ± 0.4)

1002 (4.5 ± 0 4)

1001 (44 ± 0.3)

1073 (4.2 ± 0.4)

36°N

237°E

238°E

239°E

36°N
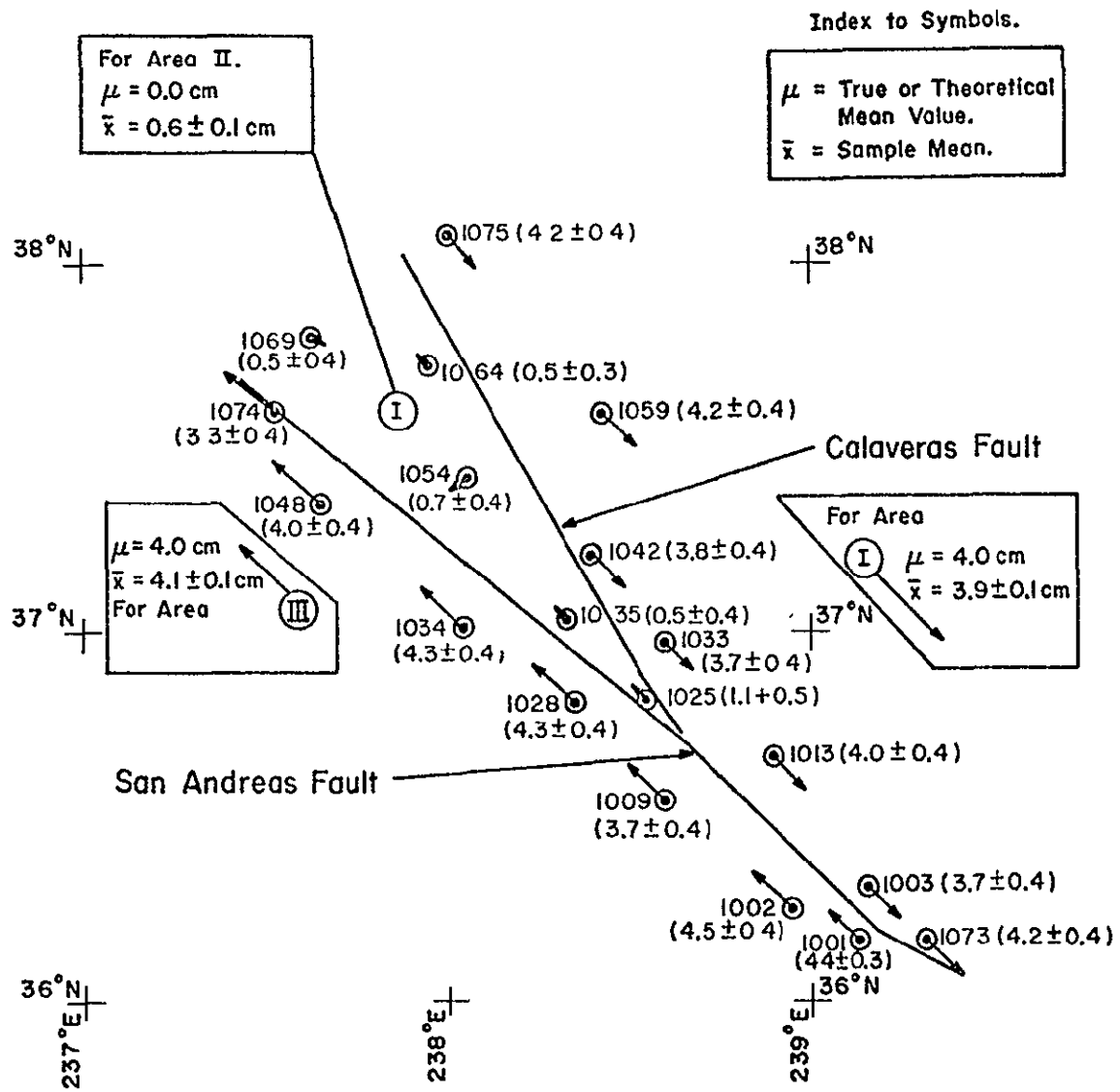
Figure 5-7   Recovery of Velocity Vector (cm) , Geometric Mode
              (250 observations to each station; σ_r = 2 cm; Solution
              Nos. 1-4 and 1-9).

Table 5-10

Recovery of Velocity Vector for Grid Stations, Geometric Mode

(250 Observations to Each Station, $\sigma_r = 2$ cm)

Recovery of Velocity Vector for Individual Stations	Velocity Vector	True or Theoretical Value μ	Sample Recovery $\overline{V}_i$		Standard Deviation $\sigma_{\overline{V}_i}$ ^{s}	Confidence Interval for $\overline{V}_i$ at $\alpha = 0.05$	Rejection Criteria $\Delta\overline{V}_i$ for	
			Magnitude				Power $1-\beta$ = 0.80	Power $1-\beta$ = 0.90
			Min.	Max.				
Area I	Magnitude(cm)	4.0	3.2	4.5	0.4	$3.2 < \overline{V}_i < 4.8$	1.1	1.3
	Direction Cosines	0.30	0.06	0.41	0.04	$0.22 < \overline{V}_i < 0.38$	0.11	0.13
		-0.72	-0.85	-0.66	0.06	$-0.84 < \overline{V}_i < -0.60$	0.16	0.19
		-0.63	-0.72	-0.49	0.08	$-0.79 < \overline{V}_i < -0.47$	0.22	0.26
Area II	Magnitude(cm)	0.0	-0.2	1.0	0.5	$-1.0 < \overline{V}_i < 1.0$	1.4	1.6
	Direction Cosines	not defined	-0.84	0.87	0.57*	Columns 7 to 9 Not Applicable		
			-0.95	0.97	0.80*			
			-0.59	0.91	0.49*			
Area III	Magnitude(cm)	4.0	3.3	4.8	0.4	$3.2 < \overline{V}_i < 4.8$	1.1	1.3
	Direction Cosines	-0.30	-0.45	-0.04	0.10	$-0.50 < \overline{V}_i < -0.10$	0.28	0.32
		0.72	0.64	0.85	0.08	$0.56 < \overline{V}_i < 0.88$	0.22	0.26
		0.63	0.49	0.71	0.08	$0.47 < \overline{V}_i < 0.79$	0.22	0.26

*Values fluctuate between wide limits.

^{s} Tabulated values indicate the worse case in Figure 5-7

Table 5-11

Recovery of Velocity Vector for Area Blocks[1], Geometric Mode

(250 Observations to Each Station; σ_r = 2 cm)

Recovery of Velocity Vector (Weighted Mean) for Area Blocks	Velocity Vector	True or Theoretical Value μ	Sample Mean $\overline{V}$ [2]		Confidence Interval for $\overline{V}$ at α = 0.05	Rejection Criteria $\Delta\overline{V}$ for	
			Magnitude	Standard Deviation		Power $1-\beta$ = 0.80	Power $1-\beta$ = 0.90
Area I	Magnitude (cm)	4.0	3.9	0.1	$3.8 < \overline{V} < 4.2$	1.5	1 5
	Direction Cosines	0.30	0.22	0.01	$0.28 < \overline{V} < 0.32$	0.15	0.15
		-0.72	-0.71	0.01	$-0.74 < \overline{V} < -0.70$	0.15	0.15
		-0.63	-0.66	0.02	$-0.67 < \overline{V} < -0.59$	0.30	0.30
Area II	Magnitude (cm)	0.0	0.6	0.1	$-0.2 < \overline{V} < 0.2$	1.5	1.5
Area III	Magnitude (cm)	4.0	4.1	0.1	$3.8 < \overline{V} < 4.2$	1 5	1.5
	Direction Cosines	-0.30	-0.21	0.02	$-0.34 < \overline{V} < -0.26$	0.30	0.30
		0.72	0.74	0.02	$0.68 < \overline{V} < 0.76$	0.30	0.30
		0.63	0.61	0.02	$0.59 < \overline{V} < 0.67$	0.30	0.30

[1] Refer Figure 3.2.

[2] Sample size n = 25.

For area II, only values pertaining to magnitude are given.

These results also show that a small value of direction cosine (say
< 0.30) will be more difficult to recover satisfactorily. However, in areas
of no motion—or extremely small rate of crustal motion, say less than 1.5
cm (a value obtained from the rejection criteria in Table 5-10, columns 8 and
9, line 5)—the recovery of direction of motion will continue to be unsatis-
factory due to its extreme sensitivity to station position recovery and its lack
of definition in the case of no motion.

Using the rejection criteria of 1.6 cm (with power $1-\beta = 0.90$) as the
most conservative case of recovery for velocity magnitude of 4 cm per year,
the minimum time Δt is given as follows:

$$\Delta t = \frac{1.6}{4.0} \quad \text{year}$$

$$\approx \quad 5 \quad \text{months}$$

Time intervals for different direction cosines (Table 5-10, lines 3 and
4) can similarly be computed.

It may be pointed out here that in a system's recovery for velocity
vector (as set up between solutions 1-4 and 1-9), the recovery is extremely
sensitive to the number of observations to each station, station grouping, and
participation of three LFS's in an event, but not to the satellite pass configur-
ations (Figure 2-3). More so, in this study, the observations are assumed to
be free of systematic error and to have a diagonal weight matrix—an assump-
tion which may not be fully met in practice. As regards the equality of variance-
covariance matrices (Section 2.2.6), the test as suggested by Box [Winer,
1962] could not be successfully applied for the large size of matrices involved
in the present study. To avoid this difficulty of testing the equality of ΣX_{t_0}
and ΣX_{t_1}, the recovery of velocity vectors (Figure 5-7)was performed by
using ΣX_{t_0} for both the epochs t_0 and t_1. In another recovery, the variance-
covariance matrix ΣX_{t_1} was used for these epochs. The results do not show any

significant variations and are quite stable in spite of some noticeable differences being present in variances and covariances between ΣX_{t_0} and ΣX_{t_1}.

However, additional statistical analysis for equality of variance-covariance matrices and Hotelling's T^2 test [Rao, 1973] to test the hypothesis that the entire set of velocity vectors obtained for a network is compatible with the theoretical model are recommended.

Furhter, the results of Table 5-10 can be projected for comparative system recovery with respect to ranging accuracy $\sigma_r = 10$ cm. The corresponding time interval in a similar experimental setup for recovery of magnitude only would be 25 months. Appropriate increase in time interval would also be necessary if the rate of crustal motion is less than 4 cm per year (Section 3.2).

5.2 Short Arc Mode

In view of the basic necessity of fundamental stations and the constraints applied to them to obtain the definition of system origin and orientation (Section 2.2.3 (b)) for short arc mode, only a recovery analysis was performed for quantities least affected by the systematic modeling errors, namely, the distances between the grid stations and represented in terms of differences $D_{R_{ij}}$ between the recovered distances and the true distances between them. The representative chain (Figure 5-2) of chords between the station was also used in this mode with suitable modifications in case of regional solutions (Section 3.4.2).

In the final analysis which compares the geometric mode against the short arc mode, the common denominator of the analysis was this recovery of the distances between the grid stations.

5.2.1 Number of grid stations per pass

In this section, four main categories of number of stations per pass, viz., 33%, 50%, 67%, and 100% of the total number of stations in the grid,

were considered (Section 3.4.2). The investigations were carried out as follows:

(a) Firstly, to obtain a broad outlook about the system's capability for recovery of any station-to-station distance, a general plot (Figure 5-8) of differences $D_{R_{ij}}$ (cm) against the corresponding chord distances R_{ij} (km) between any two grid stations of Figure 5-2 was prepared. It is noticed that all the recovered differences (in short arc mode solution) are negative—a scale-type effect. The reason for this effect is unexplained at the present time.
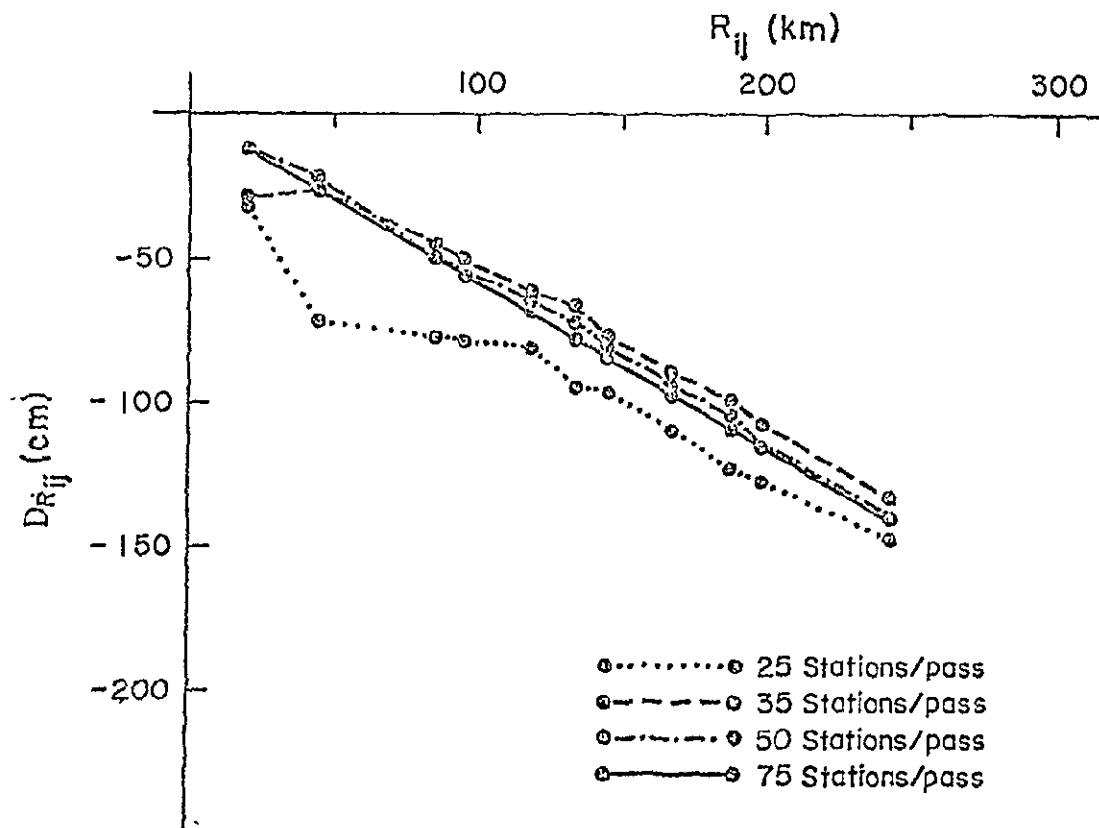
Figure 5-8   Effect of Number of Grid Stations per Pass on Recovery of Chords, Short Arc Mode
(500 Observations to Each Station; $\sigma_r = 10$ cm)

The differences $D_{R_{ij}}$ increase almost linearly with the chord distances when all 75 stations are observed by the satellite in all the passes and the maximum difference is 1.39 m for a corresponding R_{ij} of 243 km.

However, this linear trend starts showing deviations with the decrease in number of grid stations observed per pass. In the case of 35 stations (about 50% of the total grid stations) observed per pass, the differences are greater for $R_{ij} < 45$ km and smaller for $R_{ij} > 45$ km when compared to the case of 75 stations observed per pass. The recovery trend deteriorates further with the decrease in number of stations observed per pass to 25 (about 33% of the total number of grid stations).

(b) Secondly, the analysis of these recovered differences $D_{R_{ij}}$ was narrowed to chords between adjacent grid stations only (Figure 5-2). Table 5-12 shows the percentage recovery for various differences (for $R_{ij} \leq 60$ km) grouped according to their magnitude in seven intervals.

The above results show that the decrease in number of stations (from the total grid) observed in a pass does influence adversely the system's recovery and a limiting value for the same may be about 50% in any grid. In addition, it was observed during the setting up of these experiments that a grid station must be observed in at least two satellite passes for satisfactory recovery.

5.2.2 Selection of fundamental stations

The importance of observing three "distant" fundamental stations in any pass and inclusion of such observations in a short arc mode solution has already been established in the earlier study (Section 1.2). The study under this section was carried out to investigate whether such fundamental stations can be selected from the grid stations themselves. The results obtained are presented as follows.

(a) Table 5-13 shows a general recovery with the three different types of fundamental stations (Section 2.2.3 (b)) and there seems to be no significant change as the distance between fundamental stations is altered from 80 km (in

Table 5-12

Effect of Number of Grid Stations Observed per pass on

Recovery of Chords ($R_{ij} \leq 60$ km), Short Arc Mode

(500 Observations to Each Station; $\sigma_r = 10$ cm)

| Solution No.	Total No. of Stations in the Solution	No. of Stations per Pass	Fundamental Stations Used	Percentage of Absolute Differences $\lvert D_{R_{ij}} \rvert$							Maximum $\lvert D_{R_{ij}} \rvert$		Relative Precision [1]
				0-5 cm	5-10 cm	10-15 cm	15-20 cm	20-25 cm	25-30 cm	>30 cm	cm	ppm	$\sigma_{R_{ij}} / R_{ij}$ ppm
2-1	75	75	3 GFS	—	10	24	16	20	10	20	64.8	10	3
2-2	75	50	3 GFS	—	9	24	14	18	13	22	62.9	12	4
2-3	75	35	3 GFS	—	5	15	20	15	20	25	60.2	12	4
2-4	75	25	3 GFS	—	4	35	10	12	14	25	74.7	15	12

[1] The number tabulated refers to the worst case in the solution.

Table 5-13

Effect of Fundamental Stations on Recovery of Chords, Short Arc Mode
(500 observations to each station, $\sigma_r = 10$ cm)

Solution No.	Total Stations in the Solution	Stations per Pass	Funda-mental Stations Used[1]	Maximum Absolute Differences $D_{R_{ij}}$ (cm) for Different Chord Lengths (km)									
				< 20	20 to 40	40 to 60	60 to 80	80 to 100	100 to 120	120 to 140	140 to 160	160 to 180	180 to 200
2-3	75	35	3 GFS	31	28	36	70	76	68	75	84	95	120
2-5	75	35	3 PFS	29	53	39	41	46	54	55	76	79	83
2-6	75	35	3 LFS	19	31	31	44	45	53	63	72	77	87

[1] Section 3.1.2

case of GFS) to 1000 km (incase of LFS). The trend in absolute differences

$D_{R_{i\,j}}$ to increase with the chord distance between grid stations is present

in all the three cases but the rate of deterioration in the recovery being more

in the GFS case as compared to the other two cases.

In case of solutions Nos. 2-3 and 2-5 having three fundamental stations

selected from the grid itself, unusually large residuals pertain (in practically

all the cases) to chords having one of their end points at these PFS and GFS

stations.

This adverse characteristic of GFS or PFS would then rule out the

possibility of their selection as fundamental stations in any recovery through

short arc mode.

(b) In view of the preceding subsection (a), further investigations were

restricted to the three distant LFS case only. Table 5-14 contains the recovered

differences $D_{R_{i\,j}}$ for chords in two categories, viz., $R_{i\,j} \leq 20$ km and from 20

km to 60 km in length.

In order to study in more detail the recovery of chords ($R_{i\,j} \leq 20$ km)

and to make the sample more representative, 35 additional chords (other than

those included in Figure 5-2) were investigated in this category.

Thus, it will be seen that as the station network was extended from the

preliminary grid of nine stations (Section 1.2) to the present grid of 75 stations

(Section 3.1), the short arc mode has shown signs of deterioration in recovery

of relative positions. Even for chords ($R_{i\,j} \leq 20$ km), 28% of the cases now

have differences (between the recovered and the "true" relative positions)

greater than 10 cm as compared to none in the preliminary study (Table 1-1,

line 6).

A likely reason for this adverse trend in system's recovery may also be

attributed here to the "decrease" in percentage of the number of stations

observed in any satellite pass in the present solution as compared to all the

grid stations observed in all the passes--a very stringent condition in itself to

fulfill.

Table 5-14

Recovery of Chords[1], Short Arc Mode

(500 observations to each station; $\sigma_r = 10$ cm)

Solution No.	Total Stations in the Solution	Stations per Pass	Funda- mental Stations Used	Percentage of Absolute Differences					Maximum Differences cm
				0-5 cm	5-10 cm	10-15 cm	15-20 cm	>20 cm	
$R_{ij} \leq 20$ km									
2-6	75	35	3 LFS	38	34	14	14	0	19.8
20 km < $R_{ij} \leq 60$ km									
2-6	75	35	3 LFS	18	24	20	20	18	31.4

[1]Total number of chords tested: 109

5.2.3 Regional approach

To obviate the practical difficulty in meeting the requirement of "minimum" number of stations (in an extended network) being observed by the satellite in any pass (Section 5.2.1), another possible approach considered for investigation was to "break" up the area under study into smaller regions (Section 3.4.2) with some common stations in the overlapping zones.

In this setup, the problem may give rise to the following two questions:

(1) How is the recovery of relative positions within a region affected with this "break-up" when compared with the recovery of the total network.

(2) How is the recovery of "inter-regional" relative positions between two adjoining regions when compared with the recovery of the same relative positions within the total network.

(1) <u>Recovery of relative positions within any one region.</u> Figure 5-9 shows a general study for the recovery of relative positions between stations in case of regions "A" and "B" (Section 3.4.2) in comparison to a 75-station solution for the total network.

All three solutions plotted in Figure 5-9 have the same percentage ($\sim 67\%$) of the number of stations observed in any satellite pass and the three GFS as fundamental stations.

The "smaller" regional solutions, in general, show an improvement of about 15-20% in the recovery of relative positions as compared to the 75-station solution.

Further, Table 5-15 shows a more specific investigation regarding the recovery of relative positions ($R_{ij} \leq 20$ km) in case of regional solutions.

The results indicate that about 20% differences are still not recovered within 10 cm limit (Table 1-1, line 6). However, the results in Tables 5-14 when compared with those in Table 5-15 (and reviewed in light of Figure 5-9) indicate a possible deterioration in the system recovery with the increase in number of stations in the solution.

106

Figure 5-9   Recovery of Chords in Regional Solutions, Short Arc Mode
(500 observations to each station; σ_r = 10 cm)
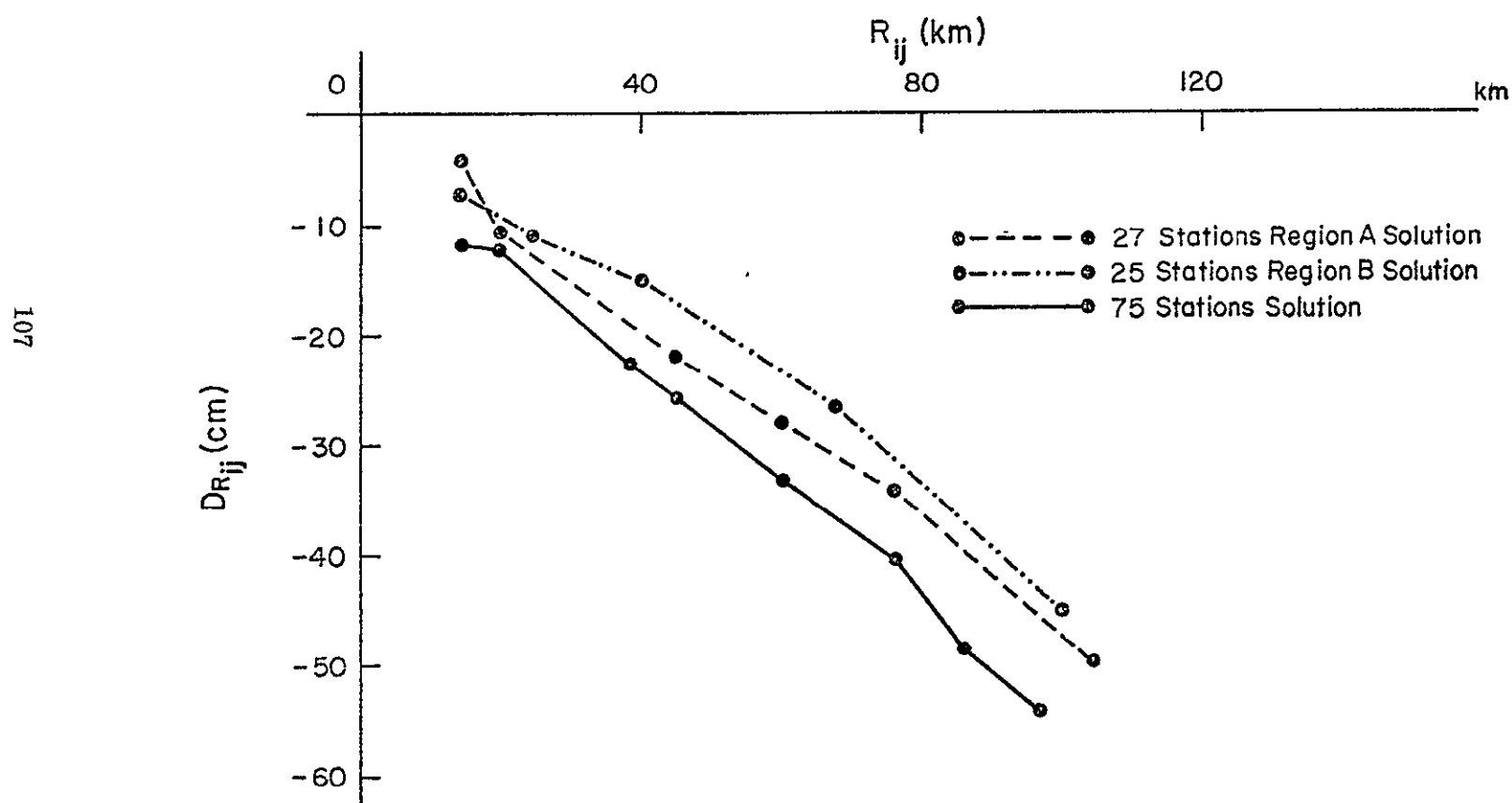
Table 5-15

Recovery of Chords ($R_{ij} \leq 20$ km) in Regional Solutions,

Short Arc Mode

(500 Observations to Each Station; $\sigma_r = 10$ cm)

Solution No.	Total No. of Stations in the Solution	No. of Stations Observing Any Pass	Percentage of Absolute Differences			Maximum Difference	
			0-5 cm	5-10 cm	>10 cm	cm	ppm
2-7	27	17	40	40	20	13.1	8
2-8	25	16	41	42	17	11.8	7

(2) <u>Recovery of inter-regional relative positions</u>. Table 5-16 shows the recovery of absolute differences for inter-regional chords between two adjoining regions, say "A" and "B" in the present case, from the two separate regional solutions (Nos. 2-7 and 2-8) and from a solution (No. 2-2) containing total network.

The results in both the cases are of the same quality, and thus indicate towards the possible approach of breaking a large network into smaller regions and expecting comparable results, if not better.

5.2.4 <u>Recovery of station coordinates</u>

In order to study the recovery of station coordinates, Figure 5-10 shows
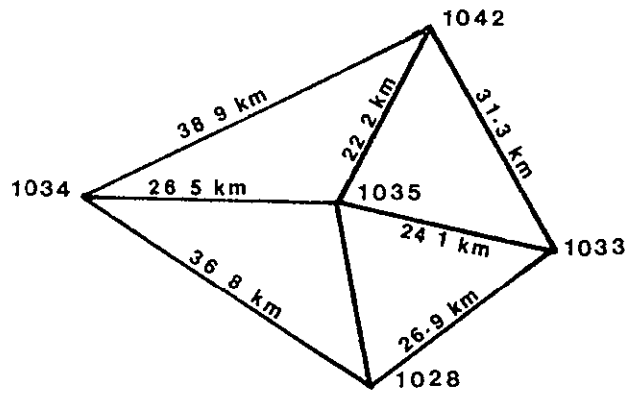
Figure 5-10 A Typical Five-Station Setup

Table 5-16

Recovery of Inter-regional Chords, Short Arc Mode

(500 observations to each station; $\sigma_r = 10$ cm)

Solution No.	Total Stations in the Solution	Stations per Pass	Maximum Absolute Differences (cm) for Different Chord Lengths (km)					
			< 20	20 to 40	40 to 60	60 to 80	80 to 100	> 100
2-7 2-8	27 25	17 16	16.7	22.6	32.1	37.0	48.4	67.3
2-2	75	50	14.0	23.8	36.6	42.9	59.0	79.9

a typical centered pentagon as taken from Figure 5-2. The recovery in terms of the above five grid stations for the solution No. 2-6 with three "distant" fundamental stations (Section 5.2.2) are listed in Table 5-17.

Subtracting the residuals in X, Y, Z of station No. 1035 (the central station in Figure 5-10) from all the other stations and plotting the differences, Figure 5-11 shows clearly that the distances between the grid stations were not recovered in the desired centimeter level. Studies of other similar figures in the grid also showed residual patterns of a type similar to those in Figure

Table 5-17

Recovery of Grid Station Coordinates, Short Arc Mode
(500 observations to each station; σ_r = 10 cm)

Solution No.	Grid Station No.	Correction to Station Coordinates		
		Δx (m)	Δy (m)	Δz (m)
2-6 (with 3 LFS)	1028	1.32	0.11	0.33
	1033	1.37	0.31	0.19
	1034	1.44	0.01	0.25
	1035	1.32	0.27	0.28
	1042	1.28	-0.40	0.42

5-11 and indicated no systematic pattern.

5.2.5 Accuracy estimation

With reference to Section 5.1.6, Figure 5-12 shows the error ellipses for φ and λ at the selected grid stations and chords for short arc mode solution No. 2-6. This solution can be compared to solution No. 1-9 of the geometric mode (Figure 5-6).

In the present case, the errors, both for the station positions in φ and λ and for middle points of the chords, are about one order of magnitude larger than the geometric mode. Figure 5-12 also shows that the system's recovery is definitely not in the centimeter level for the short arc mode in its present state.

110

$\delta \triangle X$ (cm)

$\delta \triangle Y$ (cm)

$\delta \triangle Z$ (cm)
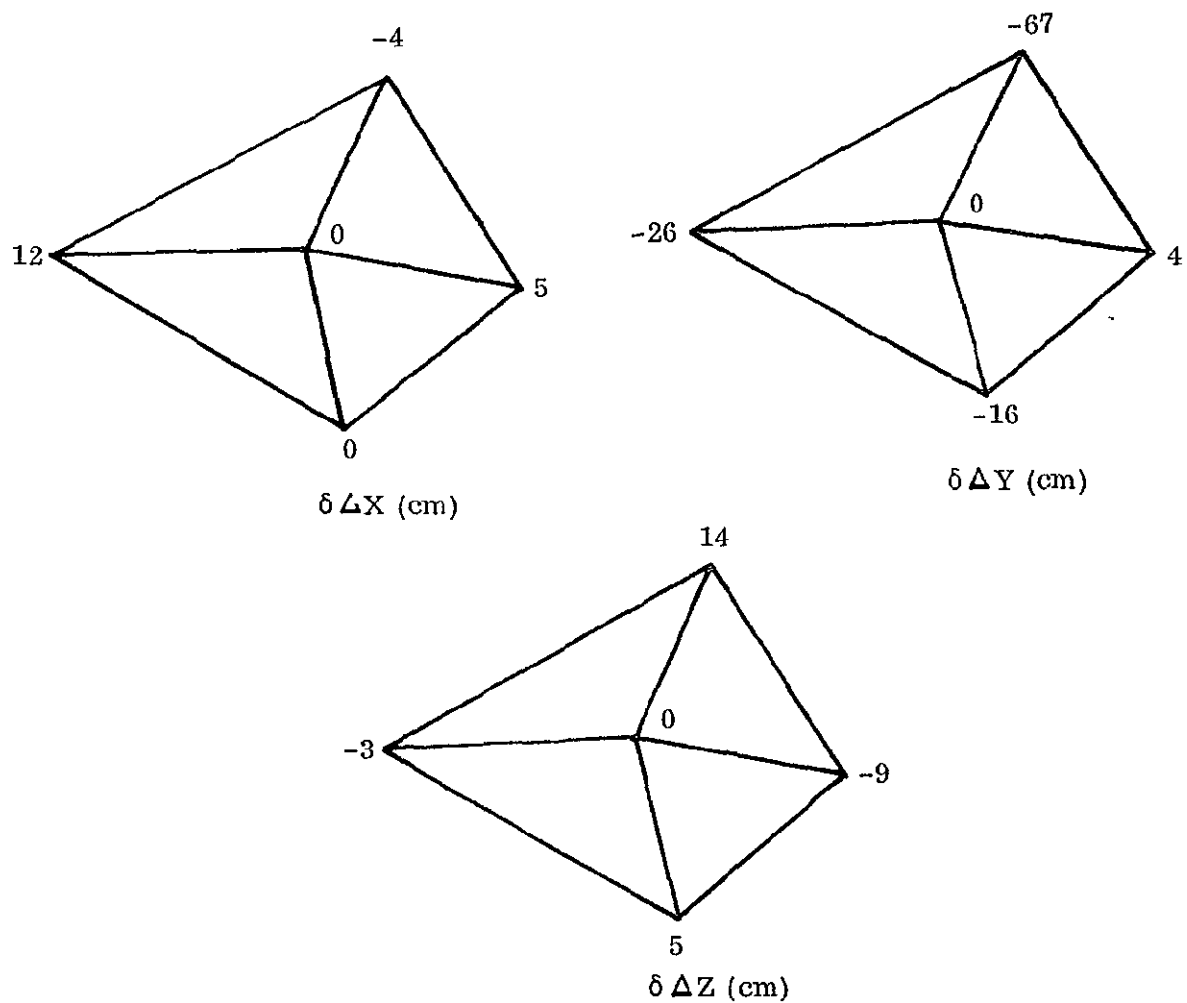
Figure 5-11   Relative Recovery of Station Coordinates,
Short Arc Mode
(Refer to Table 5-17)
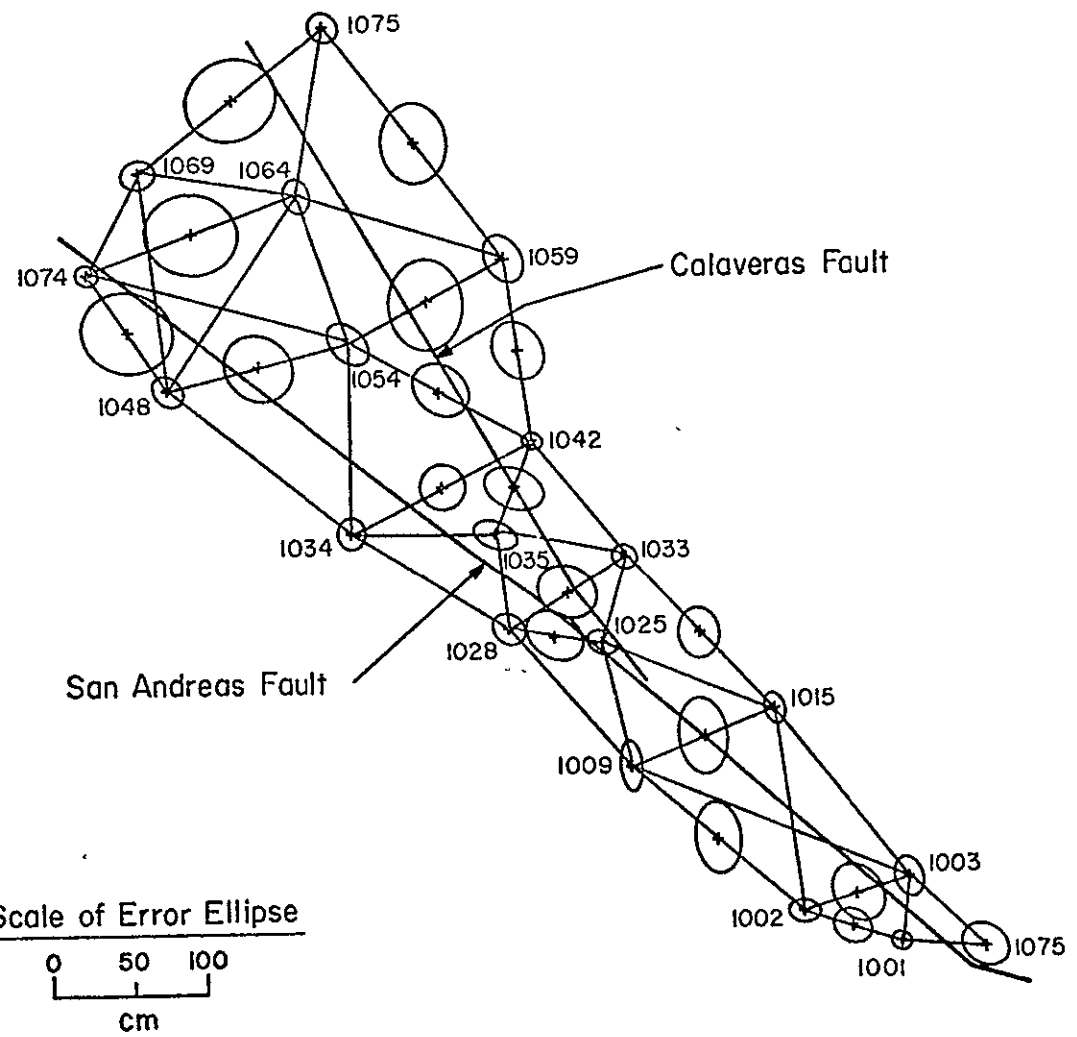
Figure 5-12   Error Ellipses for Solution No. 2-6 with Three
Laser Fundamental Stations (LFS) Held Fixed,
Short Arc Mode

112

6. SUMMARY AND CONCLUSION

The present simulation study to monitor crustal movements in the San Andreas fault zone by a satellite-borne ranging system takes off from the findings and the results of its predecessor [Mueller et al., 1975]. In this investigation, the scope of the experiment has been extended to enlarge the station network to 75 stations, to simulate crustal movements through the introduction of changes in the relative positions of the grid stations, to model weather effect for intervisibility between station and satellite and subsequent loss of observations due to bad weather, and to study the recovery of relative positions and motion rates.

The station grid covers an area between 36°N and 38°N latitudes, and 237°E and 239°E longitudes, with station-to-station distance varying from 5 - 30 km with roughly half of the stations on either side of the faults. In addition, the following two features were also incorporated:

(a) Ten original grid stations (Nos. 1021 to 1030) were replaced by ten stations at one-minute intervals as an attempt for densification of control. The recovery of relative positions in this close network was then studied as an additional feature.

(b) The location/selection of three distant "fundamental stations" was also investigated and three possible choices have been included as alternatives. In the first case these stations have been located at ground laser station sites outside the grid and termed as laser fundamental stations (LFS), while in the other two choices these stations are parts of the grid itself and their locations within the grid are the distinguishing feature--peripheral fundamental station (PFS)--when they are located at the periphery of the grid, or grid fundamental station (GFS) when

113

they are located within the grid.

The laser radar has been retained as the main measurement system in the study pending final selection from many possible candidates. In addition to the already feasible laser precision of 10 cm, the ranges have also been generated, both in simultaneous and (nonsimultaneous) sequential modes, for standard deviations σ_r equal to 2 cm. In place of circular polar orbits in the previous study, the satellite orbit has been inclined at 110° and made eccentric to provide ranging to orbital altitudes from 370 km to 930 km. The feature of airplane flights at 10 km altitude has also been retained. The software used for generating satellite orbits and airplane flights was the Goddard Trajectory Determination System (GTDS).

The ranges generated were in two observational modes, simultaneous and nonsimultaneous (or sequential), and were utilized in the following two methods and computer programs to study the station recovery.

A. Geometric Adjustment -- This method uses the geometry of an event which has been observed from the satellite simultaneously to four or more ground stations. From the numerous possible station grouping and observational patterns, four schemes for satellite and one for airplane case have been investigated. The computer program utilized was The Ohio State University Geometric and Orbital (Adjustment) Program (OSUGOP) for satellite observations after suitable modifications [Reilly et al., 1972; Appendix C]. The system's recovery was expressed in terms of estimable quantities, the chord lengths between grid stations and the angles between chords, and was also analyzed through the standard deviations of the recovered chords and angles.

The weather effect has been modeled in a straightforward and simplified manner as compared to real nature. The "probability of sighting" or the probability factor ($0 < PF < 1$) assigned to any station in the grid signifies the probability whether that station may or may not be able to participate in any observational scheme. This affects the system in two ways: (1) total

114

number of stations observed simultaneously in any event, and (2) total number of observations to a station finally available for inclusion in the solution. In overall effect, the weather scheme included has resulted in about 10% observations to a station.

The crustal motion model was simulated by creating actual changes in the relative positions of the grid stations. The constant rate of motion, as assumed in this study, represents about 3 cm drift in latitudinal and longitudinal directions which is about 4 cm total horizontal motion per year. No vertical motion was considered. Using this motion rate, two time epochs, t_0 and t_1 $(= t_0 + 12$ months) were considered and station locations referred to these epochs were then designated as CM00 and CM12. The station position as a function of time between two epochs was then utilized to investigate the recovery of motion rate for (1) the minimum time interval required between two sets of observations for a given ranging accuracy, say $\sigma_r = 2$ cm, and (2) the effect of a change in ranging accuracy on this minimum time interval. For this three distant laser stations (LFS) were assumed stationary and were held fixed in both the recoveries at epoch t_0 and t_1 .

In the statistical analysis of the recovery of motion rate, both α and β type errors were investigated. The α error signifies a preassigned chance of rejecting the hypothesis in cases when the hypothesis is true. Using the same, say at 0.05 level, the computed confidence interval provided an insight towards the quality of the recovered velocity vectors. In the case of β error, the power $1-\beta$ provided the rejection criteria at preassigned levels of 0.80 and 0.90 when the hypothesis is not true.

Further, accuracy of station recovery was estimated through error ellipses and also compared in two types of constraints used in this study, viz., inner and absolute constraints at three LFS's.

B. Short Arc Adjustment — This approach applies the orbital constraints on the satellite points used and as such can also make use of non-simultaneous (or sequential) observations. Due to the positional constraints

on fundamental stations the recovery was mainly investigated in terms of
differences $D_{R_{i,j}}$ between true and adjusted chords. In addition, an error
ellipse analysis was also performed for comparison with geometric mode
(Figure 5-6). The software used for this adjustment was Short Arc Geodetic
Adjustment (SAGA) program (Appendix B).

In addition to the necessary and essential requirement of three funda-
mental stations observed in "all" the satellite passes, the importance of total
number of grid stations observed in any single pass was also recognized. As
the station grid would increase in number and the extent of ground coverage,
the percentage of stations (from the entire network) which can be observed in
any single pass would also affect the success of an observational scheme.
Four alternative schemes--where all the stations (100%) or some of the sta-
tions (say, 67%, 50%, and 33%) from the total grid stations are observed in a
pass--were investigated.

As an alternative to mitigate the above practical difficulty of a large
number of grid stations being observed from a large network in any single pass,
the breaking of the complete network into smaller regional networks was also
investigated.

6.1 Geometric Mode Results

The limiting critical degeneracies of this mode were reduced through
(1) extension of the station grid over a larger area, (2) separation of stations
in heights up to 1555 m as topographically permitted in central California, (3)
generation of ranges from different altitudes through selection of an elliptic
orbit and the addition of airplane flights, and (4) selection of suitable observa-
tional scheme.

The results in respect of recovery of station-to-station distances with
various setups of observational patterns and ranging accuracies and inclusion
of observations from airplane or to three fundamental stations included in
events has significant improvement on the system's recovery. In such cases,

116

even a loss of about 10% in total observations to each station due to adverse weather has only marginal effect (Table 6-1).

The results also indicate that any three grid stations, suitably located (either at the periphery or at the vertices of a triangle) within the grid, can replace three "distant" fundamental stations lying outside the grid.

Two station recoveries with 250 observations to each station observed in groups of eight or nine (including three LFS's) with $\sigma_r = 2$cm were performed at epochs t_0 and t_1 ($=t_0+$ 12 months). Table 6-2 gives the results for the recovery of velocity vector in the above case for two areas, one with 4 cm per year motion rate and one with no motion. The values tabulated for area blocks (Figure 3-2) are weighted according to individual variances. The recoveries of motion rate for magnitude at individual grid stations and for the area blocks, with or without motion, are within the confidence interval (except for area block type II) for α significance level equal to 0.05. The chance of rejecting the hypothesis (say for individual stations) $\overline{V} = 4.0$ cm (if the recovered velocity is < 2.7 cm or > 5.3 cm) is 0.90. Taking the worst case for $\Delta\overline{V}$ (line 9 and Col. 7, Table 6-2) the minimum time Δt for recovery of velocity vector magnitude comes out to be 5 months. It may be pointed out here that an approximately normal distribution has been assumed for $\overline{V}$ as the sample considered is large.

In case of direction for the velocity vector, the recovery of either small direction cosine values (Table 6-2, line 2) or direction cosines for areas of no motion (or with extremely small motion of 1-2 cm per year) will have individual characteristics. Each such recovery may require consideration on its own merit.

Thus, it will be seen that in general, the magnitude of the velocity vector is recovered better compared to its direction. The table can be appropriately modi-fied for changes in ranging accuracy of the system used, experimental setup, ob-servational errors and the velocity vector for rate of crustal motion involved.

In the error analysis for the station positions and the chords between grid stations, comparative study between two solutions, one with inner cons-traints and another with absolute position constraints on three LFS's, with identical data was also made through error ellipses. This showed that for the

117

Table 6-1

Recovery of Chords ($R_{ij} \leq 60$ km), Geometric Mode

(500 Observations to Each Station)

Total Stations Co-observed in an Event	Fundamental Stations Used	Weather Effect Modeling	σ_r cm	Observation Type		Percentage of Absolute Difference $|D_{R_{ij}}|$							Maximum Difference		Relative Precision [1]
				Satellite	Airplane	0-1 cm	1-2 cm	2-3 cm	3-4 cm	4-5 cm	5-10 cm	>10 cm	cm	ppm	$\sigma_{R_{ij}}/R_{\cdot\cdot}$ (ppm)
4	--	--	10	S	-	3	2	5	8	5	22	55	66 7	14 0	281
6	--	--	10	S	-	18	15	5	8	7	22	25	28.2	7 0	11
6	--	--	10	S	A	47	31	12	10	--	--	--	3.9	1 0	2
8 or 9	--	--	10	S	-	22	10	10	30	10	13	5	13.3	3.0	7
8 or 9	3 GFS	--	2	S	-	85	15	--	--	--	--	--	1.3	0.3	1
8 or 9	3 GFS	--	10	S	-	57	20	17	4	2	--	--	5.0	2.5	6
8 or 9	3 GFS	--	10	S	A	62	20	16	2	—	--	--	3.1	1.5	2
8 or 9	3 GFS	yes	10	S	A	57	18	15	8	2	--	--	4 8	2 5	6
8 or 9	3 GFS	yes	10	S	-	50	16	8	14	10	2	--	6.8	2 8	7
8 or 9	3 LFS	--	2	S	-	92	8	--	--	--	--	--	1.1	0 2	0.4
12	3 PFS	--	10	S	-	77	20	3	--	—	--	--	3.0	0.5	2

[1] The number tabulated is for the worst case in the solution.

Table 6-2

Recovery of Velocity Vector, Geometric Mode[1]

(250 Observations to Each Station; σ_r = 2 cm)

Type of Area (Figure 3-2)		Velocity Vector	True or Theoretical Value $|\mu|$	Sample Recovery $\overline{V}$ [s]			Confidence Interval for $\overline{V}$ at α = 0.05	Rejection Criteria $\Delta\overline{V}$ for	
				Magnitude		Standard Deviation		Power 1-β = 0.80	Power 1-β = 0.90
				Min.	Max.				
Area I or III	Individual Station	Magnitude(cm)	4.0	3.2	4.8	0.4	3.2 < $\overline{V}$ < 4.8	1.1	1.3
		Direction Cosines	0.30	0.04	0.45	0 10	0.10 < $\overline{V}$ < 0.50	0.28	0.32
			0.72	0.64	0.85	0.08	0.56 < $\overline{V}$ < 0.88	0.22	0.26
			0.63	0.49	0.72	0.08	0.47 < $\overline{V}$ < 0.79	0.22	0.26
	Area Block	Magnitude(cm)	4.0	3.9	4.1	0.1	3 8 < $\overline{V}$ < 4.2	1.5	1 5
		Direction Cosines	0.30	0.21	0.22	0.02	0.26 < $\overline{V}$ < 0.34	0.30	0.30
			0.72	0.71	0.74	0.02	0 68 < $\overline{V}$ < 0.76	0.30	0.30
			0.63	0.61	0 66	0.02	0.59 < $\overline{V}$ < 0.67	0.30	0.30
Area II	Individual Station	Magnitude(cm)	0.0	-0.2	1 0	0.5	-1 0 < $\overline{V}$ < 1.0	1.4	1.6
		Direction Cosines	not defined	-0.84	0.87	0.57*	Columns 7 to 9 Not Applicable		
				-0.95	0.97	0.80*			
				-0.59	0.91	0.49*			
	Area Block	Magnitude(cm)	0.0	0.6	0.6	0.1	-0.2 < $\overline{V}$ < 0.2	1.5	1.5

[1]Station grouping of 8 or 9 including 3 laser fundamental stations (LFS) and LFS considered stationary.
*Values fluctuate between wide limits.
[s]Tabulated values for area I or III are absolute and correspond to the worst case.

119

solution with inner constraints, the errors show a better trend in the center of the grid. However, in the case where three LFS's were held fixed, the errors showed a very uniform trend and maximum error was also less compared to the first case.

6.2 Short Arc Mode Results

In spite of having some inherent practical advantages in comparison to the geometric mode, the short arc mode approach showed signs of rapid decrease in quality of system's recovery as the total number of stations in the grid were increased to 75. Even three trial choices for fundamental stations, viz., from three "distant" ground laser station sites to three PFS's or GFS's within the grid itself, and inclusion of the extreme case when all the grid stations are observed in all the passes did not help the recovery of relative positions to desired centimeter level.

Further, even though the number of grid stations observed in any pass may not be as clear cut and decisive a factor as the inclusion of three fundamental stations observed in a pass, a pass of four-to-ten minute lengths for satellites at altitudes varying between 400 - 1000 km is so short a duration that favorable weather conditions occurring simultaneously at three "distant" fundamental stations and a definite minimum percentage, say 50 or over (Table 6-3, line 4), of all the grid stations in the network might be an extremely stringent requirement to meet. In the case where this percentage is below 50 (Table 6-3, line 3), the recovery deteriorates rapidly.

In an effort to bring the "distant" fundamental stations nearer and possibly select them from the grid stations themselves, it was noticed that unusually large differences occurred between the true and recovered station-to-station chords whenever these fundamental stations lay at one of the ends of these chords. This recovery feature thereby ruled out the possibility of selecting fundamental stations from the grid itself.

Table 6-3 contains the recovery results for short arc mode with respect to station-to-station chords ($R_{ij} \leq 60$ km) in various setups of number of

Table 6-3

Recovery of Chords ($R_{ij} \leq 60$ km), Short Arc Mode

(500 Observations to Each Station; $\sigma_r = 10$ cm)

Solution No.	Total Stations in the Solution	No. of Stations per Pass	Fundamental Stations Used	No. of Satellite Passes Used	Percentage of Absolute Differences $|D_{R_{ij}}|$							Maximum Difference		Relative Precision[1]
					0-5 cm	5-10 cm	10-15 cm	15-20 cm	20-25 cm	25-30 cm	>30 cm	cm	ppm	$\sigma_{R_{ij}}/R_{ij}$ (ppm)
2-8	25	16	3 GFS	7	4	15	20	21	20	16	4	32.7	7	3
2-7	27	17	3 GFS	7	4	12	19	26	19	15	5	34.2	8	4
2-4	75	25	3 GFS	7	-	4	35	10	12	14	25	74.7	15	12
2-3	75	35	3 GFS	7	-	5	25	15	15	20	20	60 2	12	4
2-5	75	35	3 PFS	7	-	10	26	16	22	16	10	52.9	12	4
2-6	75	35	3 LFS	7	-	16	24	20	18	20	2	31.4	7	3
2-2	75	50	3 GFS	7	-	9	24	14	18	13	22	62.9	12	4
2-1	75	75	3 GFS	7	-	10	28	16	16	10	20	64.8	10	3

[1] The number tabulated refers to the worst case in the solution.

stations in the solution, number of stations per pass, and different choices of three fundamental stations. Table 6-4 shows the spread in recovery of corrections in terms of grid station coordinates for solution No. 2-6 (35 stations per pass for complete grid with three "distant" fundamental stations (LFS)) as the best case of recovery in Table 6-3.

The spread in recovery of station coordinates in terms of corrections obtained through a least squares adjustment, as indicated in Table 6-4, also brings out the limitations in the final recovery of chords and velocity vector.

Table 6-4

Recovery of Station Coordinates, Short Arc Mode
(35 stations per pass, with LFS, σ_r = 10 cm)

Solution No.	Absolute Corrections for Station Coordinates					
	Δx (m)		Δy (m)		Δz (m)	
	Min.	Max.	Min.	Max.	Min.	Max
2-6	1.37	2.29	0.06	1.12	0.02	0.50

A regional approach in breaking up a large network into smaller grid, with or without a common station, did show a slight improvement in recovery of relative positions, both within a region and inter-regional distances. However, this procedure may also develop trade-off limits with the increase in total number of stations under investigation.

In addition, an error ellipse analysis showed that the average error under this mode for stations and chords is about 15 cm.

As a comparative study, the difference between short arc mode results (Table 6-3) with geometric mode results (Table 6-1) is quite striking. In an extended station network from the preliminary grid of nine stations (Figure 1-2), the deterioration in system's recovery through short arc adjustment is very

122

significant and definitely not in the desired centimeter level under the present investigative setup and mathematical model.

6.3 Conclusions

Based on the results obtained in this study, it can be concluded that the short arc mode in its current form will not be able to yield the desired accuracy at centimeter level for recovery of station positions, chords and therefore for the velocity vector. However, the geometric mode seems promising under suitable experimental setup, ranging accuracy, station grouping, etc.

In view of the above and the questions raised in Section 1.3, the following observations/conclusions pertaining to the geometric mode can be summarized:

A.   Recovery of Chords

The inclusion of three fundamental stations in the observational scheme of any event from the satellite is strongly indicated and their selection from the grid itself is also possible. However, with reference to subsection C below, the final choice goes only for three "distant" laser stations.

The minimum optimum number of grid stations simultaneously observed in any event is eight including three fundamental stations. Any increase over eight stations per event strengthens the geometry and improves the recovery.

The inclusion of any number of grid stations in a solution is only restricted by computer system limitations in core memory and has no adverse effect on the system's recovery. These remarks will also hold if the station-to-station distances are reduced up to one kilometer for densification of network. However, in any event consisting of eight or more stations, it will always be advantageous in any observational scheme to group and mix the grid stations of varying station-to-station distances for better geometry.

The adverse weather results in a loss of observations to any station (both within an event and in total number) and this affects the system's recovery only marginally so long as the loss of observations is about 10%. An optimum

number for observations to any grid station, other than three fundamental stations, is about 500.

The ranging accuracy is an important factor in achieving the desired centimeter level in system's recovery and thus the recommended standard deviation for ranging (σ_r) is 2 cm (see subsection C below).

The observations from airplanes improve significantly the system's recovery and their inclusion is strongly recommended.

B. Accuracy Estimation

The error ellipse analysis shows that the recovery trend for station positions and the chords over a network is more uniform and significantly improved when three "distant" fundamental stations are held fixed as compared to a solution with inner constraints only.

C. Recovery of Velocity Vector at any Grid Station

For the recovery of the motion rate at any grid station, the inclusion of three "distant" fundamental stations in the observational scheme is imperative. As this recovery will be relative to these fundamental stations, their selection should be "distant" enough from the area of crustal motion so that they can be considered stationary over the time span of the motion involved.

For a specified ranging accuracy (say σ_r = 2 cm), suitable experimental setup as described earlier in this section and preassigned α equal to 0.05 and power 1-β equal to 0.90, the recovery of velocity vector (Table 6-2) may be further subdivided as follows.

Magnitude (4 cm/yr):	Time interval required is five months between two sets of station recovery.
Direction Cosines.	Time interval required varies according to the magnitude of the direction cosine. In cases of small values of direction cosines (say about 0.30) and of very small motion rate (< 2 cm/yr), each recovery may have to be considered on its own merit. In

other cases (Table 6-2, lines 3 and 4), the time interval required is five months.

In view of the above, a motion rate for magnitude of 2 cm/yr would need a time interval of ten months for the above specified setup or a change of σ_r to 10 cm would accordingly require an interval of 25 months to recover motion rate of 4 cm/yr.

D. <u>Recovery of Velocity Vector for a Plate (or Area Block)</u>

For the specified ranging accuracy (σ_r = 2 cm) and taking sample size as 25, the time interval required for recovery of velocity magnitude for the area blocks under consideration is five months between two sets of recoveries.

It may be stressed here, as a statement of caution, that the above time intervals are relative to specific design of experiment and will have their statistical limitations. In practice or in experiments of similar nature the above figures may show minor deviations. Refer to Section 5.1.7 also.

BIBLIOGRAPHY

Agreen, R.W. and D.E. Smith. 1973. "A Simulation of the San Andreas Fault Experiment." GSFC Report No. X-592-73-216, Goddard Space Flight Center, Greenbelt, Md.

Anderson, D.L. 1971. "The San Andreas Fault." Scientific American 225, 5.

Anderson P.H., C.G. Lehr, L.A. Maestre, and G.L. Snyder, 1966. "Laser Experiment for Determining Satellite Orbits." Journ. of Quantum Electronics, QE-2, 8.

Bird, J.M., and Bryan Isacks, 1972. Editor, "Plate Tectonics." Selected papers from Journal of Geophys. Res., American Geophysical Union, Washington, D.C.

Blaha, G. 1971a. "Inner Adjustment Constraints with Emphasis on Range Observations." Dept. of Geod. Sci., Report No. 148, The Ohio State University, Columbus, Ohio.

Blaha, G. 1971b. "Investigations of Critical Configurations for Fundamental Range Networks." Dept. of Geod. Sci., Report No. 150, The Ohio State University, Columbus, Ohio.

Bjerhammar, A. 1973. Theory of Errors and Generalized Matrix Inverses, Elsevier Scientific Publishing Co., New York.

Brown, D.C. and J.E. Trotter. 1969. "SAGA, A Computer Program for Short Arc Geodetic Adjustment of Satellite Observations." Air Force Cambridge Res. Lab., Report No. AFCRL-69-0080, Bedford, Mass.

Brown, D.C. and J.E. Trotter. 1973. "Extension to SAGA for the Geodetic Reductions of Doppler Observations." Report No. AFCRL-TR-73-0177, Air Force Cambridge Research Laboratories, Bedford, Mass.

Brown, R.L., Jr. 1975. "A Dislocation Approach to Plate Interaction." Ph.D. Dissertation, M.I.T., Cambridge, Mass.

Brown, S.C., and R.R. Jayroe, Jr. 1973. "Terrestrial Environment (Climatic) Criteria Guidelines for Use in Aerospace Vehicle Development." NASA Tech. Memo., NASA TM X-64757, edited by Glenn E. Daniels, Marshall Space Flight Center, Huntsville, Alabama.

Bufe, C.G., F.W. Lester, K.L. Meagher, and R.L. Wesson. 1975. "Catalog of Earthquakes Along the San Andreas Fault System in Central California, April-June 1973." Open File Report 75-125, U.S. Geological Survey, Nat. Center for Earthquake Res., Menlo Park, California.

Bureau International de L'Heure. 1973. "Universal Time and Coordinates of the Pole." Circular D 74.

Byrns, D.A., and C.R. Cooke. 1975. "The Next Generation Satellite Laser Ranging System." Abstract of paper presented at the 1975 National Fall Convention, AGU, San Francisco, EOS 56,12.

Cox, Allen, 1968. Editor, Plate Tectonics and Geomagnetic Reversals, W.H. Freeman and Co., San Francisco.

Daniels, G.E. 1973. Editor, "Terrestrial Environment (Climatic) Criteria Guidelines for Use in Aerospace Vehical Development." NASA Tech. Memo., NASA TMX-64757, Marshall Space Flight Center, Huntsville, Alabama.

Dixon, W.J., and F.J. Massey, Jr. 1957. Introduction to Statistical Analysis, Second Edition, McGraw-Hill Book Company, Inc., New York.

Drake, C.L., O.L. Anderson, C.A.Burk, A.V. Cox, J.R. Goldsmith, L. Knopoff, J.C. Maxwell, F. Press, E.M. Shoemaker, T.H. van Andel and P.J. Hart. 1973. U.S. Program for the Geodynamic Project, Scope and Objective. National Academy of Science, Washington, D.C.

Escobal, P.R., K.M. Ong, O.H. von Roos, M.S. Shumate, R.M. Jaffe, H.F. Fliegel and P.M. Muller. 1973. "3-D Multilateration : A Precision Geodetic Measurement System." Tech. Memo. 33-605, Jet Propulsion Lab., Pasadena, California.

Grafarend, E., and B. Schaffrin. 1974. "Unbiased Free Net Adjustment." Survey Review, XXII, 171.

Greensfelder, R.W. 1972. "Crustal Movement Investigations in California: Their History, Data, and Significance." Special Publication 37, California Div. of Mines and Geology, Sacramento, California.

Hartwell, J.G. 1968. "A Power Series Solution for the Motion of an Artificial Satellite and its Concomitant Variational Equations." Report for GEOS Observation System Intercomparison Investigation, NASA Contract No. NAS 5-10588, Washington, D.C.

Holdahl, S.R. 1973. "Studies of Precise Leveling at California Fault Sites." Reports of Geodetic Measurements on Crustal Movement, 1906-71, Stock No. 0317-00167, U.S. Government Printing Office, Washington, D.C.

Krakiwsky, E.J., and A.J. Pope. 1967. "Least Squares Adjustment of Satellite Observations for Simultaneous Directions or Ranges." Dept. of Geod. Sci. Report No. 86, The Ohio State University, Columbus, Ohio.

Lerch, F.J., C.A. Wagner, J.A. Richardson, and J.E. Brownd. 1974 "Goddard Earth Models (5 and 6)." GSFC Report X-921-74-145, Goddard Space Flight Center, Greenbelt, Md.

Meade, B.K. 1971. "Horizontal Movement Along the San Andreas Fault System", Bulletin 9, Royal Society of New Zealand, Wellington, N.Z.

Meade, B.K. 1973. "Annual Rate of Slippage Along the San Andreas Fault." Reports of Geodetic Measurements of Crustal Movement, Stock No. 0317-00167, U.S. Government Printing Office, Washington, D.C.

Mueller, I.I., M. Kumar, J.P. Reilly, N. Saxena, and T. Soler. 1973. "Global Satellite Triangulation and Trilateration for the National Geodetic Satellite Program (Solutions WN 12, 14, and 16)." Dept. of Geod. Sci. Report No. 199, The Ohio State University, Columbus, Ohio.

Mueller, I.I., B.H.W. van Gelder, and M. Kumar. 1975. "Error Analysis for the Proposed Close Grid Geodynamic Satellite Measurement System (CLOGEOS)."Dept. of Geod. Sci., Report No. 230, The Ohio State University, Columbus, Ohio.

National Oceanic and Atmospheric Administration, 1973. "Reports on Geodetic Measurements of Crustal Movement, 1906-71." Stock No. 0317-00167, U.S. Government Printing Office, Washington, D.C.

Oliver, J., L. Sykes and B. Isacks. 1969. "Seismology and the New Global Tectonics." Tectonophysics, 7, Elsevier Publ. Co., Amsterdam.

Pope, A.J. 1966. "Strain Analysis of Repeated Triangulation for the Investigation of Crustal Movement." Master Thesis, Dept. of Geod. Sci., The Ohio State University, Columbus, Ohio.

Rao, C.R. 1973. Linear Statistical Interference and Its Applications, Second Edition, John Wiley Inc., New York.

128

Reilly, J.P., C.P. Schwarz, and M.C. Whiting. 1972. "The Ohio State University Geometric and Orbital (Adjustment) Program (OSUGOP) for Satellite Observations." Dept. of Geod. Sci., Report No. 190, The Ohio State University, Columbus, Ohio.

Rinner, K., K. Killian, and P. Meissl, 1969. "Beitrage zur Theorie der Geodatischen Netze im Raum." Deutsche Geodätische Kommission, Reihe A., 61.

Rodgers, D.L. 1975. "Deformation, Stress, Accumulation and Secondary Faulting in the Vicinity of the Transverse Ranges of Southern California." Ph.D. Dissertation, Brown University, Providence, R.I.

Savage, J.C., and R.O. Buford. 1970. "Accumulation of Tectonic Strain in California." J. of Geophys. Res., 60, 6.

Savage, J.C., and R.O. Buford, 1973. "Geodetic Determination of Relative Plate Motion in Central California." J. of Geophys. Res. 78, 5.

Scholz, C.H., and T.J. Fitch. 1969. "Strain Accumulation Along the San Andreas Fault." J. of Geophys. Res., 74, 27.

Scholz, C.H., L.R. Sykes and Y.P. Aggarwal. 1973. "Earthquake Predictions: A Physical Basis." Science, 181, 4102.

Sherr, P.E., A.H. Glaser, J.C.Barnes, and J.H. Willard. 1968. "Worldwide Cloud Cover Distributions for Use in Computer Simulations." NASA Contractor Report, NASA-CR-61226, Marshall Space Flight Center, Huntsville, Alabama.

Smith, D.E., R. Kolenkiewicz, R.W. Agreen, and P.J. Dunn. 1974. "Dynamic Techniques for Studies of Secular Variations in Position from Ranging to Satellites." GSFC Report X-921-74-161, Goddard Space Flight Center, Greenbelt, Md.

Tsimis, E. 1973. "Critical Configurations (Determinantal Loci) for Range and Range-Difference Satellite Networks." Dept. of Geod. Sci., Report No. 191, The Ohio State University, Columbus, Ohio.

Turcotte, D.L., and D.A. Spence. 1974. "An Analysis of Strain Accumulation on a Strike Slip Fault." J. of Geophys. Res., 79, 29.

Uotila, U.A., 1967. "Introduction to Adjustment Computations with Matrices." Dept. of Geod. Sci., Lecture Notes, The Ohio State University, Columbus, Ohio.

Whitten, C.A. 1967a. Geodetic Networks versus Time." Bulletin Geodesique, 84.

Whitten, C.A. 1967b. "Geodetic Measurements for the Study of Crustal Movement." Geophysical Monograph No. 12, The Crust and Upper Mantle of the Pacific Area. American Geophysical Union, Washington, D.C.

Winer, B.J. 1962. Statistical Principles in Experimental Design, McGraw-Hill Book Company, New York.

Wyman, C.L. 1970. "An Advanced Laser Tracking Technique for Future Space Guidance System." Journal Spacecraft, 7, 4.

APPENDIX A

Goddard Trajectory Determination System (GTDS)

1. **Introduction**

Presented in this appendix are the different procedures in brief which are used in the GTDS program (out of its many-facet capabilities) to give an extremely accurate orbit. The system version described here refers to the status as was operational in June 1974.

2. **Coordinate and Time System**

   2.1 **Coordinate Systems**

The GTDS program has the capacity to use different coordinate systems including subgroups, and it can convert from one system to another as needed. The integration is done referred to mean of 1950.0 or to a specified epoch.

The parameters like obliquity, $\delta \epsilon$, $\delta \psi$, etc. are input to GTDS by fitting polynomials through the Jet Propulsion Laboratory (JPL) ephemeris data while polar motion information is taken from publications of the U.S. Naval Observatory.

   2.2 **Time Systems**

The GTDS uses the atomic time system A.1 in the integration of equations of motion and the output time is Universal Time Coordinated (UTC). The UTC is derived from A.1 and since January 1, 1972 is kept synchronous with earth rotation derived time UT1 within ± 0.7 sec by step size adjustment of exactly one second when needed. The transformation between ephemeris time (ET) and A.1 is done by the relation:

$$ET = A.1 + 32\overset{s}{.}15$$

where the suspected discrepancy is about two parts in 10^9. In the case of transformations between A.1, UTC and UTI, they are done by time difference polynomials based on information from the U.S. Naval Observatory and between UT0, UT1 and UT2 on information from the BIH.

3. Spacecraft Dynamics

3.1 Gravitational Acceleration

In the N-body case the GTDS can include sun, earth, moon and all the planets in inertial mean of 1950.0 or true of epoch system and for the nonspherical gravitational field, up to degree and order 15 for earth and degree and order 4 for moon in body-fixed true of date system.

3.2 Drag and Atmospheric Models

The air drag force model considers a rotating atmosphere of "dynamic" type where the accounted factors are air density, altitude, position, season of the year, time of day, position relative to sun and solar energy influx. The three solar effects modeled in GTDS are as follows: (i) diurnal, (ii) 27 day, and (iii) solar wind (11-year cycle).

For air density the GTDS uses either Jacchia or Harris-Priester (default) models.

3.3 Solar Radiation Pressure

The GTDS modeling of radiation pressure takes into account the surface reflectivity, luminosity of the sun and eclipse factor (or shadow effect).

4. Integration of Equations of Motion

While integrating equations of motion, the GTDS takes advantage of another system of linear differential equations, called variational equations, and their integration is then carried out at the same time.

132

The GTDS has three main integration options (analytical, semi-analytical and numerical) and local error control is achieved by variable step size and different error bounds, both automatically or as a function of the distance "r" from the primary body.

5. Modifications/Alterations Made at OSU

5.1 Sequential Output of Satellite Ephemeris

In addition to the options already available, a new simplified output choice was introduced in GTDS on unit FT98T001 to write the satellite ephemeris in the format as required by Laser Range Generation Program (Appendix D). In this simplified version, the output contains the state vector $(\bar{R}, \bar{\dot{R}})$ and the corresponding time (Julian date in UTC).

5.2 Density of Printed Output

In the case where the satellite ephemeris density written on unit FT98F001 (Section 5.1) has to be time-wise very close, an option was introduced in GTDS to control the density for printing this ephemeris on paper. A data input card is introduced as the "first" card in front of the "normal" input deck of GTDS and an integer number punched in I5 format (columns 1-5) on this card then reduces the paper output by not printing all the satellite ephemeris, e.g., a number 11 will only allow every eleventh satellite position on unit FT98F001 to be printed.

Bibliography

Wagner, W.E. and E.C. Valez, eds. 1972. "Goddard Trajectory Determination Subsystem Mathematical Specifications." GSFC Report No. X-552-72-244, Goddard Space Flight Center, Greenbelt, Md.

COSMIC (Computer Software Management and Information Center). 1974. "User's Guide for Goddard Trajectory Determination System (GTDS)." Document ID No. 0013763 (Volumes 1 and 2), University of Georgia, Athens, Ga.

APPENDIX B

Short Arc Geodetic Adjustment (SAGA) Program

1. Introduction

The Short Arc Geodetic Adjustment (SAGA) program employs a power series solution to the equations of motion and is "general" enough in its approach to handle a wide variety of data types.

Since the time when the first SAGA was written, the program has been primarily modified for improved tropospheric refraction, option to use precise NWL ephemeris, automatic detection and removal of errors in cycle count, option for handling integrated Doppler, Geoceiver, and laser data, and define coordinate system by inner constraints.

2. Normal Equations

The normal equations are built up in set patterns and their solution is-obtained by second-order partitioned regression in the program, thus taking advantage of auto-regressive feedback. This method also enables the computation of the inverse of the variance-covariance matrix of the observations analytically.

3. Refraction and Geopotential Modeling

3.1 Refraction

The model used in SAGA is from Willmann and Hopfield with an expected uncertainty of 10-30 cm for elevation angles of $10°$ or greater. The program can also include refraction parameters in the model for adjustment along with other unknowns.

3.2 Geopotential

To enforce the use of precise ephemeris, the SAGA in its original form accommodated a potential model of degree and order 8.

4. Cycle Count Editing

In the event of utilization of raw data, the program has the built-in option to edit cycle count in Geoceiver data.

5. Restart and Subset Merging

5.1 Restart

The program now stores simultaneously the processed information: (a) in the event of a computer malfunction during a run, the last iteration is still maintained on unit FT02F001, and/or (b) to retain a subset data to be run for simultaneous adjustment with other subsets after independent editing (see Section 5.2).

5.2 Subset Merging

This is a stand-alone program capability which can merge two or more independent and pre-edited subsets as restart (Section 5 1) for simultaneous adjustments.

6. Observation/Parameter Specifications

Table 6-1 gives the details about the various specifications, capabilities and limitations of the SAGA program in its original form.

Table 6-1

General Information About SAGA

Observations per Pass	300 (if more, then the pass can be treated/broken into two or more sections)
Number of Passes per Solution	No limit
Number of Stations (a) per pass (b) in solution	19 40
Model Parameters (a) per pass (b) for refraction, etc.	17 29
Constraints	(a) Spherical coordinates φ, λ and h (b) Chord (c) Azimuth (d) Inner constraints

7. Modifications Made at OSU

7.1 Core Storage

The computer program was restructured at its link-edit stage to allow an 'overlay' processing of subroutines and this procedure then cut down the core storage requirement to one-third enabling cheaper and efficient running.

7.2 Number of Stations

With the availability of overlay structure the total number of stations in any solution was raised to 100.

Another modification removed the restriction of having 'lesser' number of stations (than the overall total) per pass—now SAGA can handle passes

136

being observed by less or all the stations in the solution.

7.3 Constraints

In the new option the rectangular coordinates x, y, and z can be constrained for any station in the following two choices:

(a) At Data Input Stage—In this case the constraints are read along with the station coordinates and used in the normal sequence of the adjustment as required,

(b) At Solution Stage—In this choice the normal matrix is developed without constraints. This normal matrix, being singular, can then be used repeatedly to investigate the effect of different constraints.

7.4 Recovery of Chords and Angles

A new feature has been added to compute and print chords and space angles with their statistics through error propagation (see Section 2.2.4 of the main report) in selected combinations of grid stations. This output can then be used to study the quality of recovery of relative positions between stations and angles between chords in any short arc solution.

Bibliography

Brown, D.C. and J.E. Trotter. 1969. "SAGA, A Computer Program for Short Arc Geodetic Adjustment of Satellite Observations." Report No. AFCRL 69-0080, Air Force Cambridge Research Laboratories, Bedford, Mass.

Brown, D.C. and J.E. Trotter. 1973. "Extension to SAGA for the Geodetic Reductions of Doppler Observations." Report No. AFCRL-TR-73-0177, Air Force Cambridge Research Laboratories, Bedford, Mass.

Hopfield, Helen S. 1971. "Tropospheric Range Error at the Zenith." paper presented at the 14th Plenary Meeting, June 17 - July 2, Seattle, Wash.

Trotter, J.E. 1972. "Input Instructions to the Modified Versions of SAGA." paper prepared for AFCRL under Contract No. F 19628-71-C-0043, Air Force Cambridge Res. Lab., Bedford, Mass.

APPENDIX C

The Ohio State University Geometric and Orbital

(Adjustment) Program (OSUGOP)

for Satellite Observations

1. Introduction

The OSUGOP is extremely efficient program to perform geodetic least squares adjustment, both in the geometric and orbital modes, from either optical or range data, and in double or quadruple precision.

The program has built-in capability of rejecting single "bad" observations, or an event or all observations from a station as the case may be on some preassigned specification and or specifying/altering the rejection criteria, e.g., in the case of ranges, any event having less than four observations is automatically rejected.

2. Time System

In the geometric mode the time for observation is required to separate the event, and hence can be in any system or even fictitious so long as the difference for any two consecutive events is greater than 0.0002 sec. In the orbital mode, however, the input time is in UT1.

3. Normal Equations

The normal equations generated in the program are before the applications of any constraints and, therefore, are singular. Thus it is sufficient to form the normals once and then run different solutions by varying constraints. Normals can be generated both from uncorrelated or correlated data.

The OSUGOP can also combine normals from different systems into one adjustment according to their individual weights.

138

4. Constraints

The OSUGOP can apply both absolute and weight constraints, but in the case of absolute constraints, the following considerations are applied:

(a) When constraint is defined as weight, a very large number as weight (as compared to weights used for observations, parameters, etc.) is included.

(b) When constraint is defined as inverse of variance, a very small number (not zero) as variance is included.

The program can include the following five types of constraints:

(i) Station coordinates--Rectangular (u,v,w) and Spherical (φ, λ, h)

(ii) Chord distance (R)

(iii) Relative Position ($u_i - u_j$, $v_i - v_j$, $w_i - w_j$)

(iv) 'Inner' constraints for origin, scale and orientation (Blaha, 1971)

The OSUGOP has the capability of performing a solution even with constraints only. One important factor to note is that the constrained value cannot be zero, whence the program takes the 'approximate' value of the parameter from the input as default value for the constraint. In such a case the constraint value can be given as an extremely small number (but not zero).

5. Data Input/Output

In the latest version the options for input/output of data have been enlarged as under:

(a) Observational Data--The observational data can be input either through IBM cards or magnetic tape (in a single file or multiple file). There is no limit on the number of observations which can be processed in the program.

(b) Processed Data--The print output density for processed observations can be controlled, both station-wise and event-wise.

(c) Normal Equations--In this case the output for normal equations can be selected on paper, IBM cards, and/or magnetic tape. However, any one set of normal equations to be read in as input must be only in one single file of a tape.

(d) Variance-Covariance Matrix--The output for variance-covariance matrix can also be selected on paper, IBM cards, and/or magnetic tape.

6. Analysis of Estimable Quantities

A new feature has been added to the OSUGOP to compute and print chords and space angles with their statistics through error propagation (see Section 2.2.4 of the main report) in selected combinations of grid stations. This output has special significance for analysis when the solution has been obtained with inner constraints only.

Bibliography

Blaha, G. 1971. "Inner Adjustment Constraints with Emphasis on Range Observations." Department of Geodetic Science Report No. 148, The Ohio State University, Columbus, Ohio.

Reilly, J.P., C.R. Schwarz and M.C. Whiting. 1972. "The Ohio State University Geometric and Orbital (Adjustment) Program (OSUGOP) for Satellite Observations." Department of Geodetic Science Report No. 190, The Ohio State University, Columbus, Ohio.

APPENDIX D

## Laser Range Generation Program (LRGP)
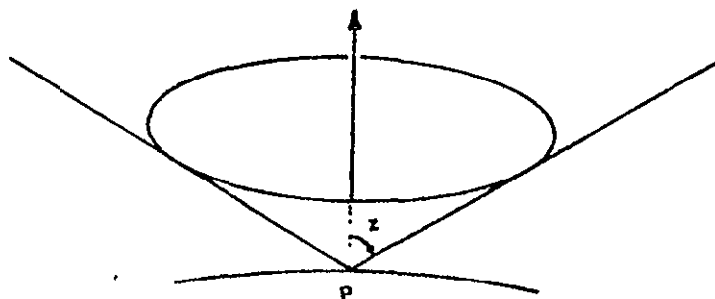
1. Introduction

This computer program was written specifically to set up an algorithm to generate ranges between the statellite and the station positions for use in the solution programs SAGA (Appendix B) and OSUGOP (Appendix C). The algorithm could be kept relatively simple as the program uses the satellite positions (and velocities) in a body-fixed coordinate system as generated by GTDS (Appendix A).

The generated ranges can be either in simultaneous or non-simultaneous sequential form with desired density and, if generated event-wise in the simultaneous mode, the program can also sort them station-wise in non-simultaneous mode for subsequent use in SAGA. In addition, the program also simulates crustal motion or weather effect.

2. Range Generation

From the satellite positions as obtained from GTDS the actual ranges are computed by checking if a particular satellite position happens to be in the observable cone :

The observable cone is visualized as a cone with its vertex coinciding with the observing station, its axis being along the zenith axis of that station, and its vertex semi-angle being equal to the maximum specified cut-off zenith distance. As soon as a satellite pass (or the satellite position) would reach within this observable cone, the data generation by the program starts and this process stops when the satellite leaves the cone. In the simultaneous mode, the range generation only starts when minimum of four (or any other specified number > 4) stations of a group can sight the satellite within their respective cones and stops as soon as the number of stations which can sight the satellite within their respective cones falls below four or the specified minimum.

3. Accuracy and Precision of Ranges

The computer program LRGP uses the subroutines GAUSS and RANDU from the Fortran's Scientific Subroutine Package to superimpose Gaussian noise on the ranges generated.

In its present form, the subroutine RANDU will not repeat before 2^{29} entries.

4. Weather Effect

This effect is modeled in subroutine CLOUD through a probability factor (PF) associated with each station (Section 3.4, main report). A value (PF = 1) for any station signifies a sighting/participation of that station in any event.

In case PF < 1, the computer generates an uniformly distributed random real number between 0.0 and 1.0 for each 'entry' and if this random number is less than the associated PF value of the station in question at that particular 'entry,' the range observation is generated. Otherwise, this

station is ignored and the cycle is continued with the next station.

In order to safeguard against the possibility of any station with PF<1 missing an observational simulation completely, a provision has also been made in the program to override the generated random number after a certain number 'k' of consecutive entries and trials to observe a station in which it has been missed by the satellite. In this case, PF is restored equal to 1 and observation generated. After this observation, PF value is again changed to its original value for subsequent 'entry.'

5. Crustal Motion

The crustal motion is generated by the subroutine DRIFT by introducing changes in the relative position between the stations.

6. Input/Output of Data

The satellite ephemeris input is through a magnetic tape as generated by GTDS (Section 5, Appendix A).

Using the above input together with the station coordinates, information regarding density of observations, etc., the program generates another magnetic tape containing ranges, simultaneous or sequential, together with the observational time as output.

ERRATA

If you have a copy of   Reports of the Department of Geodetic Science

Report No. 228

THE OSU 275 SYSTEM OF SATELLITE TRACKING
STATION COORDINATES

by

Ivan I. Mueller and Muneendra Kumar

August 1975

Please replace page 22, with the attached page.